AZLACTONE SUPPORTED DUALLY CROSS-LINKED SUPRAMOLECULAR GELS AS MOLECULAR SENSORS

A DISSERTATION
SUBMITTED TO THE DEPARTMENT OF CHEMISTRY
AND THE COMMITTEE ON GRADUATE STUDIES
OF PADERBORN UNIVERSITY
IN PARTIAL FULFILLMENT OF THE REQUIRMENTS
FOR THE DEGREE OF
DOCTOR OF SCIENCE

JIE LI
July 2018

ABSTRACT

Gels as sensor materials are payed much attention by scientist due to their easy manufacture, high responsibility, and good reversibility. Among them, dually cross-linked supramolecular gel (**DCSG**) containing multiple cross-linkers exhibits responsive properties and maintains the construction of the network during the response process. Surface plasmon resonance combining optical waveguide spectroscopy (SPR-OWS) was utilized to quantitatively detect (bio)molecules by using a three dimensional hydrogel layer. In this thesis, diverse **DCSG** systems were designed and developed as SPR-OWS sensors for target small molecules detection.

Template copolymers poly(*N,N*-dimethyl acrylamide-*co*-2-(dimethyl maleimido)-*N*-ethyl-acrylamide-*co*-2-vinyl-4,4-dimethylazlactone), poly(*N,N*-dimethylacrylamide-*co*-2-vinyl-4,4-dimethylazlactone) and poly(methyl acrylate- *co*-2-(dimethylmaleimido)-*N*-ethyl-acrylate-*co*-2-vinyl-4,4-dimethylazlactone) were synthesized via reversible addition-fragmentation chain transfer polymerization. These copolymers containing azlactone moieties, which were easily modified with nucleophilic amine groups bearing biotin, β-cyclodextrin, ferrocene, Hamilton receptor, and thymine to obtain **P1-P5**, in which the molecular recognition pairs were introduced. The dually cross-linked supramolecular gel systems were prepared onto a gold surface after spin coating, photo cross-linking and equilibrating in solvents. The sensor chip was responsive to target molecules by using SPR-OWS measurements.

As a first example, thin hydrogel layer based on biotin for streptavidin recognition was developed as a sensor for quantitative detecting of streptavidin in the concentration range from 0.5 to 200 μg/mL.

Then, the dually cross-linked supramolecular hydrogel based on β-cyclodextrin and ferrocene as noncovalent bonding pair was built as sensor, which could quantitatively detect adamantane in the range from 1×10^{-5} to 1×10^{-3} M. Also, the sensor was able to detect other small molecules. Interestingly, the sensor was further used to

selectively and quantitatively detect a cancer biomarker lysophosphatidic acid.

Finally, the dually cross-linked supramolecular gel based on Hamilton receptor and thymine as the molecular recognition pair was developed to detect hydrophobic barbiturates. Hamilton receptor and barbiturates has three order of magnitudes higher binding affinity than that of Hamilton receptor and thymine.

The new strategy to develop a sensor chip using SPR-OWS measurements was successfully demonstrated by diverse dually cross-linked supramolecular gel systems. They are expected to be used as a novel molecular sensor system in chemical and biological applications.

ZUSAMMENFASSUNG

Gele als Sensormaterialien werden von Wissenschaftlern aufgrund ihrer einfachen Herstellung, hohen Sensitivität und guten Reversibilität viel Aufmerksamkeit geschenkt. Unter ihnen zeigen zweifach vernetzte supramolekulare Gele (**DCSG**), die mehrere Vernetzer enthalten, responsivee Eigenschaften und behalten die Konstruktion des Netzwerks während des Reaktionsprozesses bei. Oberflächenplasmonresonanz-Kombiniete-Lichtwellenleiterspektroskopie (SPR-OWS) wurde verwendet, um (Bio-) Moleküle unter Verwendung einer dreidimensionalen Hydrogelschicht quantitativ nachzuweisen. In dieser Arbeit wurden verschiedene **DCSG**-Systeme als SPR-OWS-Sensoren für die Detektion kleiner Zielmoleküle entwickelt.

Templatcopolymere Poly (*N,N*-dimethylacrylamid-*co*-2-(dimethylmaleimido) -*N*-ethylacrylamid-*co*-2-vinyl-4,4-dimethylazlacton), Poly(*N,N*-dimethylacrylamid-*co* -2(vinyl-4,4-dimethylazlacton) und Poly(methylacrylat-*co*-2-(dimethylmaleimido) -*N*-ethylacrylat-*co*-2-vinyl-4,4-dimethylazlacton) wurden über eine Reversible Additions-Fragmentierungs-Kettentransfer Polymerisation synthetisiert. Diese Copolymere enthielten Azlactoneinheiten, die leicht mit nukleophilen Amingruppen modifiziert wurden, die Biotin, β-Cyclodextrin, Ferrocen, Hamilton-Rezeptor und Thymin trugen, um **P1**-**P5** zu erhalten, in dem die molekularen Erkennungspaare eingeführt wurden. Die zweifach vernetzten supramolekularen Gelsysteme wurden nach Rotationsbeschichtung, Photovernetzung und Äquilibrierung in Lösungsmitteln auf einer Goldoberfläche hergestellt. Der Sensorchip reagierte im SPR-OWS-Messungen auf entsprechende Zielmoleküle.

Als erstes Beispiel wurde eine dünne Hydrogelschicht basierend auf Biotin- und Streptavidin-Erkennung als Sensor zum quantitativen Nachweis von Streptavidin im Konzentrationsbereich von 0,5 bis 200 µg/ml entwickelt.

Danach wurde ein zweifach vernetzte supramolekulare Hydrogel auf der Basis von β-Cyclodextrin und Ferrocen als nichtkovalente Bindungspaar als an einen Sensor gebaut, der Adamantan im Bereich von 1×10^{-5} bis 1×10^{-3} M quantitativ detektieren

konnte. Der Sensor konnte ebenfalls andere kleine Moleküle erkennen zu können. Interessanterweise wurde der Sensor weiter dazu verwendet, einen Krebs-Biomarker Lysophosphatidsäure selektiv und quantitativ nachzuweisen.

Schließlich wurde das zweifach vernetzte supramolekulare Gel auf Basis des Hamilton-Rezeptors und Thymins als molekulares Erkennungs-Paar genutzt, um hydrophobe Barbiturate nachzuweisen. Der Hamilton-Rezeptor und Barbiturate haben eine um drei Größenordnungen höhere Bindungsaffinität als der Hamilton-Rezeptor und Thymin.

Die neue Strategie, einen Sensorchip durch zweifach vernetzte supramolekulare Gelsysteme mit SPR-OWS-Messungen zu entwickeln, wurde erfolgreich demonstriert. Sie werden voraussichtlich als neuartige molekulare Sensorsysteme in chemischen und biologischen Anwendungen eingesetzt werde können.

ACKNOWLEDGEMENTS

Undertaking this PhD has been a truly life-changing experience for me and it would not have been possible to do without the support and guidance that I received from many people. I would like to extend thanks to the many people, in different countries, who so generously contributed to the work presented in this thesis.

Special mention goes to my enthusiastic supervisor, Prof. Dirk Kuckling. My Ph.D. has been an amazing experience and I thank Dirk wholeheartedly, not only for his tremendous academic support, but also for giving me so many wonderful opportunities. I appreciate all his contributions of time, ideas, and funding to make my Ph.D. experience productive and stimulating. I am also thankful for the excellent example he has provided as a science researcher with rigorous and comprehensive scholarship, and humorous and positive attitude toward life.

Similar, profound gratitude goes to Prof. Meizhen Yin, who has been a spiritual and life mentor. The suggestions and encouragement she gives upon her experience help me getting through tough time in the Ph.D. pursuit. I am also appreciative to her kind help with my research work for quantitatively detect binding affinities of molecular recognition pairs.

Special mention goes to Prof. Jan Paradies, Dr. Hans Eglod and Ralf Hamann. Prof. Jan Paradies helps to simulate the binding process of the molecular recognition pair. Dr. Hans Eglod helps to build decent methods for calculating binding affinity and gelation point by using NMR measurements. Ralf Hamann helps to technically prepare gold layer utilizing PVD method. Thanks for their professional skills and kind help.

This PhD study would not have been possible without the corporation and support by all the members in the work group of Kuckling. To Dr. Artjom Herberg and Dr.

Jingjiang Sun, for helping me to test the GPC and for providing me with a fantastic lab training. To Dr. Wolfgang Birnbaum, for teaching me to operate the SPR spectroscopy. To Xiaoqian Yu and Patrik Berg, for helping me to operate DLS and UV-Vis spectroscopy. To Mariola Zukowski, for measuring the HRMS and ordering chemical agents. To Annette Lefarth and Angelika Kröber, for dealing with the daily lab organization and clerical work.

Dr. Chendong Ji was kind enough to undertake the correction work and help improving my research work, and I acknowledge the meticulous work he has done. I also very thanks to the contribution of other members in the work group of Prof. Yin in BUCT.

Personally, I owe a lot to my friends who encouraged and helped me at every stage of my personal and academic life, and longed to see this achievement come true. We spend lots of good times for celebrating Chinese festival, for travelling to different countries and doing sports. I acknowledge all my friends for your kind help and encouragement.

Finally, but by no means least, thanks go to mum, dad and my sister for almost unbelievable support. They are the most important people in my world and I dedicate this thesis to them.

DECLARATION

I, Jie Li declare that this thesis and the work presented in it are my own and has been generated by me as the result of my own original research.

The title of the doctoral thesis is

Azlactone supported dually cross-linked supramolecular gels as molecular sensors

I confirm that:

1. This work was done wholly or mainly while in candidature for a research degree at this University;
2. Where any part of this thesis has previously been submitted for a degree or any other qualification at this University or any other institution, this has been clearly stated;
3. Where I have consulted the published work of others, this is always clearly attributed;
4. Where I have quoted from the work of others, the source is always given. With the exception of such quotations, this thesis is entirely my own work;
5. I have acknowledged all main sources of help;
6. Where the thesis is based on work done by myself jointly with others, I have made clear exactly what was done by others and what I have contributed myself.

Signed: ……

Date: ……

CONTENTS

Chapter One: Motivation

In the past decades, gels were one of the hottest topics as interests ranged from chemical building blocks to various applications. Among them, a kind of gels which is built up by noncovalent bonding showing easy manufacture, high responsibility, and good reversibility has much more bright future as a functional material. Further, when two or more driving forces of covalent bonding and noncovalent bonding synergistically construct a gel, the gel show either outstanding mechanical properties or good responsibility through the volume swelling or shrinking. As a sensitive gel called dually cross-linked gel, the quantitative detection of its responsive behaviors is still a challenge.

Since it is long time that surface plasmon resonance combining optical waveguide spectroscopy (SPR-OWS) has being investigated in our working group. This method was used to detect layer thickness as well as refractive index of a gel layer on a gold surface. In our group, diverse responsive hydrogels were developed to detect their responsive behaviors upon different stimuli such as temperature dependent swelling of poly(*N*-isopropylacrylamide), pH dependent swelling of poly(*N*,*N'*-dimethylacrylamide) or poly(acrylacid). By using SPR-OWS, the layer thicknesses of these hydrogels were quantitatively detected and their dynamic processes of the swelling were also investigated. Therefore, it is thought that the SPR-OWS is a powerful method to investigate the responsive behavior of functional gels.

When a dually cross-linked gel system with responsive behavior was compelled to the SPR-OWS method it allows to quantitatively detect the responsive behaviors of gels. Taking these two technologies into account, it is assumed that a dually cross-linked gel even more detailed called dually cross-linked supramolecular gel would be able to swell along one dimension as response to stimuli signal. When the signal is a chemical molecule, the dually cross-linked gel could be used as a molecular sensor.

Normally, a sensor will contain two functional components, namely a recognition

element providing the specific binding to the targeting analyst and a reporter component transferring the signaling of the binding reaction. Dually cross-linked supramolecular gels have the feasibility to be used as a sensor due to its dually cross-linking structures responding with a volume change in the presence of the analyte. Thus, the signal of binding reaction is transferred to volume change of the gel, which is related to layer thickness as well as the refractive index monitored by the SPR-OWS.

Therefore, in this thesis, a series of dually cross-linked supramolecular gels were designed and constructed. Both organogel and hydrogel were prepared to detect hydrophobic molecules in organic solution and hydrophilic molecules in aqueous solution, respectively. In order to make the dually cross-linked supramolecular gel more universal, a functional monomer was introduced called 2-vinyl-4,4-dimethylazlactone (VDMA), which could be easily reacted with nucleophilic groups such as amine, hydroxyl and thiol groups via ring-opening reaction. The VDMA was copolymerized with other monomers by using reversible addition-fragmentation chain transfer (RAFT) polymerization to ensure a relatively uniform composition in each polymer chain. The dually cross-linked system was composed from dimethyl maleimide group as covalent bonding via photo cross-linking and molecular recognition pairs as noncovalent binding via multiple hydrogen bonding or host-guest interaction.

Next, the dually cross-linked supramolecular gels were immobilized onto a gold surface to prepare a SPR-OWS sensor chip. Different types of sensor chips were developed according to the different molecular recognition pairs based on supramolecular chemistry. The sensor chip based on dually cross-linked supramolecular hydrogel in which the biotin was collected as a recognition molecule would be used to quantitatively detect streptavidin. The results were shown in **Chapter three**. Another dually cross-linked supramolecular hydrogel system was created by introducing β-cycdextrin and ferrocene as a molecular recognition pair. This system was developed to quantitatively detect small molecules by using SPR-OWS measurements as shown in **Chapter four**. Interestingly, the system was further developed to selectively detect a cancer biomarker in mimic plasma condition (**Chapter five**). Further, the dually cross-linked supramolecular gel based on

hydrophobic monomers was used to prepare a sensor chip to detect hydrophobic molecules. Hamilton receptor and thymine was used as a molecular recognition pair to response to barbiturates as shown **Chapter six**.

The new strategy to develop a sensor chip using SPR-OWS measurements was successfully demonstrated by diverse dually cross-linked supramolecular gel systems. They are expected to be used as a novel molecular sensor system in chemical and biological applications.

Chapter Two: Dually cross-linked single networks: structures and applications

2.1 Introduction

Cross-linking of polymer chains is a traditional tool to improve materials properties and it enables forming materials that cannot be obtained from non-cross-linked polymers like elastomers or gels. Recently, networks with two kinds of cross-links were prepared.[1] one kind of networks called interpenetrating networks or double networks, which was formed by two or more kinds of polymers possessing network in each polymer and combining each other with interpenetrating or noncovalent bonding.[2,3] The other kind of networks can be called dually cross-linked single polymer networks (DCN), which was formed by same type of polymers containing two or more cross-linkers. Considering that a cross-link might be covalent (irreversible) or non-covalent (reversible) three different combinations are possible for DCNs: A – both are irreversible, B – one is irreversible and one reversible and C – both are reversible. While route A is mainly used to improve mechanical properties,[4] routes B and C yields materials changing their properties in response to different stimuli.[5,6] More recently, DCN structures with improved mechanical properties as well as stimulative responsibilities have been created[7,8] and applications as biological scaffold materials[9], shape memory materials[10], sensors[11], self-healing materials[12] and molecular carries[13] have been proposed. Mostly, the reversible cross-links in DCN formed by dynamic covalent bond or noncovalent bond are based on the principles of supramolecular chemistry.

Supramolecular chemistry to form polymers, as a concept firstly created by Lehn in 1970s, has been extensively and deeply investigated by scientists.[14] They are based on dynamic covalent bond or noncovalent bond of small molecules.[15,16] Despite the controllable polymerization or degradation of supramolecular polymers as well as their

functionality such structures are not comparable with the traditional polymers due to their non-controlled molecular weight and poor mechanical properties.[17] Therefore, supramolecular polymers were created having the host and guest structures as side or end groups of covalent polymers to synergistically improve the performance as a soft material by forming gels or elastomers.[18,19] Indeed, supramolecular polymers with covalent or noncovalent bonds in a precise manner to generate functional scaffolds have the ability to echo complex assemblies and multiple response of nature.[20] Various applications were developed such as self-healing[21,22], drug delivery[23,24], sensors[25], and adhesives[26]. A number of reviews have been published by different work groups covering both polymer architectures[27–29] and applications[30–32].

Typically, first polymers with functional side groups were prepared and then different polymers were combined to form supramolecular structures interacting with each other via varied covalent or noncovalent bonding. Supramolecular polymers with one driving force, called singly cross-linked supramolecular polymer organize themselves through a sol-gel transformation.[33] When there is more than one driving force for cross-linking the structures are called double or multi cross-linked supramolecular polymers.[34] Such supramolecular polymers will response to multiple signals changing e.g. their swelling behaviors with maintaining their skeleton structures.[35] Multi cross-linked supramolecular polymers, normally, possessed superior mechanical properties.[18] These unique properties of double cross-linked supramolecular polymers aroused great interest by scientists to create new networks or improve mechanical and responsive preferences of these networks in the past decades.

Creatively, double networks (DN) were developed integrating two or more independent cross-linked networks together. Gong et al.[36] reported the first DN gel system with high mechanical strength (fracture compressive stress of 12.7 KPa and strain of 92%) due to non-covalent interactions between the networks. poly(2-acrylamido-2-methylpropanesulfonic acid) formed the first network with rigid and brittle properties combining with poly(acrylamide) as the second network with soft and ductile properties in an interpenetrating network (IPN) manner. There are several reviews on double networks reported by Gong[37], Zheng[38] and Schmidt[39]. Although

different cross-linking was used to form different networks DN gels will not be covered here because of their IPN structure.

Further, DCN with orthogonal covalent or noncovalent interactions have been used to design reversible and responsive gels. In this account, different aspects of DCNs are summarized ranging from preparations to applications (***Figure 2.1***). From the structure aspect DCNs were classified with covalent-covalent, covalent-noncovalent and noncovalent-noncovalent cross-linking, respectively. From the applications aspect tissue engineering, adhesive, sensor, drug delivery, shape memory, self-healing and actuator were reported covering the most popular topics in supramolecular chemistry.

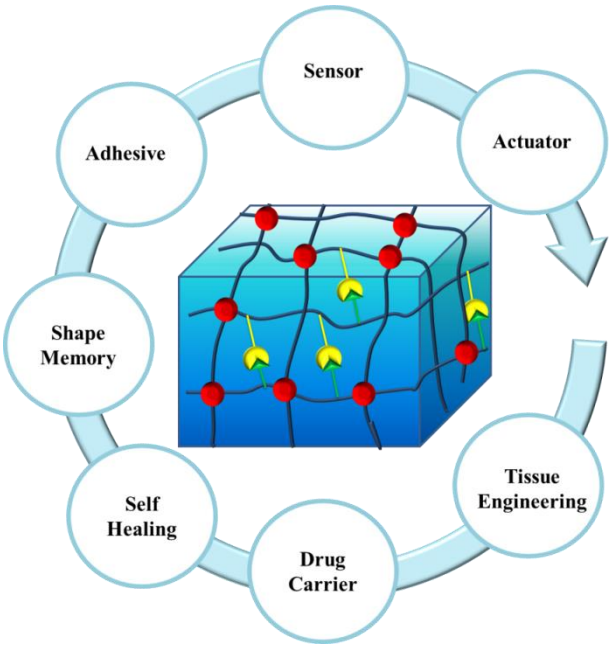

Figure 2.1. Constructions and applications of dually cross-linked single polymer network

2.2 Constructions of dually cross-linked single polymer networks

Dually cross-linked single polymer networks are constructed via covalent and non-covalent interactions between different polymer chains. Covalent bonds, compared to non-covalent bonds, have considerably stronger bonding energies that can range from 150 kJ mol^{-1} to 450 kJ mol^{-1} for a single bond. Non-covalent bonds range from 2 kJ

mol^{-1} for dispersion interactions to 300 kJ mol^{-1} for 'ion-ion' interactions.[40] Covalent interactions with high binding energy are beneficial for DCN mechanical properties, while non-covalent interactions with special binding pairs contribute to the responsive behavior. The term of "non-covalent bond" is related to a variety of interactions like ion-ion interaction, hydrogen bonding and hydrophobic interaction, which are representative interaction pairs in supramolecular polymers. Further, when these interactions are used in a cooperative manner a stable supramolecular complex with enhanced mechanical property or reversible response can exist.

2.2.1 Covalent-covalent cross-linking

DCNs with covalent-covalent cross-linking were normally prepared to improve their mechanical properties via a two-step polymerization method. There are rarely covalent-covalent cross-linking in DCNs with responsive behavior reported to our knowledge. Cui et al. developed a cross-linked microgel based on two kinds of chemical cross-linkers.[41] Divinylbenzene (DVB), ethylacrylate (EA) and methacrylic acid (MAA) were copolymerized by emulsion polymerization to form the microgels followed by modification with glycidyl methacrylate (GMA) as a second cross-linking agent. They showed that concentrated microgel dispersions can be covalently interlinked to form macroscopic hydrogels, which are termed doubly cross-linked microgels (DX MGs). Pandiyarajan et al.[42] developed a covalent-covalent dually cross-linked polymer layer to construct a surface in which the cross-link density varies continuously and gradually across the substrate in two orthogonal directions. The monomer *N*-isopropylacrylamide (NIPAAm) with photoactive methacrylyloxybenzophenone (MABP) and thermally active styrene sulfonyl azide (SSAz) was copolymerized. The presence of MABP and SSAz in the copolymer facilitates control over the cross-link density of the gel in an orthogonal manner using photo-activated and thermally activated cross-linking chemistries, respectively.

Despite the high performances of DCNs in mechanical properties, there are still some limitations for dually covalent cross-linked networks: (1) Multi-step free radical polymerizations are time-consuming and yield rather uncontrolled reproducibility in

polymer compositions; (2) Covalent-covalent cross-linked networks were just reported to be fabricated with simple shapes like sheets and dumbbells, while they are difficult to process in more complex shapes. (3) Essentially, all dually covalent cross-linked networks are short of responsibility to external stimulation and recoverability from damage.

2.2.2 Covalent-non-covalent cross-linking

To overcome the limitations of covalent-covalent cross-linking dually cross-linked gels, covalent-non-covalent cross-linked systems were developed. Here, scientists consider the mechanical property as well as the functionality of the gels by introducing different non-covalent bonds. In this case, normally, the stronger interactions like ion-ion interaction and hydrogen bonding were applied in DCNs with high mechanical strength, while the weaker but more sensitive interactions like hydrophobic interaction and π-π stacking were used to develop DCNs with responsibility and recoverability. Both systems can be used to achieve self-healing and shape memory properties. Additionally, based on hydrophobic interactions a new concept of fuse links has been introduced and gels with a reliable deformation range were achieved.[43]

Elastomers with covalent-non-covalent dual cross-linking exhibit improved mechanical properties in response to their functional properties. Tang and coworkers used a metal coordination reaction between pyridine groups and metal ions in butadiene-styrene-vinylpyridine rubber (VPR).[44] Wang and coworkers also developed an elastomer with covalent-non-covalent dual cross-linking through reversible ionic hydrogen bonds via the acid–base reaction.[45] The DCN elastomer was based on polybutadiene oligomers bearing amine group and acid group cross-linked with tri-functional thiol via the thiol-ene reaction. In hybrid DCN elastomers combining hydrogen bonds and covalent bonds sufficient chain mobility and hydrogen bond concentration were provided, when PDMS chains with proper molecular weight were used as the polymer matrix.[46]

Covalent-ionic dually cross-linked gel system was developed by the Zhou group where ferric ion coordination with carboxylic acid group as an ionic bonding was

introduced.[47] The copolymer P(AAm-co-AA) with covalent cross-linker *N*,*N*-methylene bisacrylamide (MBA) was prepared forming a soft gel. After loading with ferric ions the DCN with ultrahigh mechanical strength was obtained (***Figure 2.2a***). The optimal DCN hydrogel possessed ultrahigh tensile strength of 6 MPa, large elongation more than 700 %, ultrahigh toughness of 27 MJ/m^3 and good self-recovery property (recovering up to 87.6 % within 4 h at room temperature). More, Huang and coworkers designed a DCN based on PAA where modified silica nanoparticles was used as a covalent cross-linker and carboxylic acid-ferric ion used as a reversible non-covalent bonding.[48] A similar approach using MBA to cross-link the PAA with the same non-covalent interactions was reported by the Xie group.[49] Craig and coworkers developed a DCN by using poly(4-vinylpyridine) with dibromide hexane as the covalent and bifunctional van Koten-type pincer complex as the reversible cross-linker (***Figure 2.2b***).[50] The coordination pincer complex introduced to DCN has a surprising influence on mechanical properties. Compared to covalent cross-linked gels the dually cross-linking gel can have a much greater fracture stress and strain because the pincer complex minimized the stress concentrations that initiate crack formation and propagation. Moreover, weaker interactions like hydrophobic interaction were also used to construct DCNs with improved mechanical properties. Yan[51] and Harada[52] groups have developed host-guest interaction covalent-non-covalent DCNs based on β-cyclodextrin. Poly(ionic liquid) membranes with covalent cross-linking were synthesized from imidazolium type ionic liquid monomers, acrylic acid, acrylonitrile and divinylbenzene (***Figure 2.2c***).[51] Then the surface was modified with β-cyclodextrin and ferrocene, respectively, via coupling of carboxylic acid and primary amine groups. This polymer velcro exhibits strong adhesion in air and in aqueous solutions (including acidic and basic water, and artificial seawater, holding 100 g weight more than 3 h), and could be unfastened and fastened by mechanical and chemical means. The β-cyclodextrin and adamantane pair as host-guest interaction was grafted to polyacrylamide in combination with the covalent cross-linking agent MBA to form the DCN gel (***Figure 1.2d***).[52] The gel showed a tensile strength of ~ 12 MPa in a wet condition, which is much stronger than in normal hydrogel (~ 6.3 KPa).

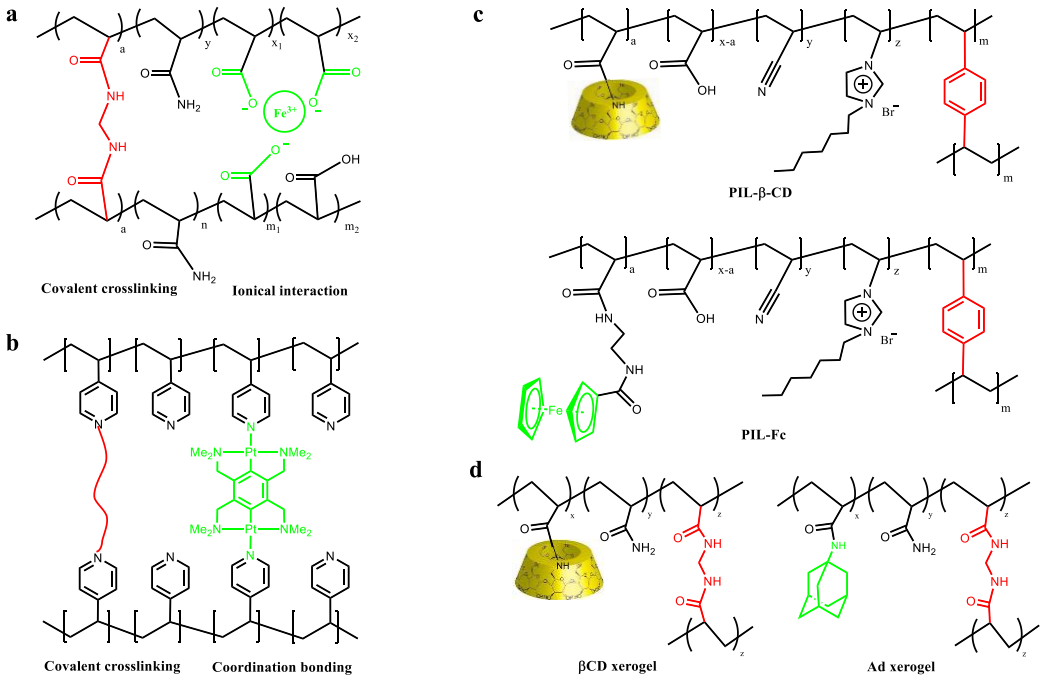

Figure 2.2. Covalent-non-covalent cross-linked DCN gels with remarkable mechanical properties. a) copolymer of P(AAm-co-AA) with MBA as covalent bonding and carboxylic acid group with ferric ion as non-covalent bonding[47]; b) homopolymer poly(4-vinylpyridine) modified with dibromide hexane as covalent bonding and Koten-type pincer as non-covalent bonding[50]; c) poly(ionic liquid) membrane PIL-β-CD and PIL-Fc containing divinylbenzene as covalent bonding and β-CD and Ferrocene as non-covalent bonding[51]; d) β-CD xerogel and Ad xerogel were obtained based on PAAm containing MBA as covalent bonding[52].

More often, the rather weak supramolecular interactions combined with covalent cross-linking forming DCN with novel functional properties. Because of the weak binding energy of non-covalent cross-links the supramolecular polymers exhibited uncompetitive mechanical properties but high responsibility and reversibility. Cyclodextrin[53], catechol[54] and boric acid[55] are three systems mostly reported for switchable DCNs.

Harada´s group developed covalent-non-covalent DCNs based on β-cyclodextrin as a host molecule. AAm, MBA and the host-guest pair (β-cylcodextrin and ferrocene) were copolymerized to form the DCN gel as shown in ***Figure 2.3a***.[56] The gel was responsive to oxidation and reduction of the ferrocene moieties resulting in expansion

or contraction of the gel volume. The host-guest pair β-cyclodextrin and dansyl was also introduced to the same backbone to form DCN gels that were responsive to pH values changes.[57] The optical spectra were used to monitor the assembly and disassembly process due to the dansyl group protonation or deprotonation in different pH environments resulting in changing its fluorescence during the process. Zhao and coworkers reported a DCN gel constructed by AAm, MBA and the host-guest pair (β-cyclodextrin and ferrocene) performing like Lego building blocks with multiple responses.[58] The Lego-inspired assembly process allows easy placement of different building blocks within the same construct. The individual hydrogel building blocks exhibit either non-responsive or merely simple swelling-deswelling responsive behaviors. Nevertheless, the assembled structure shows much more complex reversible shape changing behaviors due to the mechanical stresses between the building blocks of distinct stimuli-responsiveness. Combining the host–guest inclusion complexes of β-cyclodextrin with adamantane and ferrocene in one copolymer network, formed gel showed self-healing ability when damaged and responded to redox stimuli by expansion or contraction. Moreover, the gel showed a redox responsive shape-morphing effect.[59]

The Qiao group[60] has reported DCNs using α-CD and azobenzene as the non-covalent bonding and norbornene as the secondary covalent bonding (***Figure 2.3b***). Poly(*N*-(2-hydroxyethyl)acrylamide) (PHEAm) was selected as the backbone followed by modification of the hydroxyl group with each functional moieties to form the DCN particles. Upon short exposure to UV light, the non-covalent cross-links were disrupted resulting in increased permeability and burst release of the cargo. As sunlight contains UV light at low intensities, the particles can potentially be incorporated into systems used in agriculture, environmental control, and food packaging, whereby sunlight could control the release of nutrients and antimicrobial agents. Burdick and coworkers[61] designed covalent-non-covalent cross-linked DCN based on hyaluronic acid, which was modified with a covalent cross-linking pair for Michael addition (methacrylate and thiol) as well as a non-covalent cross-linking pair for host-guest interaction (β-cyclodextrin and adamantane) as shown in ***Figure 2.3c***. This hydrogel demonstrated its

potential in a range of applications where the precise delivery of hydrogels with tunable properties is desired. With the similar strategy they designed a DCN for the 3D printing process using the UV light initiated covalent cross-linking of methacrylate.[62]

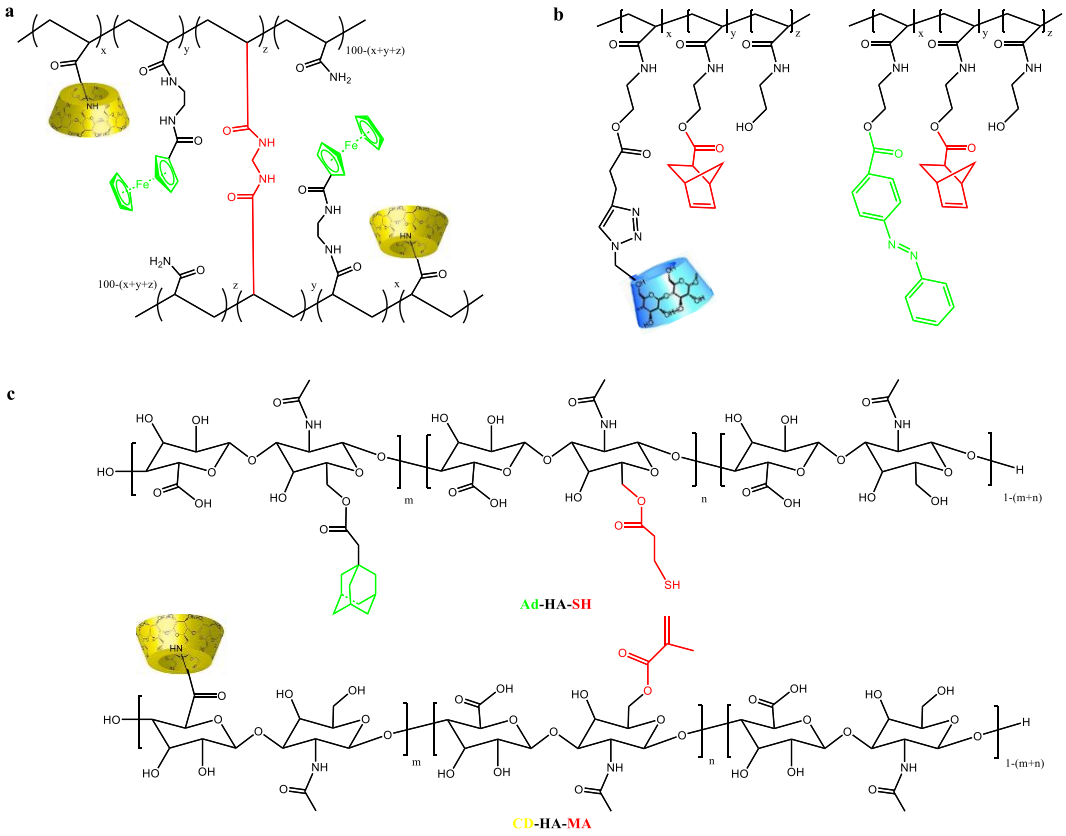

Figure 2.3. DCN supramolecular polymers based on cyclodextrin. a) DCN gel copolymerized with AAm, BMA and host-guest pair (β-CD and Ferrocene)[56]; b) DCN gel constructed by modification of PHEAm with norbornene as covalent bonding and host-guest pair (α-CD and azobenzene) as non-covalent bonding[60]; c) DCN supramolecular gel obtained from hyaluronic acid, which was modified with Michael addition pair (methacrylate and thiol) and host-guest pair (β-CD and adamantane)[61].

Adhesive proteins from mussels contains a large numbers of 3,4-dihydroxy phenylalanine residues having the key role to fix the mussel to organic and inorganic surface.[63] Dopamine is the simplified structure of this functional group, which has been reported widely in supramolecular chemistry. The Takahara group[54,64] reported the DCN synthesis with copolymer chains containing catechol groups. The catechol

group can form two different types of cross-links either through oxidation of two catechol groups or coordination with ferric ions. Ren and coworkers[65] reported the similar process of dual cross-linking of modified chitosan via catechol groups. The Harada group[66] combined catechol with boronic acid side groups to construct the non-covalent bonding as well as MBA as the covalent bonding. The assembly and disassembly of the gels are reversibly switched by varying the pH of the medium.

Boronic acid is known as a non-covalent bonding moiety owing to its responsibility to diol-containing molecules[67], which potentially can be used as a sensor. A DCN gel sensor based on a polymerized crystalline colloidal arrays (PCCA) matrix has been designed.[68] AAm and MBA were photo polymerized to form the covalently bonded hydrogel that later was modified with phenylboronic acid by reaction to the acrylamide side group. The gel was shrinking at a certain glucose level due to the secondary non-covalent bonding, while it was swelling when abundant glucose was used to react with the boronic acid in a 1:1 ratio. Later they developed another similar system built up on a PVA backbone that can interact with phenyl boronic acid as a non-covalent cross-linker.[55] The dually cross-linked gel would de-cross-link of the non-covalent in the presence of glucose molecules.

Besides the irreversible covalent bonding, dynamic covalent bonding was also used to construct DCNs. Zhang et al.[69] designed a dually cross-linked supramolecular gel based on a backbone of poly(2-hydroxyethyl acrylate), which contained dynamic covalent furan-maleimide Diels-Alder adducts and hydrogen bonds from the 2-ureido-4[1H]-pyrimidinone (UPy) moiety. They constructed self-healing material containing relatively rapidly exchanging hydrogen-bonded and slowly exchanging Diels–Alder based cross-linkers. Xu et al.[70] used poly(2-aminoethylmethacrylamide hydrochloride)-block-poly(2-hydroxypropylmethacrylamide) (PAEMA-b-PHPMA) to construct DCNs via dynamic covalent bond with pyridine-2,6-dicarbaldehyde and metal coordination with copper and zinc ions. Further, based on the boronate–catechol interactions between a disulfide-containing, boronic acid-based cross-linker, and a catechol-functionalized poly(*N*-isopropyl acrylamide), a multitasking hydrogel with double dynamic network was developed.[71] By integrating the inherent heat-responsive

property of poly(*N*-isopropyl acrylamide) and bioadhesion of catechol moieties with the reversibility and dynamic features of boronate ester and disulfide bonds, the final hydrogel is endowed with not only temperature, pH, glucose, and redox quadruple stimuli sensitiveness, but also autonomic self-healing property and biomimetic adhesion ability.

2.2.3 noncovalent-noncovalent bonding

Non-covalent-non-covalent cross-linked gel systems were investigated to design environmentally responsive materials that can act as a generalist. The Fiore group[72] used hydrogen bonding and metal coordination to design DCN with orthogonal interactions and multifunctional stimuli-responsive behavior. Polymer blends based on a poly(ethylene-co-butylene) core (PEB) terminated with either 2-ureido-4[1H]-pyrimidinone (UPy) hydrogen-bonding motifs (UPy-PEB-UPy) or 2,6-bis(1'-methylbenzimidazolyl)pyridine (Mebip) ligands coordinated to metal ions ([M(Mebip-PEB-Mebip)]$^{2+}$ (M = Zn, Fe)) were assembeled in an orthogonal fashion. Weng et al.[73] designed an orthogonal metal-ligand coordination and hydrogen bonding DCN as well. Polymer bearing tridentate 2,6-bis(1,2,3-trizol-4-yl)pyridine (BTP) ligand units in the chain center and two ureidopyrimidinone (UPy) motifs on the chain ends with a linker of PEG. The Holten-Andersen group[74] used the dually non-covalent bonding process to decouple spatial structure and mechanical performance of polymer materials. 4-Arm polyethylene glycol polymers, where the end of each arm was functionalized with a histidine moiety (4PEG-His), were designed to coordinate with different metal ion like Ni^{2+}, Cu^{2+} or Zn^{2+}. The gel exhibited different relaxation time by adjusting the ratio of metal ions opening a new method to control the properties of soft materials. Linear polyurethanes with two non-covalent bonding moieties (hydrophobic interaction and hydrogen bonding) were developed with a thermo-induced triple shape memory effect and a pH-sensitive dual shape memory effect.[75] Finally a triblock copolymer containing two non-covalent interactions was designed that could further create complex secondary structures by orthogonal self-assembly and fold into well-defined polymeric nanoparticles.[76]

2.3 Applications of dually cross-linked single networks

2.3.1 Tissue engineering

Materials for tissue engineering whether form natural derivatives or from synthetic polymers are extremely important for tissue replacement and regeneration.[77] They are expected to exhibit suitable physical parameters such as degradation period and mechanical properties and well biological parameters like cell adhesion and biocompatibility.[78] Injectable hydrogels are considered as one of the most brightly candidates as a tissue engineering matrix rather than covalently cross-linked materials like aliphatic polyesters, which requires the surgeon to make incisions sufficiently large to enable placement of the polymer/cell constructs. Various hydrogel systems were developed with covalent or non-covalent cross-linking that are composed of a broad range of natural and synthetic macromolecules, such as poly(ethylene glycol) (PEG)[79], poly(vinyl alcohol) (PVA)[80], agarose[81], alginate[82], chitosan[83], gelatin[84], fibrin[85], chondroitin sulfate[86] and hyaluronic acid[87]. However, it should be noted that natural polymers are mechanically weak with inconstant composition and often possess a high affinity for proteins present in serum. Further, synthetic systems inherently lack biologically active sites which limit proliferation, migration and organization of incorporated cells. Therefore, an ideal model to design hydrogel for tissue engineering is combining synthetic polymers with natural polymers to construct DCN hydrogels.[88]

2.3.2 Drug and biomolecule carrier

Generally speaking, drugs and biomolecules like protein are hard to release from carriers to the host site by a controlled manner.[89] The controlled release approach aims to achieve benefits like maintaining the cargo stable and the concentration within the therapeutic window over an extended period of time and, thus, enhance the therapeutic efficacy by lowering the drug dosage while reducing side effects.[24] Hydrogels are beneficial in preserving drug and protein stability at mild conditions (aqueous environment, room temperature). Hence, they belong to the most promising candidates

for drug and biomolecule carrier.[90] DCN hydrogels were developed to carry drugs and proteins and to control their release due to their stable skeleton as well as responsible properties.[32]

To increase the phase transition efficiency DCNs were developed as drug carriers. Dually cross-linked particles with β-CD-azobenzene host−guest interactions chemically cross-linked by ring-opening metathesis polymerization of norbornene and with different sized silica particles as a template. Upon short exposure (5 s) to UV light, the non-covalent cross-links were disrupted resulting in increased permeability and burst release of the cargo (50 mol-% within 1 s).[60] Dually cross-linked nanogels containing cholesteryl group-bearing pullulan (CHA) as the non-covalent interaction as well as the chemical interaction with copolymerization of 2-methacryloyloxyethyl phosphorylcholine (MPC) were prepared using a seed growing method. The hybrid nanogels exhibited the ability of trapping denatured carbonic anhydrase B (CAB) and then releasing CAB in its native form.[91] DCN hydrogels with tunable swelling ratio and mechanical properties can be synthesized employing hydrazide based click reactions. Substantial shear thinning and rapid recovery make these hydrogels suitable injectable materials at high storage modulus.[92]

2.3.3 Self-healing

Materials used in industrial applications are designed with a specific service life, but during the time loss of structural capacity or functionality can occur because of incidental damage or degradation.[93] If materials have the ability to self-reorganize and heal from damage, then this material will be called self-healing material. DCNs exhibit multiple interactions between different polymers making it easier to design self-healing materials. Hu et al.[94] designed dually non-covalent cross-linked supramolecular gels utilizing clay nanoparticles through the interaction of hydrogen bonds with poly(acrylamide-co-acrylic acid). The reinforcing fillers can relax the applied stress and defer the complete fracture of hydrogels, which significantly increased the stretchability of dually cross-linking gel. Because of its unique physical reversible network structures, these DCN hydrogel could sufficiently reconstruct its network

structures, resulting in good self-recovery from damages without any external stimuli. Huang et al.[48] introduced silica nanoparticles with vinyl groups to chemically cross-link polyacrylic acid gels, in which the hydrogen bonding leads to the self-healing property. The Binder group[95] has developed a self-healing system based on star polymer containing azide-alkyne click reactions as a covalent bonding and thymine groups for non-covalent bonding. Poly(isobutylene)s (PIBs) based star polymer with a prominent rubbery plateau showed a complete self-healing after 72 h at 20 ^{o}C and after 24 h at 40 ^{o}C, respectively. Dynamic covalently and as well as hydrogen bonded were partially healed at room temperature while fully healed after treated at high temperature owning to cross-linking by the dynamic covalent bonding.[69] DCN hydrogels containing host-guest interactions of β-cylcodextrin and ferrocene complex could be redox stimulated to control self-healing properties such as re-adhesion between cut surfaces.[53]

2.3.4 Shape memory

In principle, shape memory polymer should consist of two phases: a stable fixing phase determining the permanent shape, and a switching phase for temporary shape fixing and recovery. DCNs are beneficial for this application due to the presence of multiple cross-linking agents with both stability and reversible response. The tri-stimuli-responsive formation/dissociation of α-cyclodextrin-azobenzene acts as molecular switch freezing or increasing the molecular mobility. The resulting film can be processed into temporary shapes and recovers its initial shape upon the application of light irradiation, heating, or chemical agent independently.[96] The introduction of Zn^{2+}-pyridine coordination[44] or ion-ion interactions[45] into a chemically cross-linked rubber increased its mechanical properties as well as create a shape memory behavior. The Anthamatten group[97] used ureidopyrimidinone (UPy) as a noncovalent bonding moiety to construct a shape memory elastomer. H-bonding is temperature dependent and, hence, was considered as a driving force for shape recovery switching between 5 °C and 66 °C as shown in ***Figure 2.4***.

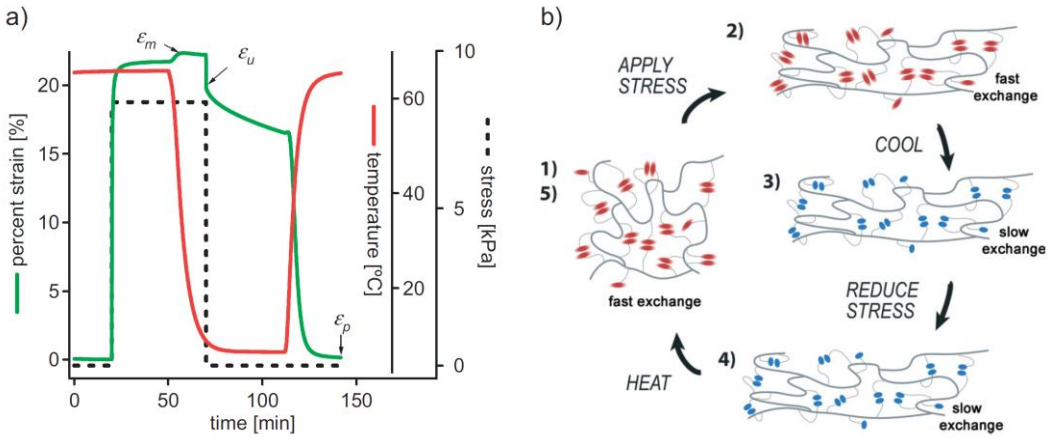

Figure 2.4. a) Typical shape-memory response curve of an elastomer containing 2 mol% UPy pendent side groups, 1.5 mol% TMP-TMA, and 96.5 mol% BA. b) Cartoon of proposed shape-memory mechanism involving thermo-reversible H-bonding. Colored side-groups represent H-bonding groups in the hot (red) and cold (blue) states, and the darker lines represent the lightly cross-linked covalent network. Reprinted with permission from[97]. Copyright 2007 Wiley-VCH.

The noncovalent bonding with weak interaction was also investigated that was focused on the morphologies rather than the mechanical properties. Two different kinds of host–guest inclusion complexes of β-cyclodextrin with adamantane and ferrocene were used to bind polymers together to form a DCN. Since ferrocene is responsive to oxidation and reduction conditions the gel showed a redox-responsive shape-morphing effect (***Figure 2.5a***).[59] Carboxylic acid modified polyurethane containing PEG fragments was used to construct another shape memory material.[75] Due to the dually cross-linking moieties of hydrophobic interaction and hydrogen bonding, this supramolecular gel exhibited almost complete recovery as shown in ***Figure 2.5b***.

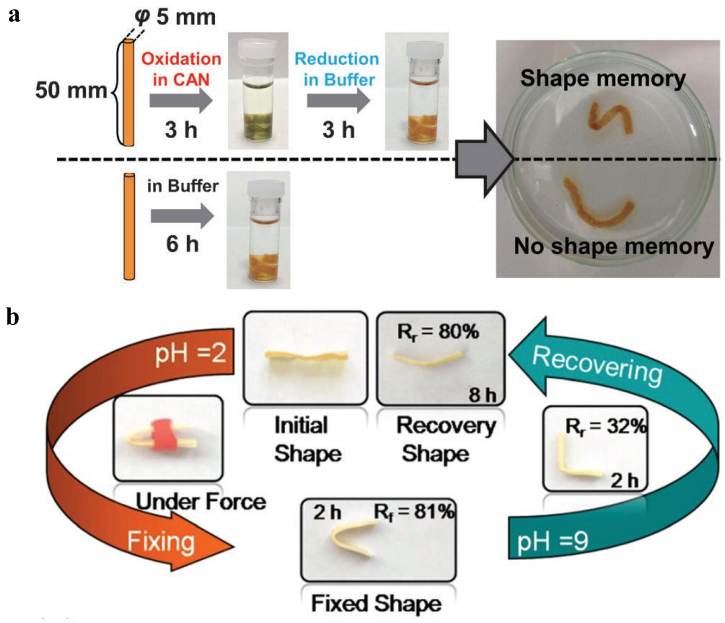

Figure 2.5. The shape memory property of dually cross-linked single network supramolecular gel with weak noncovalent interactions. a) a linear-cylindrical piece of βCD-Ad-Fc pAAm gel (2,1,1) (φ: 5 mm, length: 50 mm) was oxidized in an aqueous buffer containing CAN (25 mm) for 3 h, during which time it adopted a helical shape. Subsequently, the gel was reduced by immersion in the original buffer. When the gel was shaken in the buffer for 3 d, it retained its helical shape (top). This shape-memory effect did not occur without the oxidation–reduction cycle (bottom). Reprinted (adapted) with permission from[59]. Copyright 2015 Wiley-VCH; b) pH-Sensitive memory effect of PEG-30%-MDI-DMPA, it was firstly immersed in an alkaline solution for 2 h to damage the carboxylic dimers (Initial Shape). Then it deformed into a new shape and was immersed in acid to reform the carboxylic dimers to fix this temporary shape (Fixed Shape). Next, the sample was returned to the alkaline state, and the fixed shape gradually recovered to the initial shape (80 %). Reproduced (in part) from [75] with permission of The Royal Society of Chemistry (2016).

2.3.5 Adhesives

A tough adhesive DCN was constructed, which was based on hydrogels with a cationic imidazolium substituent and intercalative properties of micromica.[98] When the imidazolium group was entrapped in the interlayers of the layered inorganic

compound micromica, the hydrogels adhered together supporting a tensile load of 10 kg (with a hydrogel containing 20 wt-% water). DCN based on host-guest interactions of β-cyclodextrin showed adhesive properties as well when combined with adamantane[52] and ferrocene[51] moieties, respectively. In the latter case the polymer adhesion reversibility was electrochemically controlled by an applied potential.

2.3.6 Sensors

Detection of chemical and biological agents plays a fundamental role in biomedical, forensic and environmental science as well as in anti-bioterrorism applications.[99] Normally, a sensor will contain two functional components, namely a recognition element providing the specific binding to the targeting analyst and a reporter component transferring the signaling of the binding reaction.[100] DCNs have the feasibility to be used as a sensor due to its dually cross-linking structures responding with a volume change in the presence of the analyte. Molecule-responsive micro-sized hydrogels with β-cyclodextrin as ligands are prepared by photo polymerization. The molecule-responsive micro-hydrogels show ultra-quick shrinkage in response to target bisphenol A.[101]

DCNs respond to the change of the glucose concentration of the surroundings, which has a promising future within the application of diabetes treatment.[102] Scientists have already developed glucose sensors in different manners including boronic acid systems. Ganesan et al.[103] designed a DCN based on ferrocene on a gold surface, which exported the signal electrochemically (***Figure 2.6a***). In another approach sulfonamide was used as the acid to indicate the glucose-responsive signal by exhibiting a swelling transition in the pH range of 6.5 - 7.5 existing only in the presence of glucose.[104] Braun and coworkers[55,68] designed DCNs as glucose sensor by using boronic acid, which provides a specific interaction with glucose. PAAm was modified with boronic acid that physically interacted with 1,3-diols like PVA forming the dually cross-linked supramolecular sensor (***Figure 2.6b***). By adjusting the composition of boronic acid and the volume resetting agent (PVA), the sensor exhibits a linear fast response to glucose as well as minimal hysteresis and signal drift under simulated

physiological conditions.

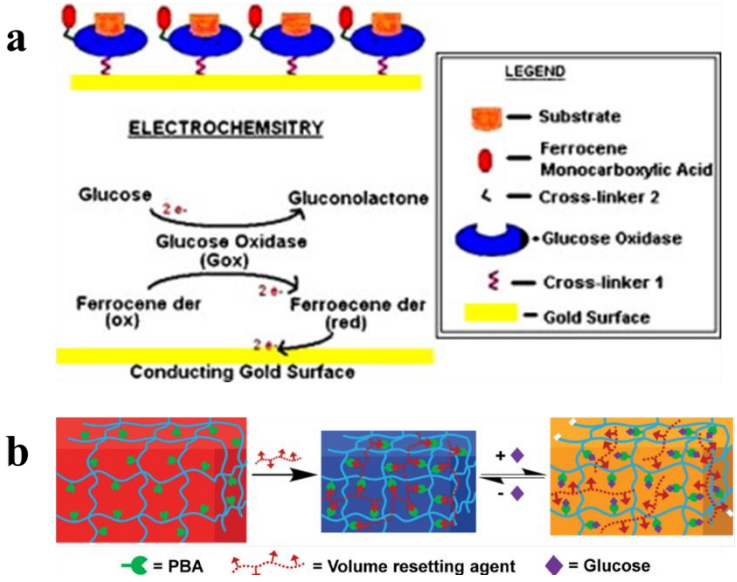

Figure 1.6. a) Reaction schema of the proposed dually cross-linked Gox biosensor (top) and the reaction electrochemistry (bottom). Reprinted (in part) from [103] ith permission of Elsevier (2005); b) General design protocol of the glucose responsive hydrogel. Reproduced (in part) with permission from [55]. Copyright 2014 Wiley-VCH.

2.3.7 Actuators

Certain DCN gels possess a covalent bonding to maintain the gel structure while a non-covalent bonding can be used to increase or decrease the cross-linking densities of the structure. Thus, the hydrogel has expansion–contraction ability when treated with a stimulating factor leading to the response of the non-covalent bonding. A hydrogel actuator was created using the inclusion complexes between β-cyclodextrin and ferrocene as a non-covalent cross-linking, which could be expanded to 111 % in oxidated state (***Figure 2.7a***).[56] A supramolecular hydrogel actuator based on PDMAAm containing a chemical cross-linker MBA and a guest moiety of dialkoxynaphthalene was combined with PNIPAM end-functionalized with tetrathiafulvalene, which interacted with another host molecule (cyclobis(paraquat-p-phenylene)). The host molecule would interact with the dialkoxynaphthalene moiety as the temperature was raised above the LCST leading a swelling of the hydrogel with a

ratio of 1.6 (***Figure 2.7b***).[105] Sheikos group[106] created an autonomous actuator without any external stimuli. They used a DCN with lightly chemical cross-linking and abundant hydrogen bonding. Through strain-induced and time-dependent reorganization of the reversible hydrogen-bonds, the some gel flowers were designed with shape transformations on timescales from seconds to hours (***Figure 2.7c***).

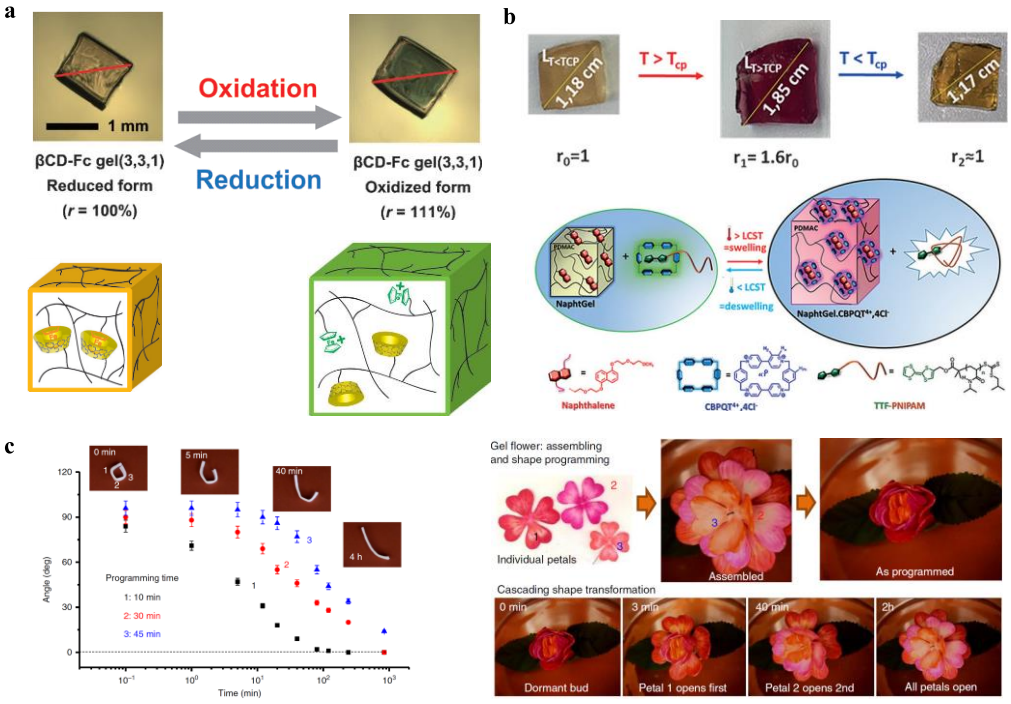

Figure 2.7. Polymer actuators with dually cross-linking supramolecular structures. a) Photographs and Illustration of the βCD-Fc gel(3,3,1) soon after immersion in Tris/HCl buffer with CAN (50 mm) (left) and after one hour (right). Red lines indicate the lengths of gels. Scale bar: 1 mm. Reprinted with permission from[56]. Copyright 2013 Wiley-VCH; b) Illustration of the heating-induced swelling of the three-component supramolecular system based on NaphtGel, TTF-PNIPAM, and $CBPQT^{4+}$. Reprinted from [103]; c) Upper panel: three petal-shape sheets of different sizes are cut from 50:50 MAAc-co-DMAA gel (70 wt% water) and coloured for easy distinction. The petals are then assembled and folded in air for different times (1:1 min; 2:10 min; 3:30 min) to create a dormant 'bud'. Lower panel: sequential 'blooming' after immersing the programmed 'bud' in pH 3 buffer at 22 °C. Reprinted from[106].

Chapter Three: Biomolecule sensor based on azlactone copolymer hydrogel films

3.1 Introduction

Surface plasmon resonance (SPR)-based sensors for the analysis of molecular interactions as a real-time, free label technique has been widely studied. [107,108] Therefore, applications of SPR sensors for detecting analytes related to biomolecular recognition[109,110], medical diagnostics[111], environmental monitoring[112] and food safety[113] have been reported. However, conventional SPR sensors still needs an improvement in stability of immobilized layer, selectivity to target molecules and usability in wide concentration ranges.[108] Later, three dimensional hydrogel binding matrices were developed showing larger binding capacity and lower steric hindrance than that of two dimensional self-assembled monolayers.[114,115] In addition to the surface plasmon, optical waveguide modes occur as the hydrogel layer gets thick enough (> 500 nm).[116] Thus, the combination of SPR with optical waveguide spectroscopy (OWS), utilizing Kretschmann configuration, allows the sensor chip to independently determine layer thickness and refractive index at the same time.[117]

Hydrogels, as a hydrophilic polymer network, received much attention as advanced materials due to their versatile compositions, easy functionalization and superior mechanical properties and responsivities.[11] Photo cross-linkable polymers are considered as good candidates for preparing thin hydrogel layers that could be manufactured with nanometer dimensions.[118] Dimethylmaleimide was reported as a photo cross-linker to build up thin hydrogel layer.[116–118] Furthermore, polymer chains containing reactive moieties, which could be further functionalized or modified with certain molecules, are also important for hydrogel layer as sensor chips.[119] Thus, a general design strategy of a template polymer for constructing a stable gel structure and

improving optical response of the sensing platform is required in order to develop SPR-based sensors.

Herein, it was reported the synthesis of a terpolymer containing *N,N*-dimethyl acrylamide (DMAAm), 2-(dimethylmaleimido)-*N*-ethyl-acrylamide (DMIAAm) and 2-vinyl-4,4-dimethylazlactone (VDMA) as a template for constructing thin hydrogel layers (***Figure 3.1***). The terpolymer was obtained via reversible addition-fragmentation chain transfer (RAFT) polymerization to ensure a relatively uniform terpolymer composition. The azlactone moiety was introduced into the terpolymer due to its reactivity with nucleophiles like hydroxyl, amine and thiol groups under mild conditions.[120–122] Thus, the terpolymer could easily be modified with amino functionalized biotin. On this basis, SPR sensor chips capable of sensing streptavidin (SAV) were developed. Changes in hydrogel layer thickness upon presence of SAV were detected by SPR-OWS measurements.

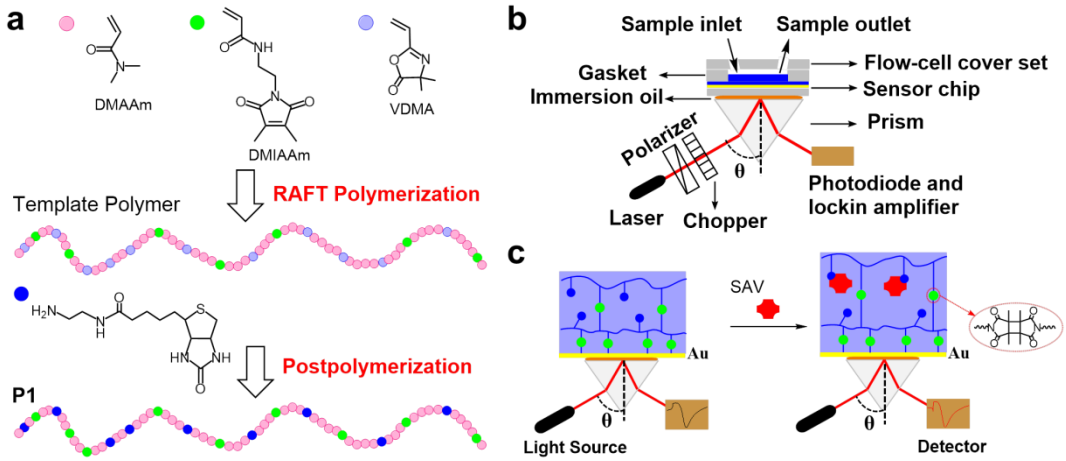

Figure 3.1. a) Design strategy of template copolymer and further post-polymerization with biotin; b) Optical setup of a sensor chip for detection of biomolecules via SPR-OWS; c) Schematic illustration of a thin gel layer responding to streptavidin by changing layer thickness.

3.2 Experimental section

3.2.1 Materials and Instruments

N,N-dimethylacrylamide (> 99.0 %, TCI) was purchased from TCI and distilled

before used. 2,2'-azobis(2-methylpropionitrile) (AIBN) was purchased from Acros Organics and recrystallized from methanol before use. Dialysis membrane for 3.5 kDa molecular weight cut off was obtained from Spectrum (USA). 2-(Dodecylthiocarbonothioylthio)-2-methylpropionic acid (DDMAT) was synthesized according to the literature.[123] The following chemicals were purchased from commercial sources and used as received. 1,2-Diaminoethane (98 %, Acros Organics), 2-Methylalanine (> 98.0 %, TCI), acryloyl chloride (96 %, Alfa Aesar), allylamine (98+ %, Alfa Aesar), biotin (> 98 %, TCI), dimethymaleic anhydride (97 %, Acros Organics), di-*tert*-butyl-dicarbonate (99 %, Acros Organics), ethyl chloroformate (99 %, Fluka), HCl in dioxane (3 M, Alfa Aesar), *N*-(3-dimethylaminopropyl)-*N'*-ethylcarbodiimide hydrochloride (EDC) (> 98.0 %, Sigma Aldrich), *N*-hydroxysuccinimide (NHS) (98.0 %, Sigma Aldrich), *N,N*-diisopropylethylamine (97 %, Alfa Aesar), streptavidin (lyophilized powder, ≥13 units/mg protein, Sigma Aldrich), thioacetic acid (> 97 %, Fluka), triethylamine (TEA) (99 %, Acros Organics). All other normal chemicals and solvents were of analytical grade and were used without further purification.

^{1}H- and ^{13}C-NMR spectra were recorded on a Bruker AV-500 spectrometer (500 MHz for ^{1}H and 125 MHz for ^{13}C), with chemical shifts (δ) reported in ppm relative to the solvent peak (7.26 ppm for $CDCl_3$ and 2.50 ppm for DMSO) and coupling constants (*J*) reported in Hz. High-resolution mass spectra (HRMS) were recorded by electrospray ionization (ESI) on a Waters SYNAPT™ G2 HDMS™. Determination of molar mass distributions was performed by a modular gel permeation chromatography (GPC) system at a flow rate of 1 mL/min with a Knauer Smartline RI Detector 2300 and a Merck Hitachi L-4200 UVVIS Detector. The instrument was equipped with a PSS-SDV 10^5 Å and a PSS-SDV 10^3 Å column and all samples were calibrated by poly(methylmethacrylate) standards. Photo cross-linking process was performed by an OmniCure® S1500 spot UV curing lamp with a 200 Watt Intelli-Lamp.

3.2.2 Synthesis of primary amine modified biotin[124]

Synthesis of tert-Butyl(2-(5-(2-oxohexahydro-1H-thieno[3,4-d]imidazol-4-yl)

pentanamido)ethyl)carbamate (1)

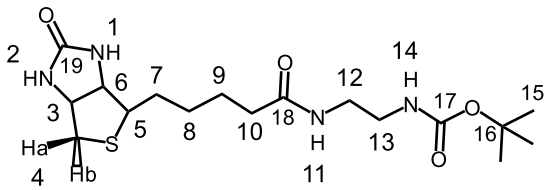

Biotin (1.20 g, 4.92 mmol) and EDC (1.44 g, 7.32 mmol) were mixed and added into a flask followed by adding DMF (10 mL) with stirring under argon atmosphere. After 20 min, NHS (624 mg, 5.2 mmol) was added into the mixture followed by stirring for another 12 h. Then, *tert*-butyl (2-aminoethyl)carbamate (0.80 g, 5.00 mmol) and DIPEA (4.32 mL, 24.00 mmol) were added into the mixture followed by stirring for 4 h at room temperature. After the reaction, the mixture was poured out on 100 mL crushed ice. The solid was obtained after melting the ice and then washed with cooled water yielding the final product as white solid (1.116 g, 2.887 mmol, 58.7 %). ^{1}H NMR (500 MHz, MeOD) δ (ppm) = 4.50 – 4.48 (m, 1H, H3), 4.31 (dd, ^{3}J = 7.9, 4.5 Hz, 1H, H6), 3.26 – 3.20 (m, 3H, H5 and H12), 3.14 (t, ^{3}J = 6.1 Hz, 2H, H13), 2.93 (dd, ^{2}J = 12.7, ^{3}J = 5.0 Hz, 1H, H4a), 2.71 (d, ^{2}J = 12.7 Hz, 1H, H4b), 2.21 (dd, ^{2}J = 10.7 Hz, ^{3}J = 4.5 Hz, 2H, H10), 1.79 – 1.55 (m, 4H, H7 and H9), 1.51 – 1.38 (m, 11H, H8 and H15). ^{13}C NMR (126 MHz, MeOD) δ (ppm) = 173.51 (C19), 163.26 (C18), 155.74 (C17), 77.31 (C16), 60.50 (C3), 58.79 (C6), 54.07 (C5), 38.16 (C12), 37.66 (C13), 33.96 (C4), 26.88 (C10), 26.59 (C9), 25.90 (C8 and C7), 23.89 (C15). HRMS (ESI-TOF: m/z (%)): $[M+Na]^{+}$: Calc. 409.1885, Found 409.1881 (100).

Synthesis of N-(2-Aminoethyl)-5-(2-oxohexahydro-1H-thieno[3,4-d]imidazol-4-yl)pentanamide hydrochloride (2)

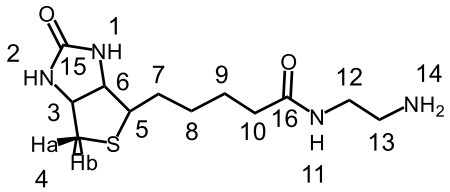

Compound **1** (0.60 g, 1.55 mmol) was added into a flask followed by adding HCl/Dioxane (10 mL, 3 M) under stirring with argon. The mixture was stirred for 2 h at room temperature. After that the solvent was evaporated and the residue was

dissolved in MeOH (5 mL). The solution was precipitated in Et_2O and the solid was collected and washed with Et_2O yielding the final product as light yellow solid (474 mg, 1.47 mmol, 90.3 %). ^{1}H NMR (500 MHz, MeOD) δ (ppm) = 4.63 (dd, ^3J = 7.8, 4.9 Hz, 1H, H3), 4.44 (dd, ^3J = 7.9, 4.4 Hz, 1H, H6), 3.49 – 3.43 (m, 2H, H13), 3.28 (dd, ^3J = 9.0, 4.7 Hz, H5), 3.07 (t, ^3J = 6.0 Hz, 2H, H12), 2.99 (dd, ^2J = 13.0 Hz, ^3J = 4.9 Hz, 1H, H4a), 2.78 (d, ^2J = 12.9 Hz, 1H, H4b), 2.29 (dd, ^2J = 11.0 Hz, ^3J = 4.5 Hz, 2H, H10), 1.82 – 1.54 (m, 4H, H7 and H9), 1.51 – 1.43 (m, 2H, H8). ^{13}C NMR (126 MHz, MeOD) δ (ppm) = 175.96 (C15), 164.42 (C16), 62.88 (C3), 61.31 (C6), 55.42 (C5), 39.54 (C12), 39.29 (C13), 36.82 (C4), 35.13 (C10), 28.35 (C9), 27.99 (C7), 25.03 (C8). HRMS (ESI-TOF: m/z (%)): $[M+H]^+$: Calc. 287.1542, Found 287.1541 (100).

3.2.3 Synthesis of adhesion promotor[125]

Synthesis of 1-Allyl-3,4-dimethyl-1H-pyrrole-2,5-dione (3)

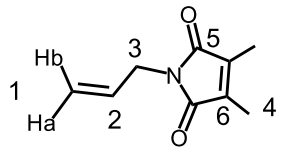

Dimethylmaleic anhydride (5.00 g, 39.70 mmol) was added into a flask followed by addition of toluene (50 mL) and allylamine (14.87 mL, 197.90 mmol) with stirring under argon atmosphere. The mixture was refluxed for 6 h at 130 ºC with a water trap to remove the water. After reaction, the solvent was removed by evaporation and the residue was purified with a short column of silica gel with DCM (30 mL) and EtOAc (100 mL). The solution was concentrated and purified with column chromatography (EtOAc/*n*-hexane = 1/2) to give the final product as a yellow liquid (6.1 g, 37.04 mmol, 93.3%). ^{1}H NMR (500 MHz, $CDCl_3$) δ (ppm) = 5.82 – 5.75 (m, 1H, H2), 5.15 (ddd, ^2J = 28.0 Hz , ^3J = 2.8 Hz, ^4J = 1.5 Hz, 1H, H1a), 5.14 (dd, ^3J = 2.5 Hz , ^4J = 1.2 Hz, 1H, H1b), 4.08 (dt, ^3J = 5.6 Hz, ^4J = 1.5 Hz, 2H, H3), 1.96 (s, 6H, H4). ^{13}C NMR (126 MHz, $CDCl_3$) δ (ppm) = 171.75 (C5), 137.24 (C6), 132.03 (C2), 117.27 (C1), 39.97 (C3), 8.65 (C4).

Synthesis of S-(3-(3,4-Dimethyl-2,5-dioxo-2,5-dihydro-1H-pyrrol-1-yl)propyl) ethanethioate (4)

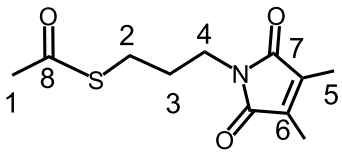

Compound **3** (2.51 g, 15.20 mmol) was added into a flask followed by addition of $CHCl_3$ (15 mL), AIBN (0.15g, 0.91 mmol) and thioacetic acid (1.62 mL, 22.90 mmol) under stirring with argon. The mixture was stirred for 4.5 h at 80 ºC followed by addition of Na_2CO_3 (30 mL) after the mixture cooled to room temperature. The organic phase was collected and the water phase was extracted with petrolether (2 × 45 mL). The organic phase was washed with saturated sodium chloride solution, dried with $MgSO_4$ and concentrated by evaporation. The final compound was obtained via purification with column chromatography (*n*-hexane/EtOAc = 4/1) as a yellow oil (1.02 g, 25.3%). ^{1}H NMR (500 MHz, $CDCl_3$) δ (ppm) = 3.54 (t, ^3J = 6.9 Hz, 2H, H4), 2.83 (t, ^3J = 7.2 Hz, 2H, H2), 2.31 (s, 3H, H1), 1.95 (s, 6H, H5), 1.89 – 1.82 (m, 2H, H3). ^{13}C NMR (126 MHz, $CDCl_3$) δ (ppm) = 195.40 (C8), 172.13 (C7), 137.20 (C6), 36.75 (C4), 30.56 (C2), 28.73 (C3), 26.31 (C1), 8.66 (C5). HRMS (ESI-TOF: *m/z* (%)): $[M+Na]^+$: Calc. 264.0670, Found 264.0675 (97.8).

3.2.4 Synthesis of photo cross-linker[126]

*Synthesis of tert-Butyl (2-aminoethyl)carbamate (**5**)*

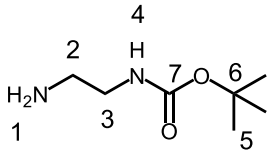

1,2-Diaminoethane (46.465 g, 0.773 mol) was dissolved in dioxane (150 mL) and added into a flask followed by addition of di-*tert*-butyl dicarbonate (21.825 g, 0.100 mol) solution with dioxane (250 mL) dropwise under room temperature within 3 h. After stirring for 48 h at room temperature the mixture was filtered to remove the precipitation and was evaporated to remove the solvent and excess 1,2-diaminoethane. The residue was suspended in water (250 mL) followed by filtration to remove the precipitation. Then sodium chloride was added forming a saturated solution followed by extracting with DCM (5 × 100 mL). The organic phase was dried with $MgSO_4$ and

evaporated to remove the solvent yielding the final product as colorless oil (14.72 g, 0.092 mol, 92 %). ^{1}H NMR (500 MHz, $CDCl_3$) δ (ppm) = 4.97 (s, 1H, H4), 3.17– 3.14 (m, 2H, H3), 2.79 – 2.77 (m, 2H, H2), 1.53 (s, 2H, H1), 1.42 (s, 9H, H5). ^{13}C NMR (126 MHz, $CDCl_3$) δ (ppm) = 156.23 (C7), 79.18 (C6), 43.29 (C3), 41.82 (C2), 28.40 (C5).

*Synthesis of tert-Butyl (2-(3,4-dimethyl-2,5-dioxo-2,5-dihydro-1H-pyrrol-1-yl) ethyl)carbamate (**6**)*

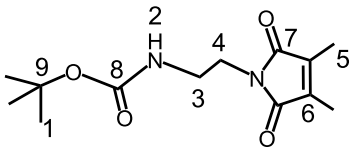

Compound **5** (8.00 g, 0.050 mol) and dimethylmaleic anhydride (6.30 g, 0.050 mol) were added into a flask followed by addition of toluene (300 mL) with stirring under argon atmosphere. The mixture was stirred for 3.5 h with a water trap to remove the water. After that, the precipitation was removed by filtration followed by evaporation to remove the solvent. The residue was resolved in chloroform (50 mL) and precipitated in cooled pentane. The solid was collected and washed with pentane to give the final product as white solid (11.76g, 0.044 mol, 87.9%). ^{1}H NMR (500 MHz, $CDCl_3$) δ (ppm) = 4.79 (s, 1H, H2), 3.61 (dd, ^{3}J = 6.3, 4.9 Hz, 2H, H3), 3.30 (d, ^{3}J = 4.1 Hz, 2H, H4), 1.95 (s, 6H, H5), 1.40 (s, 9H, H1). ^{13}C NMR (126 MHz, $CDCl_3$) δ (ppm) = 172.21 (C7), 155.91 (C8), 137.29 (C6), 79.35 (C9), 39.80 (C4), 37.97 (C3), 28.30 (C5), 8.66 (C1).

*Synthesis of 1-(2-Aminoethyl)-3,4-dimethyl-1H-pyrrole-2,5-dione hydrochloride (**7**)*

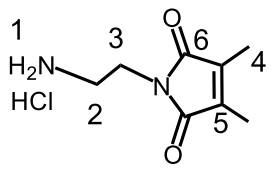

Compound **6** (8.05 g, 0.030 mol) was added into a flask followed by addition of EtOAc (100 mL) and HCl (6.17 mL) with stirring at room temperature. The mixture was stirred overnight, then the solid was collected via filtration and washed with EtOAc to give the final product as white solid (5.567g, 0.027 mol, 89.9%). ^{1}H NMR (500 MHz, DMSO)

δ (ppm) = 8.22 (s, 3H, H1), 3.65 (t, ^{3}J = 6.2 Hz, 2H, H3), 2.94 (m, 2H, H2), 1.90 (s, 6H, H4). ^{13}C NMR (126 MHz, DMSO) δ (ppm) = 172.07 (C6), 137.41 (C5), 37.79 (C3), 35.52 (C2), 8.93 (C4). HRMS (ESI-TOF: *m/z* (%)): $[M+H]^{+}$: Calc. 169.0977, Found 169.0978 (100).

*Synthesis of N-(2-(3,4-Dimethyl-2,5-dioxo-2,5-dihydro-1H-pyrrol-1-yl)ethyl) acrylamide (**8**)*

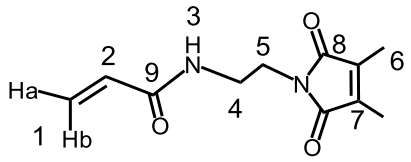

Compound **7** (4.10 g, 0.02 mol) and TEA (11.1 mL) were added into a flask followed by addition of THF (100 mL) with stirring under argon atmosphere. Acryloyl chloride (4.90 mL, 0.06 mol) mixed with THF (20 mL) was added into the flask dropwise under stirring at 0 ºC within 1 h. The mixture was stirred overnight at room temperature followed by filtration to remove the precipitation. After evaporation removing the solvent, chloroform (100 mL) was added to the residue and washed with water (3 × 50 mL), saturated sodium hydrogen carbonate (2 × 50 mL) and diluted hydrochloride acid (0.1 M, 2 × 50 mL). The organic phase was then concentrated and purified by chromatography (EtOAc/*n*-hexane = 2/1) to give the final product as white solid (2.58 g, 9.62 mmol, 48.1 %). ^{1}H NMR (500 MHz, $CDCl_3$) δ (ppm) = 6.21 (dd, ^{2}J = 17.1 Hz, ^{3}J = 1.4 Hz, 2H, H1a and H3), 6.06 (dd, ^{2}J = 17.1 Hz, ^{3}J = 10.3 Hz, 1H, H1b), 5.61 (dd, ^{3}J = 10.3 Hz, ^{3}J = 1.4 Hz, 1H, H2), 3.73 – 3.67 (m, 2H, H4), 3.52 – 3.49 (m, 2H, H5), 1.95 (s, 6H, H6). ^{13}C NMR (126 MHz, $CDCl_3$) δ (ppm) = 172.44 (C8), 165.81 (C9), 137.49 (C7), 130.85 (C2), 126.25 (C1), 39.62 (C5), 37.39 (C4), 8.70 (C6).

3.2.5 Synthesis of 2-Vinyl-4,4-dimethylazlactone (VDMA)[120]

Synthesis of N-Acryloyl-2-methylalanine (9)

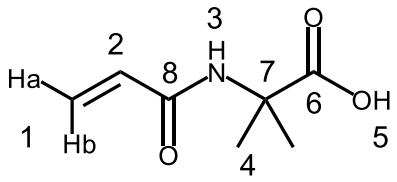

A solution of sodium hydroxide (17.68 g, 0.442 mol) in water (44 mL) was added into a flask at 0 ºC using an ice bath followed by slowly adding 2-methylalanine (20 g, 0.194 mol) and 2,6-di-tert-butyl-p-cresol (BHT) (20 mg, 0.09 mmol). When the solution was clear, acryloyl chloride (18 mL, 0.221 mol) was added dropwise under stirring at 0 ºC. The mixture was stirred for another 4 h at room temperature. Then, concentrated hydrochloric acid (23 mL) was added into the solution slowly and the white solid was obtained during the acidization. The solid was collected by passing the mixture through a filter and was recrystallized from a mixture of ethanol and water (1/1 in volume) to give the final product as a white solid (16.5 g, 0.105 mol, 54.2%). ^{1}H NMR (500 MHz, DMSO-d_6) δ (ppm) = 12.14 (s, 1H, H5), 8.21 (s, 1H, H3), 6.25 (dd, ^{2}J = 17.1 Hz, ^{3}J = 10.2 Hz, 1H, H1a), 6.05 (dd, ^{2}J = 17.1 Hz, ^{3}J = 2.2 Hz, 1H, H1b), 5.56 (dd, ^{3}J = 10.2, 2.2 Hz, 1H, H2), 1.37 (s, 6H, H4). ^{13}C NMR (126 MHz, DMSO d_6) δ (ppm) = 175.79 (C6), 164.29 (C8), 132.12 (C7), 125.65 (C2), 55.30 (C1), 25.38 (C4).

*Synthesis of 2-Vinyl-4,4-dimethylazlactone (**10**)*

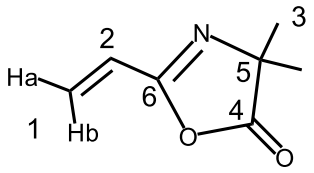

Compound **9** (8.0 g, 50.0 mmol) and TEA (10.4 mL, 75.0 mmol) were added into a flask followed by addition of acetone (150 mL) at 0 ºC using an ice bath. Then ethyl chloroformate (4.9 mL, 50.0 mmol) was added dropwise into the mixture within 1 h. The solution was stirred for another 3 h at 0 ºC. After that, the mixture was passed through a filter and washed with acetone to remove the precipitation. The solvent was then removed by evaporation and the filtrate residue was distilled under vacuum (4.5 × 10^{-2} mbar, 32 ºC) to give the final product as a colorless liquid (4.66 g, 33.5 mmol, 67.0 %). ^{1}H NMR (500 MHz, $CDCl_3$ d_1) δ (ppm) = 6.24 (dd, ^{2}J = 17.6 Hz, ^{3}J = 10.3

Hz, 1H, H1a), 6.17 (dd, ^{2}J = 17.6 Hz, ^{3}J = 1.7 Hz, 1H, H1b), 5.87 (dd, ^{3}J = 10.3, 1.7 Hz, 1H, H2), 1.40 (s, 6H, H3). ^{13}C NMR (126 MHz, $CDCl_3$) δ (ppm) = 180.52 (C4), 158.93 (C6), 128.77 (C2), 123.92 (C1), 65.62 (C5), 24.52 (C3). HRMS (ESI-TOF: *m/z* (%)): $[M+OH]^-$: Calc. 156.0661, Found 156.0659 (100).

3.2.6 Copolymerization of template copolymer P(DMAAm-*co*-DMIAAm-*co*-VDMA)

DMAAm (3.60 g, 36 mmol), DMIAAm (0.46 g, 2 mmol) and VDMA (0.29 g, 2 mmol) were added into a flask followed by addition of 2-(dodecylthiocarbonothioylthio)-2-methylpropionic acid (17.3 mg, 0.05 mmol), AIBN (3.9 mg, 0.025 mmol) and dioxane (13.3 mL). The mixture was treated with argon at room temperature for 30 min and then put into an oil bath at 70 ºC for 12 h under stirring. After cooling to room temperature, the mixture was precipitated into cooled diethyl ether (-35 ℃) yielding the polymer. Precipitation was repeated twice to obtain the final product as light yellow solid (3.02 g, 69.4 %). The product was characterized with ^{1}H NMR and GPC to obtain the composition and molar mass distribution of the terpolymer (to see ***Figure 3.3***).

3.2.7 Post-polymerization with biotin (P1)

Terpolymer (300 mg) and compound **2** (60 mg, 0.19 mmol) were added into a flask followed by addition of a mixture of DMF/DMSO (5 mL, V:V = 1:1) and TEA (50 µL). The mixture was stirred for 12 h at room temperature followed by precipitation in cooled diethyl ether (-35 ℃). After that, the solid was dissolved in water (20 mL), dialyzed in water for 48 h and freeze dried to give the final product as a white solid (290 mg, 80 %). The functional copolymer **P1** was analyzed by ^{1}H NMR to confirm its composition (to see ***Figure 3.5***).

3.2.8. Determination of layer thickness of SN supramolecular gel with SPR measurements

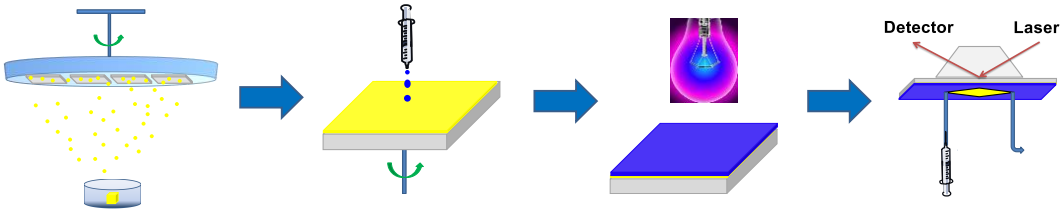

Gold layer on quartz substrate by PVD:

A size with 2.5 cm × 2.5 cm of quartz (LaSFN9) was selected as the substrate to prepare the gold surface. Before the quartz was treated with PVD, they should be carefully washed. There were two methods to cleaning the surface of quartz depending on the state of the surface. If the quartz was reused from an old one, they should be cleaned with Piranha solution firstly followed by normal process of cleaning. If the quartz was new, then they just need the normal process of cleaning method as shown below.

Normal process of cleaning quartz surface:

1) ultrasonic cleaning at 55 ºC for 15 min in water solution with 2 % of Hellmanex™ III;

2) the quartz was washed with distilled water followed by ultrasonic cleaning at 55 ºC for 15 min in triple distilled water for 2 times;

3) the quartz was washed with ethanol followed by ultrasonic cleaning at 55 ºC for 15 min in ethanol for 2 times;

4) the quartz was washed with absolute ethanol, dried with a gas gun.

The layer was then treated with PVD for deposing a gold surface with around 50 nm layer thickness. This process was started when the vacuum was under 10^{-5} mbar and was stopped when the monitor has shown a layer thickness at 70 nm. The last, SPR measurement was used to check the layer thickness of the gold layer.

Spin coating of polymer layer on gold surface

Preparation of gold surface:

The gold surface was treated with ethanol solution of adhesion promotor, which can act as an anchor to connect gold surface with dually cross-linked supramolecular gel. The concentration of adhesion promotor was 5 mM (1.2 mg/mL). The gold substrate was submerged in adhesion promotor solution for 12 h followed by washing with ethanol and dried with a gas gun.

Preparation of polymer solution:

Since the viscosity of the polymer solution has great influence in the layer thickness of polymer layers, concentration of polymer and type of solvent were selected carefully. For P(DMAAm-*co*-DMIAAm-*co*-VDMA) methanol found to be a good solvent to dissolve the copolymer. Different concentrations of polymer were checked using the same spin coating method. 10 mg/mL was found the superior concentration for the formation of polymer layers thinner than 100 nm in dry state. The polymer solution was stirred for 12 h at room temperature to ensure a complete dissolution of the polymer. After that, the solution was passed through a filter (0.45 μm) before spin coating.

Parameter setting of the spin coater:

Parameters of spin coater could influence in the quality of polymer layer, like homogeniety and layer thickness. Considering of the properties of solvents used here, the recipe of the spin coater was set as: 1) 250 rmp for 25 S; 2) 2500 rmp for 70 S; 3) 0 rmp for 2 S.

Photo cross-linking of dually cross-linked supramolecular gel

After the polymer layer was spin coated, the slice was dried overnight at room temperature in the dark. Then they were prepared to photo cross-link by using a UV-Vis lamp. Parameters of the UV-Vis lamp were shown as below. The distance between lamp and sample was 8 cm; the light intensity on the sample was 252 mW/cm^2 (43 % of the intensity from the monitor); irradiation time of the sample was 65 S.

Layer thickness detection by SPR/OWS

SPR/OWS spectra were recorded in the Kretschmann configuration with a customized setup from Max Planck Institute for Polymer Research (Mainz, Germany).

The SPR/OWS sensor was implemented by using the optical setup described in ***Figure 3.2***. Briefly, monochromatic light (He/Ne laser, λ= 632.8 nm, Uniphase) was passed through polarizers (Glan-Thompson polarizer, B. Halle) to obtain linear and transverse magnetic (TM, p) polarization and was reached to a high refractive index prism (LASFN9, refractive index n_p= 1.8449). The sensor chip was covered by a flow cell through a rubber gasket, which selected an area around 1 cm^2 from the sensor chip as the efficient area for the next responsive measurement. The prism moiety and the sensor chip were connected by using an immersion oil (Cargille Lab., USA, refractive index $n_D^{25°C}$ = 1.8000 ± 0.005), which has the similar refractive index as the prism. Then, this pack was mounted on a rotation stage (2-circle 414 with the precision 10^{-2} deg, Huber AG, Germany) to control the angle of incidence from the laser beam θ. The reflected intensity of the laser beam was measured by using a photodiode connected to a lock-in amplifier (7265 DSP Lock-in amplifier, Signal Recovery, USA, integration time 3 s).

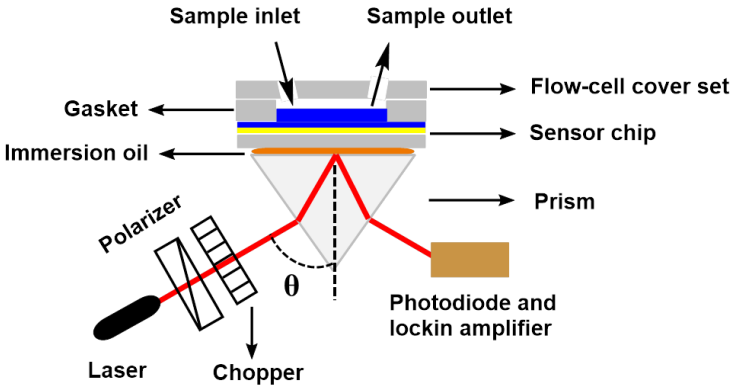

Figure 3.2. The scheme of optical setup and sensor chip for the excitation of optical waveguide (OW) and surface plasmon (SP).

The excitation of SP/OW modes from the laser beam hitting the gold layer and causing resonance with surface plasmons of the gold layer was observed from angular dependent reflectivity spectra R(θ). The modes were manifested as two distinct dips that changes with layer thickness (d_h) and refractive index (n_h), respectively. In order to determine the d_h and n_h, the angular reflectivity spectrum exhibiting SP and OW resonance dips was fitted by transfer matrix-based model through a software Winspall (MPI polymer research in Mainz, Germany).

3.3 Results and discussion

A terpolymer P(DMAAm-*co*-DMIAAm-*co*-VDMA) containing photo cross-linkable DMIAAm and azlactone moieties represents a suitable candidate for preparing polymeric sensitive hydrogels. The template polymer was prepared by RAFT polymerization in dioxane using AIBN as the initiator at 70 °C (***Scheme 3.1***). The functional copolymer **P1** was obtained by the ring-opening addition of the primary amine group of modified biotin (**2**) to the reactive, azlactone-functionalized template terpolymer. The azlactone group can easily be modified with amine or hydroxyl groups that makes the template terpolymer multifarious. Also, the photo cross-linker DMIAAm could form covalent bonds via UV-Vis irradiation, which has advantages in processing and shaping.

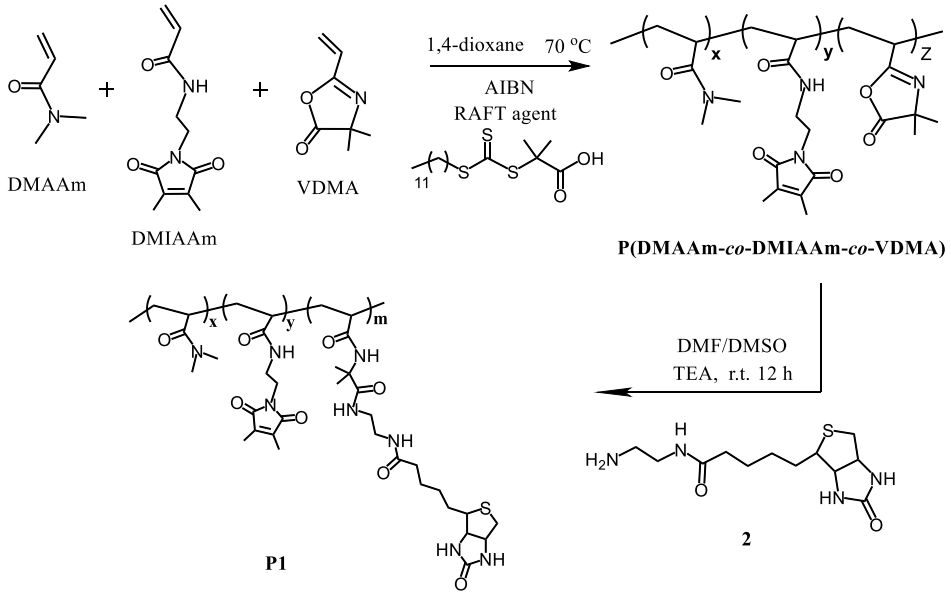

Scheme 3.1. Synthesis of a template terpolymer and the polymer analogous modification with an amino bearing biotin derivative.

In order to investigate the reactivity of the monomers DMAAm, DMIAAm and VDMA, copolymerization of these monomers was conducted in a NMR tube at 70 °C with the dioxane-d_8 as a solvent. The copolymerization was monitored in real-time by ^{1}H NMR spectroscopy. In the ^{1}H NMR spectra, signals for all of the three monomers

and repeating units could be assigned (***Figure 3.3***). Thus, the monomer compositions, terpolymer compositions and monomer conversions could be calculated for all of the monomers throughout the reaction (***Table 3.1***). After graphing the data (***Figure 3.4***), it is shown that the monomer VDMA shows the highest reactivity since its sharpest conversion curve, lower monomer composition than initial value and higher polymer composition than the ideal value. The monomer DMIAAm was slower incorporated into the polymer than VDMA and DMAAm. Anyway, the ternary copolymerization process could be operated in one pot reaction using the RAFT method to ensure a relative uniform copolymer composition in each polymer chain. The copolymerization was carried out on large scale with the same conditions as in the kinetic measurement. After copolymerization for 4 h, the overall conversion reached 63.7 % and the number average molecular weight was determined to be 12300 g/mol with a dispersity $Đ_M$ of 1.32 (***Table 3.2***). However, the number average molecular weight was lower than theoretically expected. Therefore, copolymerization at higher monomer-to-CTA-ratios was carried out. As expected, the number average molecular weight increased for higher monomer-to-CTA-ratios. But, the dispersity of the terpolymer also increased due to extension of the reaction time. Further, increasing the monomer-to-CTA-ratio to 1000/1, the polymerization, unfortunately, led to cross-linked polymer after copolymerization for 12 h.

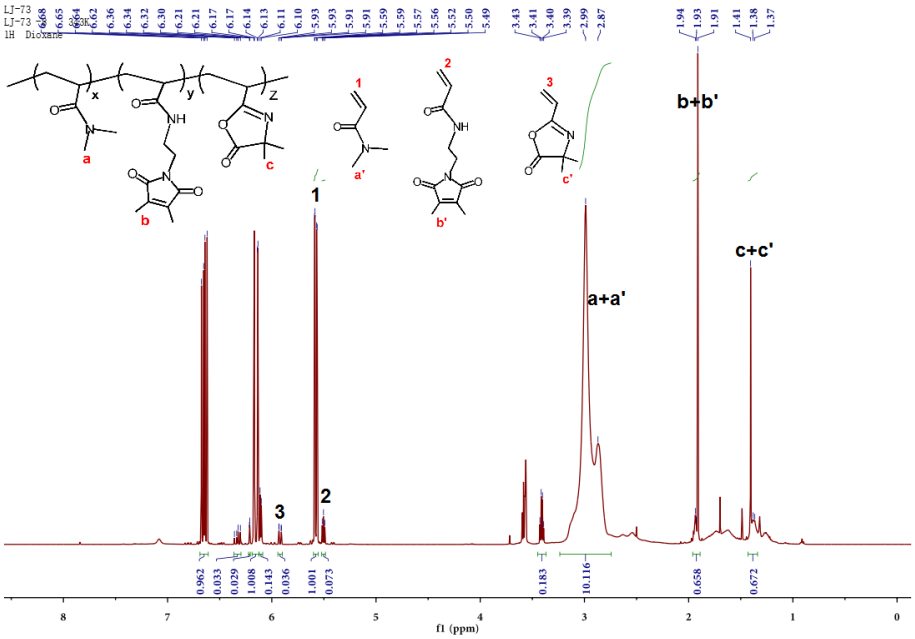

Figure 3.3. ^{1}H NMR spectrum of P(DMAAm-co-DMIAAm-co-VDMA) in dioxane-d_8 after reaction for 70 min.

Table 3.1. Kinetics of ternary copolymerization of DMAAm (M1), DMIAAm (M2) and VDMA (M3) with an initial monomer ratio of [M1]/[M2]/[M3] = 90/5/5 in dioxane-d_8 at 70 °C monitored by ^{1}H NMR spectroscopy.

Time (min)	**$[M_1]/[M_2]/[M_3]$**	**Composition $[P_1]/[P_2]/[P_3]$**	**Conversion M_1 (%)**	**Conversion M_2 (%)**	**Conversion M_3 (%)**
0	1/0.058/0.061	-	-	-	-
10	1/0.061/0.061	1/0.067/0.150	2.2	2.4	5.2
20	1/0.063/0.061	1/0.046/0.141	6.9	5.3	15.5
30	1/0.065/0.057	1/0.042/0.107	11.7	8.0	19.5
40	1/0.067/0.054	1/0.044/0.108	17.6	12.4	30.0
50	1/0.068/0.049	1/0.046/0.112	23.8	17.6	41.8
60	1/0.069/0.043	1/0.052/0.117	29.9	24.5	53.8
70	1/0.071/0.040	1/0.052/0.114	35.1	28.6	60.7
80	1/0.073/0.036	1/0.053/0.111	40.7	33.4	67.9
90	1/0.074/0.033	1/0.053/0.107	44.7	36.7	72.3
100	1/0.076/0.030	1/0.052/0.103	48.8	39.3	76.6
110	1/0.080/0.029	1/0.051/0.098	52.9	41.5	79.1
120	1/0.080/0.025	1/0.052/0.096	56.7	46.1	83.6
130	1/0.080/0.022	1/0.052/0.096	60.1	50.3	86.6

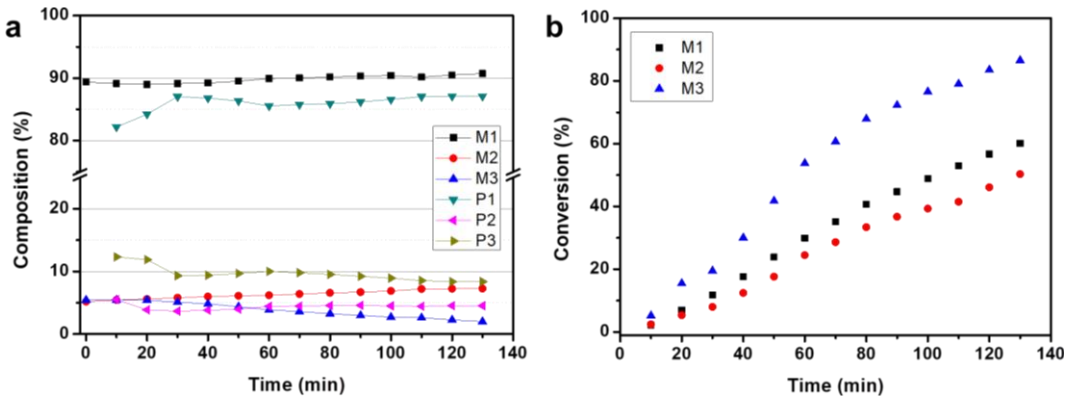

Figure 3.4. Kinetics of ternary copolymerization of DMAAm (M1), DMIAAm (M2) and VDMA (M3) with an initial monomer ratio of [M1]/[M2]/[M3] = 90/5/5 in dioxane-d_8 at 70 °C monitored by ^{1}H NMR spectroscopy. a) monomer and terpolymer compositions and b) monomer conversions against reaction time.

Table 3.2. Parameters of P(DMAAm-*co*-DMIAAm-*co*-VDMA) in copolymerization of DMAAm (M1), DMIAAm (M2) and VDMA (M3) with a monomer ratio of [M1]/[M2]/[M3] = 90/5/5 in dioxane at 70 °C.

P(DMAAm-*co*-DMIAAm-*co*-VDMA)	[M]/[CTA]/ [AIBN]	t (h)	Overall Conv.[b] (%)	M_n [a] (g/mol)	$Đ_M$ [a]	$[P_1]/[P_2]/[P_3]$[b] (%)
1	300/1/0.5	4	63.7	12300	1.32	85.2/5.1/9.7
2	800/1/0.5	6	45.1	25100	1.86	86.1/4.2/9.7
3	800/1/0.5	12	79.1	51100	2.53	86.8/4.5/8.7
4	1000/1/0.5	12	Gelation			

[a] Determined by SEC (THF) using PMMA standards. [b] Determined using ^{1}H NMR spectroscopy.

The photo cross-linker is considered to be the reason leading to cross-linking and gelation. So, bipolymerization of DMAAm and DMIAAm as well as DMAAm and VDMA was carried out to check the cross-linking behavior. After reaction for 19 h, P(DMAAm-*co*-DMIAAm) was cross-linked while P(DMAAm-*co*-VDMA) was not. Also, the number average molecular weight of P(DMAAm-*co*-VDMA) was 42300 g/mol with a dispersity of 1.59. This result suggested that P(DMAAm-*co*-VDMA) was obtained under well controlled copolymerization conditions even with longer reaction time. DMIAAm moieties tend to cross-link at longer polymerization time and high

conversions. Previous studies have shown that dimethyl maleinimide groups are able to take over the radical during free radical polymerization.[127] Due to the sterical hindrance of two methyl groups as well as low conversion in the polymerization, no cross-linking behavior was observed.[116,128] Here, however, the content of monomer was low after a longer reaction time. Also, the viscosity of the reaction system was high as the polymerization reached high conversion. These conditions would synergistically promote cross-linking of the DMIAAm groups via two radicals coupling. Terpolymer **3** showing the highest number average molar mass was used for further post-polymerization and functionalization with amino-modified biotin.

The biomolecular recognition pair of biotin and streptavidin is the most widely investigated noncovalent binding system due to its very strong binding affinity (K_a ~ 10^{13} M^{-1}).[129] Herein, this molecular recognition was used to verify the responsive behavior of the thin hydrogel film. Therefore, the amino-modified biotin derivative was attached to the terpolymer by reacting with the azlactone groups as shown in ***Scheme 3.1***. The success of biotin attachment was proven by ^{1}H NMR spectroscopy as shown in ***Figure 3.5***. 72.8 % of the available azlactone groups were modified with biotin with a total composition of 6.3% in **P1**.

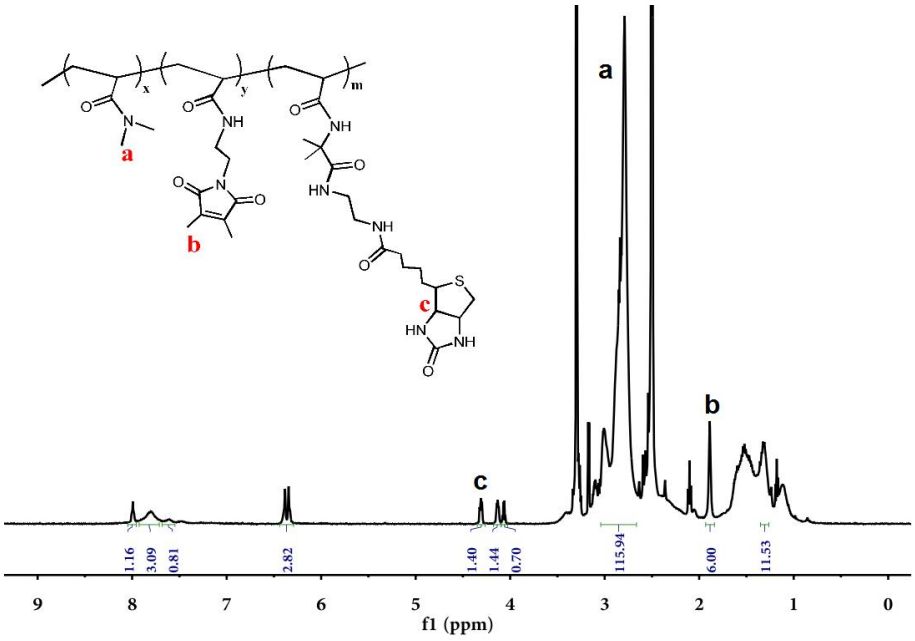

Figure 3.5. ^{1}H-NMR spectrum of **P1** in DMSO-d_6.

In the next step, the modified terpolymer **P1** was spin-coated onto a gold surface

containing an adhesion promotor based on 2,3-dimethyl-maleimide. The resulting thin polymer film was photo cross-linked and covalently bound to the gold surface to build the sensor chip. An optical setup utilizing attenuated total reflection (ATR) method with the Kretschmann configuration was used as shown in ***Figure 3.1***. The thin gel layer was investigated by SPR-OWS in different states as shown in ***Figure 3.6a***. By fitting the two distinct resonances at θ_{OW} and θ_{SP} being associated with the excitation of OW and SP modes, respectively, the layer thickness d_n and the refractive index n_h of the gel were determined independently (***Table 3.3***). After swelling in water, the corresponding layer thickness of the swollen hydrogel was 830 nm with a swelling ratio of 11.9. A highly swellable hydrogel layer was formed enabling the diffusion of target molecules into the polymer network. When the hydrogel was treated with SAV solution, the layer thickness of the hydrogel significantly increased to 1292 nm and the refractive index slightly decreased to 1.3476. The target molecule entered into the hydrogel system via diffusion and permeation then followed by interaction with the functional molecules in the hydrogel.[130] Since the molecular weight of SAV is large (52.8 kDa) and SAV has an isoelectric point around pH 5-6,[131] the network in the gel would swell as SAV diffused into the gel layer and bind to biotin. The binding of SAV to the network chains increased the driving force for water uptake by electrostatic repulsion. Therefore, the layer thickness of the gel was increasing. Due to the size of SAV, a gradient distribution along the layer thickness direction was developed. The refractive index of the hydrogel layer was almost not changed during the absorption process. SAV was not present in the bottom ~ 200 nm. This is the approximate depth that evanescent θ_{SP} field of the plasma mode can penetrate the hydrogel layer. The SAV bonding to biotin on the top of the hydrogel layer could fill the passageway and prevent the diffusion of the SAV to the bottom of the hydrogel layer. Above all, the SAV as the target molecule could interact with biotin in the hydrogel system, thereby increasing layer thickness. This change in hydrogel dimension could be read out by SPR-OWS resulting in an SAV sensor.

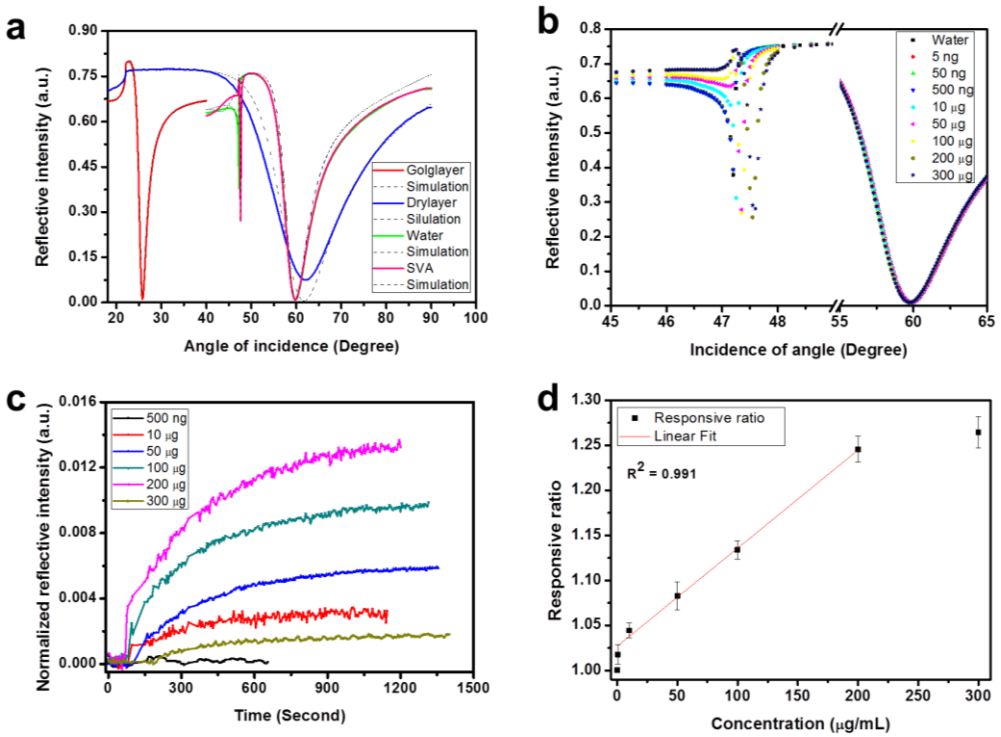

Figure 3.6. SPR-OWS measurements of SAV sensitive hydrogel film. a) representative SPR-OWS curves for the gold layer, hydrogel layer in dry state, hydrogel layer in swollen state and hydrogel layer in responsive state with streptavidin, respectively; b) concentration dependent measurements of hydrogel dimension against diverse amount of SAV, angle of incidence breaks from 49° to 55°; c) kinetics of reflectivity changes after injecting different concentrations of streptavidin solutions at a certain incidence angle of 47.5°; d) plot of responsive ratio against concentration of streptavidin based on the layer thickness from simulated parameters of SPR-OWS and their linear fitting. Indicated error bars represent the standard deviation for samples measured in triplicate, line shows a linear fit with r-square (COD) value of 0.99.

For investigation of the detection range and sensitivity of the sensor chip, SPR-OWS measurements at diverse amounts of SAV were carried out (***Figure 3.6b***). The dip below the critical angle ($\theta < \theta_c$), associated with the OW mode, gradually increased with increasing SAV concentration. But, the total reflection point was almost not changed with increasing SAV concentration. This indicated that the layer thickness (d_h) of the thin gel layer increased upon addition of SAV while the refractive index n_h remained constant. Swelling kinetics of hydrogels were studied by measuring the

reflectivity variations at a certain incidence angle of 47.5°, in which the reflection curve shows a sharp dip. As shown in ***Figure 3.6c***, the target molecule SAV diffused into the hydrogel and interacted with biotin within 20 minutes. This slow response time can be attributed to the large molecular size of SAV as well as a gradient diffusion along the layer thickness direction. It shows, nevertheless, the target molecule triggered hydrogel swelling in a certain concentration range. Taking the layer thickness of the hydrogel in water (d_w) as a standard, the responsive ratio was carried out by ds/d_w where the d_s is the layer thickness of the hydrogel in SAV solution. Plotting the concentration dependent responsive ratio (***Figure 3.6d***), which is based on the responsive layer thickness against concentration of SAV, a linear correlation of the responsive ratio data points (r-square value of 0.99). These results show a linear sensor range for SAV concentrations between 0.5 and 200 μg/mL. Thus, it allows the sensor chip reliable detection and quantification of SAV.

Table 3.3. Characteristics of the hydrogel film in different states. The SAV concentration was 50 μM.

Materials	**Layer Thickness d_n (nm)**	**Refractive Index n_h**
Gold layer	45	-3.374
Dried Hydrogel	70	1.6045
Hydrogel swelling in water	830	1.3480
Hydrogel swelling in SAV solution	1292	1.3476

3.4 Conclusions

It was reported the successful implementation of a plasmonic biosensor for the analysis of SAV using a biotin-modified hydrogel system. In a first step, a template terpolymer P(DMAAm-*co*-DMIAAm-*co*-VDMA) was synthesized by RAFT polymerization and subsequently modified with an amine group bearing biotin derivative via ring opening of the azlactone moieties in the terpolymer. Upon UV irradiation, the modified terpolymer formed a hydrogel film via photo cross-linking of

the 2,3-dimethylmaleimde groups in the polymer. Changes of hydrogel layer thickness achieved via exposure of the sensor chip to SAV were monitored by using SPR-OWS measurements. The biosensor showed an excellent concentration dependent linear detection range for SAV concentration between 0.5 μM and 200 μM. It was demonstrated that the hydrogel can be used as a binding matrix for biomolecules that can diffuse and selectively bind to the immobilized docking molecules. It is envisioned that the achieved results will pave the way to a new class of biosensor technologies which take advantage of the analysis of target molecules in a large concentration range.

Chapter Four: Dually cross-linked supramolecular hydrogel as SPR sensor for small molecules detection

4.1 Introduction

Surface plasmon resonance (SPR) measurements have been demonstrated as a useful tool in molecular sensing especially for biomolecule detection as it shows high sensitivity to target molecules.[132,133] An extension of SPR, called localized plasmon resonance, is achieved by using metallic nanostructures with advanced microfabrication and nanofabrication, which can enhance the sensitivity of target molecules with relatively large molecular weight.[134] However, the SPR based approaches still need an improvement in sensitivity for the detection of small molecules (< 500 Da), which could have large impact in fields like biomedicine, pharmacology and diagnostics.[108,135] Ultimately, the small molecule with lower polarizability decreased the resonance of the sensor, which would be limited without amplifying or transforming the signal of targeting process.[136] Moreover, the SPR based approach also generally suffer from nonspecific binding, which has impeded further application in proteomics and disease diagnostics, especially for the detection of complex biological samples.[137] Therefore, a new design strategy with SPR based approach for small molecule detection would significantly expand the range of applications.

Hydrogels with responding to external stimuli and exhibiting “smart” characteristics have achieved much progress in both mechanical performances[47,48,138] and biological applications[24,90]. Among them, dually cross-linked supramolecular hydrogel (**DCSH**) was mostly considered to construct advanced hydrogel with combination of covalent bonding and noncovalent bonding.[88,139] Based on specific noncovalent interactions of the **DCSH** including hydrogen bonding,[140] host-guest interaction,[32] metal coordination,[141] small molecular sensors were developed by

volume expansion or shrinking.[55] The **DCSH** can response to target small molecules meanwhile remaining their original structure or mechanical properties.[142] However, this responsive behavior mostly occurred in three dimensions causing technical difficulties for quantitative detection of target small molecules.

Recently, SPR combined with optical waveguide spectroscopy (SPR-OWS) was developed to characterize hydrogel layers (> 500 nm), in which the layer thickness and refractive index can be determined independently.[114,116,143,144] The SPR-OWS could be able to monitor responsive behavior of **DCSH** in one dimension by fixing other two directions with a surface attachment.[116]

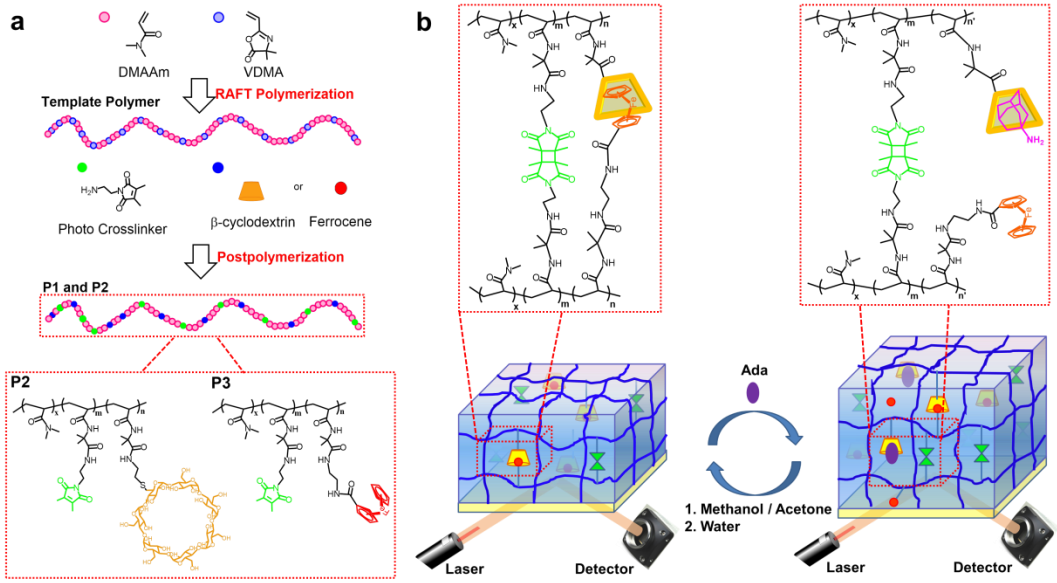

Figure 4.1. a) Schematic illustration of the synthesis of dually cross-linked supramolecular hydrogel based on azlactone template copolymer and chemical structures of **P2** and **P3**; b) Sketch of swelling behavior caused by target molecule Ada using a SPR-OWS measurement.

Herein, a **DCSH** capable of undergoing selective swelling in response to target small molecules with SPR-OWS measurements (***Figure 4.1***) was developed that was based on a new concept of competitive guest molecule interaction. The **DCSH** was constructed by simultaneously introducing host-guest interaction pairs of β-cyclodextrin (β-CD) and ferrocene (Fc), and photo cross-linker 2-

(dimethylmaleimido)-*N*-ethylamine (DMIEA). A target small molecule, in this case adamantane (Ada)[59], acted as a competitive guest molecule to break the host-guest interaction between β-CD and Fc, in which the signal of the targeting process was amplified by selective swelling of the **DCSH** resulting in decreasing the refractive index and increasing the layer thickness. The target small molecules only showing higher bonding affinity than the initial guest molecule in **DCSH** could trigger the competitive interaction that largely avoid nonspecific adsorption. This research provides a new strategy to construct **DCSH** from simply modified template copolymer and to develop a sensor for target small molecules detection via SPR-OWS measurements.

4.2 Experimental section

4.2.1 Reagents and Instruments

N,N-Dimethylacrylamide (> 99.0 %, TCI) was vacuum distillation before used. The following chemicals were purchased from commercial sources and used as received. 2,2'-Azobis(2-methylpropionitrile) (AIBN) was purchased from Acros Organics and recrystallized from methanol before use. Dialysis membrane for 3.5 kDa molecular weight cut off was obtained from Spectrum (USA). 2-(dodecylthiocarbonothioylthio)-2-methylpropionic acid (DDMAT) was synthesized according to the literature.[123] 1,2-diaminoethane (98 %, Acros Organics), 1-adamantanamine (98 %, Alfa Aesar), 1-hydroxybenzotriazole hydrate (HOBt) (> 97.0 %, Sigma Aldrich), 2,6-di-tert-butyl-p-cresol (BHT) (> 99 %, Fluka), 2-aminoethanethiol hydrochloride (> 95.0 %, TCI), 2-methylalanine (> 98.0 %, TCI), acryloyl chloride (96 %, Alfa Aesar), allylamine (98+ %, Alfa Aesar), dimethymaleic anhydride (97 %, Acros Organics), di-*tert*-butyl-dicarbonate (99 %, Acros Organics), ethyl chloroformate (99 %, Fluka), ferrocene carboxylic acid (98 %, Alfa Aesar), *N*-(3-Dimethylaminopropyl)-*N'*-ethylcarbodiimide hydrochloride (EDC) (> 98.0 %, Sigma Aldrich), *N,N*-diisopropylethylamine (97 %, Alfa Aesar), thioacetic acid (> 97 %, Fluka), tosylchloride (98 %, Alfa Aesar), triethylamine (TEA) (99 %, Acros Organics), trifluoroacetic acid (>99.0 %, TCI). All

other normal chemicals and solvents were of analytical grade and were used without further purification.

^{1}H and ^{13}C NMR spectra were recorded on a Bruker AV-500 spectrometer (500 MHz for ^{1}H and 125 MHz for ^{13}C), with chemical shifts (δ) reported in ppm relative to solvent peak (7.26 ppm for $CDCl_3$ and 2.50 ppm for DMSO) standards and coupling constants (*J*) reported in Hz. High-resolution mass spectra (HRMS) were recorded by electrospray ionization (ESI) on a Waters SYNAPT™ G2 HDMS™ mass spectra. The molar masses and molar mass distribution (M_w/M_n) were performed on a gel permeation chromatography (GPC) at a flow rate of 1 mL/min on a Merck Hitachi 655A-11 Liquid Chromatograph connected to a Knauer Smartline RI Detector 2300 and a Merck Hitachi L-4200 UVVIS Detector. The instrument was equipped with a PSS-GRAM 10^3 Å and PSS-GRAM 10^2 Å column and all samples were calibrated by poly(methylmethacrylate) standards. Supramolecular polymer size was carried out on a dynamic light scattering (DLS) apparatus of Malvern Nano-ZS at an angle of incidence of 15°. Photo cross-linking process was performed by an OmniCure® S1500 spot UV curing lamp with a 200 Watt Intelli-Lamp.

4.2.2 Synthesis of 2-Vinyl-4,4-dimethylazlactone (VDMA)

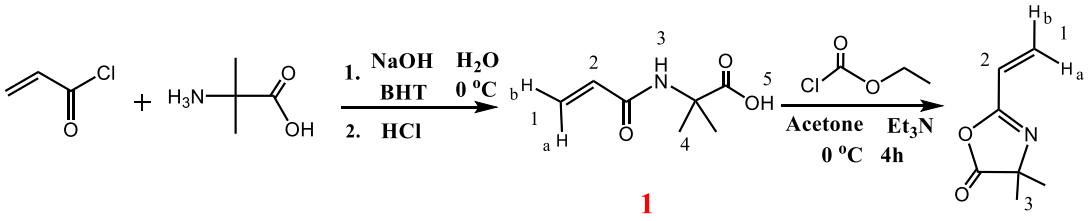

1 **2**

See 3.2.5

4.2.3 Synthesis of additional promotor and photo cross-linker

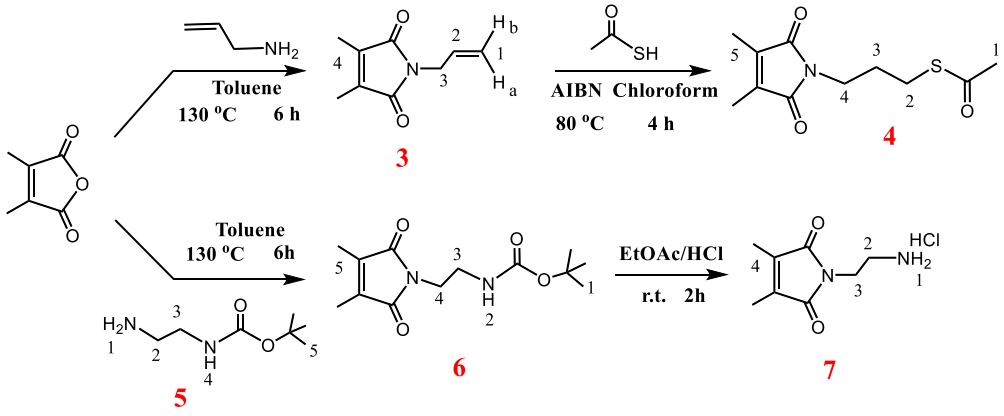

See 3.2.3 and 3.2.4

4.2.4 Synthesis of primary amine modified cyclodextrin[145,146]

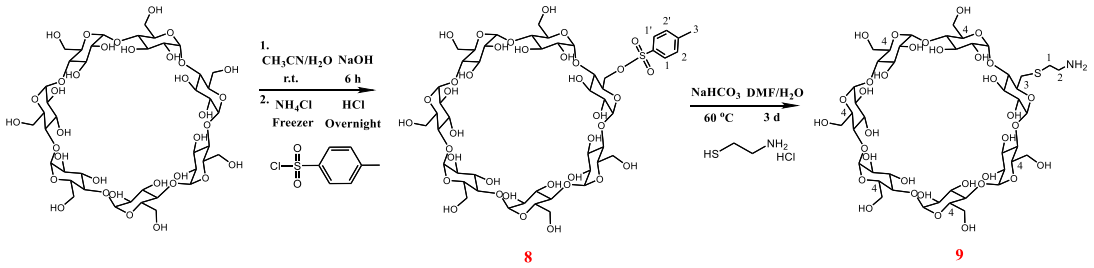

Synthesis of Mono- [6-deoxy-6-(p-toluol-sulfonyl)]-β-cyclodextrin (8):

To a flask β-CD (40.24 g, 35.24 mmol) was suspended in water (1 L) with stirring. Tosyl chloride (10.48 g, 54.52 mmol) was dissolved in acetonitrile (30 mL) and added into the suspension dropwise within 40 min. The mixture was stirred for another 6 h at room temperature followed by addition of NaOH solution (160 mL, 2.5 M) within 10 min. Then, the mixture was passed through the filter to remove the solid. After that, NH_4Cl (39.44 g) and HCl (15 mL, 10 %) were added into the solution to neutralization. A white solid was obtained after keeping the mixture in freezer overnight. The solid was collected and recrystallized from water for 3 times to give final product **8** as a white solid (8.39 g 18.3 %). ^{1}H NMR (500 MHz, DMSO) δ (ppm) = 7.76 (d, ^3J = 7.9 Hz, 2H, 1 and 1'), 7.44 (d, ^3J = 8.0 Hz, 2H, 2 and 2'), 5.85 – 5.59 (m, 14H), 4.81 (s, 7H), 4.54 – 4.29 (m, 7H), 4.26 – 4.14 (m, 1H), 3.59 (m, 26H), 3.44-3.38 (m, 5H), 3.24 (m, 3H),

2.44 (m, 3H, 3). ^{13}C NMR (126 MHz, DMSO) δ (ppm) = 145.25, 133.20, 130.35, 128.04, 102.73, 102.41, 101.78, 82.04, 81.70, 81.30, 73.83 – 73.05, 72.90, 72.51, 70.17, 69.39, 60.36, 59.91, 21.66. HRMS (ESI-TOF: *m/z* (%)): $[M+Na]^+$: Calc. 1311.3684, Found 1311.3668 (100).

Synthesis of Mono-[6-deoxy-6-(2-aminoethylsulfanyl)]-β-cyclodextrin (9):

Compound **8** (3.87 g, 3 mmol) and NH_4HCO_3 (8.31 g, 105 mmol) were added into a flask followed by addition of DMF/H_2O (60 mL, 1/3 in volume) with stirring under argon atmosphere. Then 2-aminoethanthiol hydrochloride (3.06 g, 27 mmol) was added at room temperature and reacted at 60 °C for 3 d. After that, the mixture was precipitated in acetone. The solid was dissolved in DMF/H_2O mixture and reprecipitated in acetone to give the final product **9** as a white solid (3.45 g, 96.2 %). ^{1}H NMR (500 MHz, D_2O) δ (ppm) = 5.11 (s, 1H, 3), 5.05 (s, 6H, 4), 4.08 – 3.77 (m, 26H), 3.70 – 3.48 (m, 14H), 3.21 (t, ^2J = 6.4 Hz, 2H, 1), 2.92 (t, ^2J = 6.5 Hz, 2H, 2). ^{13}C NMR (126 MHz, D_2O) δ (ppm) = 101.89, 101.56, 84.01, 81.22, 73.16, 72.94, 72.00, 71.17, 60.49, 39.41, 37.46, 36.95. HRMS (ESI-TOF: *m/z* (%)): $[M+Na]^+$: Calc. 1216.3789, Found 1216.3789 (100).

4.2.5 Synthesis of primary amine modified ferrocene[147]

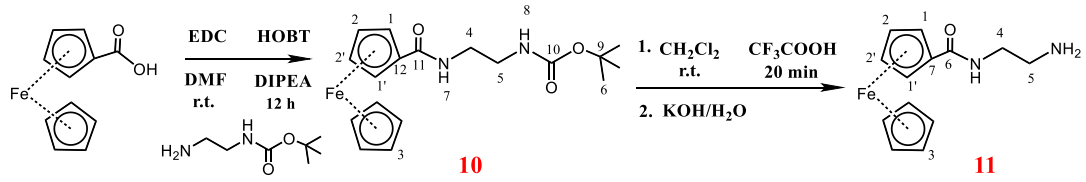

Synthesis of [((2-aminoethyl)- tert-butyl-carbamate)carbonyl]ferrocene (10):

Ferrocene carboxylic acid (2.084 g, 8.68 mmol), HOBt (2.8 g, 20.8 mmol) and EDC (3.6 g, 20.8 mmol) were added into a flask followed by addition of DMF (20 mL) with stirring under argon atmosphere. After stirring 30 min at room temperature, *tert*-butyl (2-aminoethyl)carbamate (1.36 g, 8.68 mmol) and DIPEA (3.42 mL, 20.8 mmol) were added into the mixture followed by stirring for another 12 h. After the reaction, the mixture was added water (150 mL) then extracted with EtOAc (3 × 100 mL). The

organic phase was dried with $MgSO_4$ and evaporated to remove the solvent. The residue was recrystallized from EtOAc to give the final product as an orange solid (2.717 g, 81.9 %). ^{1}H NMR (500 MHz, $CDCl_3$) δ 6.56 (s, 1H, 7), 5.04 (s, 1H, 8), 4.75 – 4.63 (m, 2H, H1 and H1'), 4.41 – 4.28 (m, 2H, H2 and H2'), 4.20 (s, 5H, H3), 3.49 (m, 2H, H4), 3.36 (m, 2H, H5), 1.46 (s, 9H, H6). ^{13}C NMR (126 MHz, $CDCl_3$) δ (ppm) = 171.22 (C11), 157.39 (C10), 79.94 (C9), 76.10 (C12), 70.54 (C1), 69.90 (C2), 68.31 (C3), 41.19 (C4), 40.82 (C5), 28.57 (C6). HRMS (ESI-TOF: *m/z* (%)): $[M+Na]^+$: Calc. 395.1034, Found 395.1042 (100).

Synthesis of [((2-aminoethyl)amino)carbonyl]ferrocene (11):

Compund **10** (980 mg, 2.63 mmol) was dissolved in DCM (15 mL) and added into a flask followed by addition of triflouroacetic acid (TFA) (5 mL) with stirring under argon atmosphere. After the mixture was stirred for 20 min at room temperature, the solvent was evaporated and KOH solution (50 mL, 1 N) was added dropwise at 0 °C followed by extracting with DCM (3 × 50 mL). The organic phase was dried with $MgSO_4$ and evaporated removing the solvent to obtain the final product as an orange solid (652 mg, 91.5 %). ^{1}H NMR (500 MHz, MeOD) δ (ppm) = 4.80 (m, 2H, H1), 4.41 – 4.38 (m, 2H, H2), 4.19 (s, 5H, H3), 3.37 (t, ^3J = 6.5 Hz, 2H, H4), 2.80 (t, ^3J = 6.5 Hz, 2H, H5). ^{13}C NMR (126 MHz, MeOD) δ (ppm) = 172.45 (C6), 75.31 (C7), 70.36 (C1), 69.43 (C2), 68.00 (C3), 41.82 (C4), 40.93 (C5). HRMS (ESI-TOF: *m/z* (%)): $[M+H]^+$: Calc. 273.0690, Found 273.0689 (100); $[M+Na]^+$: Calc. 295.0510, Found 295.0508 (100).

4.2.6 Copolymerization of P(DMAAm-*co*-VDMA)

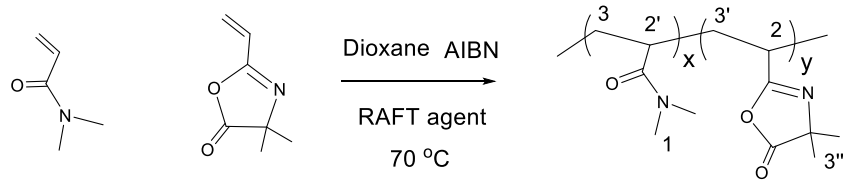

DMAAm VDMA **P(DMAAm-*co*-VDMA)**

DMAAm (5.61 g, 56.7 mmol) and VDMA (0.88 g, 6.3 mmol) were mixed and added into a flask followed by adding 2-(dodecylthiocarbonothioylthio)-2-methylpropionic

acid (DDMAT) (27.5 mg, 0.078 mmol), AIBN (2.5 mg, 0.0157 mmol) and dioxane (21 mL). The mixture was treated with argon at room temperature for 30 min and then turned into oil bath at 70 ^{o}C for 20 h under stirring. After the reaction was stopped and cooled to room temperature, the mixture was precipitated in cooled diethyl ether to obtain the polymer. The polymer again resolved in THF to repeat the process of precipitation for 2 times to obtain the final product as a white solid (4.93 g, 76.1 %). ^{1}H NMR (500 MHz, $CDCl_3$) δ (ppm) = 3.11-2.89 (m, 5.37H, 1), 2.73 – 2.17 (m, 1H, 2 and 2'), 1.98 – 1.08 (m, 2.6H, 3 and 3' and 3'').

4.2.7. Synthesis of P2

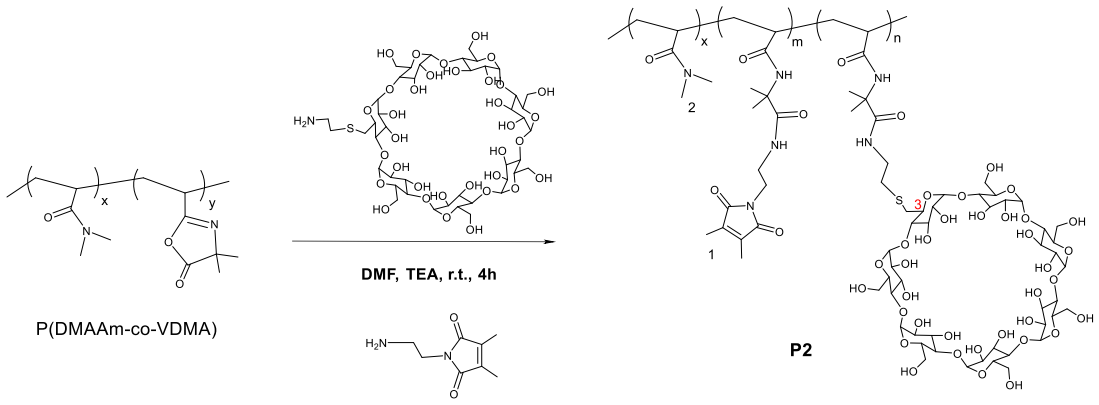

Copolymer P(DMAAm-*co*-VDMA) (300 mg), DMIEA (32.6 mg) and compound **9** (120 mg) were added into a flask followed by addition of DMF (5 mL) and TEA (0.1 mL). The mixture was stirred for 4 h at room temperature followed by precipitation in cooled diethyl ether and dried under vacuum. After that, the solid was dissolved in water (20 mL), dialyzed in water for 48 h and freeze dried to give the final product as a white solid (273 mg, 91 %). ^{1}H NMR (500 MHz, DMSO) δ (ppm) = 7.58 (m, 2.97H), 5.75 (m, 4.76H), 4.83 (m, 2.58H, H3), 4.43 (m, 1.85H), 3.66 (m, 9.8H), 2.90 (m, 137.2H, H2), 1.87 (m, 6H, H1), 1.78 – 1.20 (m, 54H), 1.11 (m, 11.6H).

4.2.8 Synthesis of P3

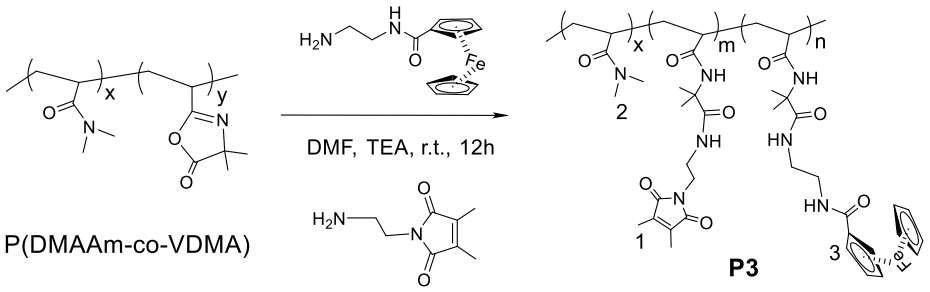

Copolymer P(DMAAm-*co*-VDMA) (300 mg), DMIEA (32.6 mg) and compound **11** (60 mg) were added into a flask followed by addition of DMF (5 mL) and TEA (0.1 mL). The mixture was stirred for 4 h at room temperature followed by precipitation in cooled diethyl ether and dried under vacuum. After that, the solid was dissolved in water (20 mL), dialyzed in water for 48 h and freeze dried to give the final product as a yellow solid (286 mg, 95.3 %). ^{1}H NMR (500 MHz, DMSO) δ (ppm) = 7.62 (m, 7.57H), 4.78 (m, 4H, H3), 4.32 (m, 4.1H), 4.16 (m, 10.9H), 2.90 (m, 250.4H, H2), 1.87 (m, 6H, H1), 1.77 – 1.21 (m, 96.1H), 1.11 (m, 21.6H).

4.2.9 Determination of layer thickness of SN supramolecular gel with SPR measurements

See 3.2.8

4.3 Results and discussion

To prepare **DCSH**, an azlactone based template copolymer was prepared through reversible addition-fragmentation chain transfer (RAFT) polymerization and then the covalent and noncovalent cross-linkers were introduced (***Scheme 4.1***). Initially, *N*, *N'*-dimethylacrylamide (DMAAm) was copolymerized with 2-vinyl-4,4-dimethylazlactone (VDMA) through a RAFT polymerization to obtain P(DMAAm-*co*-VDMA) with a relatively uniform distribution in polymer composition. The polymerization could be conducted to high conversion (> 90%) with 2-(dodecylthiocarbonothioylthio)-2-methylpropionic acid as the RAFT agent (***Table 4.1***).

The polymer composition was confirmed by calculating characteristic peaks in ^{1}H NMR spectrum, in which the VDMA shows higher reactivity than that of DMAAm (***Figure 4.2***). Next, the template copolymer was modified with covalent cross-linker (DMIEA) and non-covalent cross-linker (β-CD for **P2**, Fc for **P3**) under mild conditions to give rise to **P2** and **P3**. Cross-linker contents in **P2** and **P3** were calculated by ^{1}H NMR spectra (***Figure 4.3*** and ***Figure 4.4***). 1.4% of β-CD and 3.7% of DMIEA were introduced in **P2** and 4.3% of Fc and 2.3% of DMIEA were introduced in **P3**.

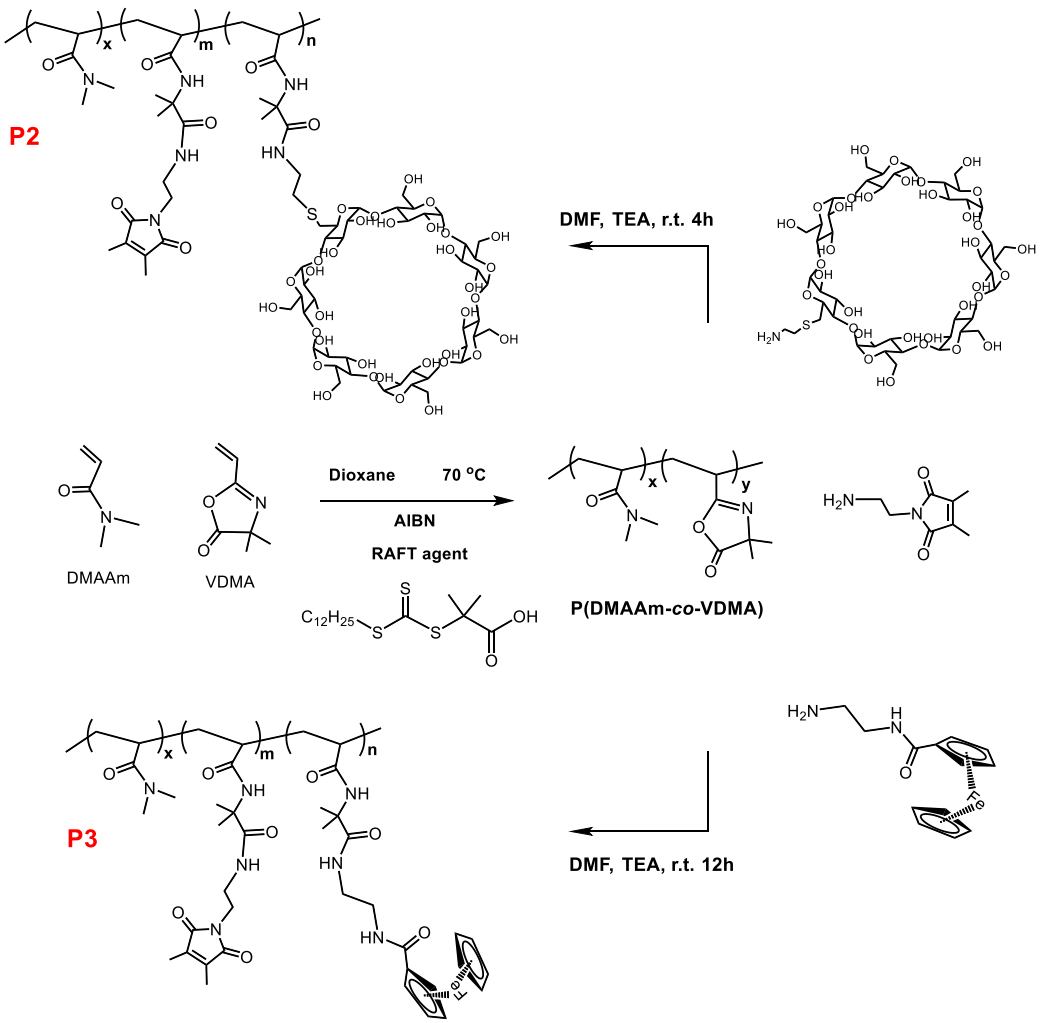

Scheme 4.1. Synthetic strategy of dually cross-linked supramolecular polymers of **P2** and **P3** based on P(DMAAm-*co*-VDMA).

Table 4.1. Parameters of P(DMAAm-*co*-VDMA) with a monomer ratio of [M1]/[M2] = 90/10 in dioxane at 70 °C.

P(DMAAm-*co*-VDMA)	[M]/[CTA]/[AIBN]	t (h)	Overall Conv. [b] (%)	Mn [a] (g/mol)	$Đ_M$ [a]	Comp. [b] $[P_1]/[P_2]$ (%)
1	500/1/0.2	12	95.2	9300	1.51	89.7/10.3
2	800/1/0.2	20	99.4	38600	1.60	89.5/10.5
3	1000/1/0.2	24	78.3	36800	1.84	86.7/13.3
4	1000/1/0.5	12	93.1	53300	1.48	89.3/10.7
5	2000/1/0.2	24	92.7	72800	1.71	89.3/10.7

[a] Determined by SEC (THF) using PMMA standards. [b] Determined using ^{1}H NMR spectroscopy.

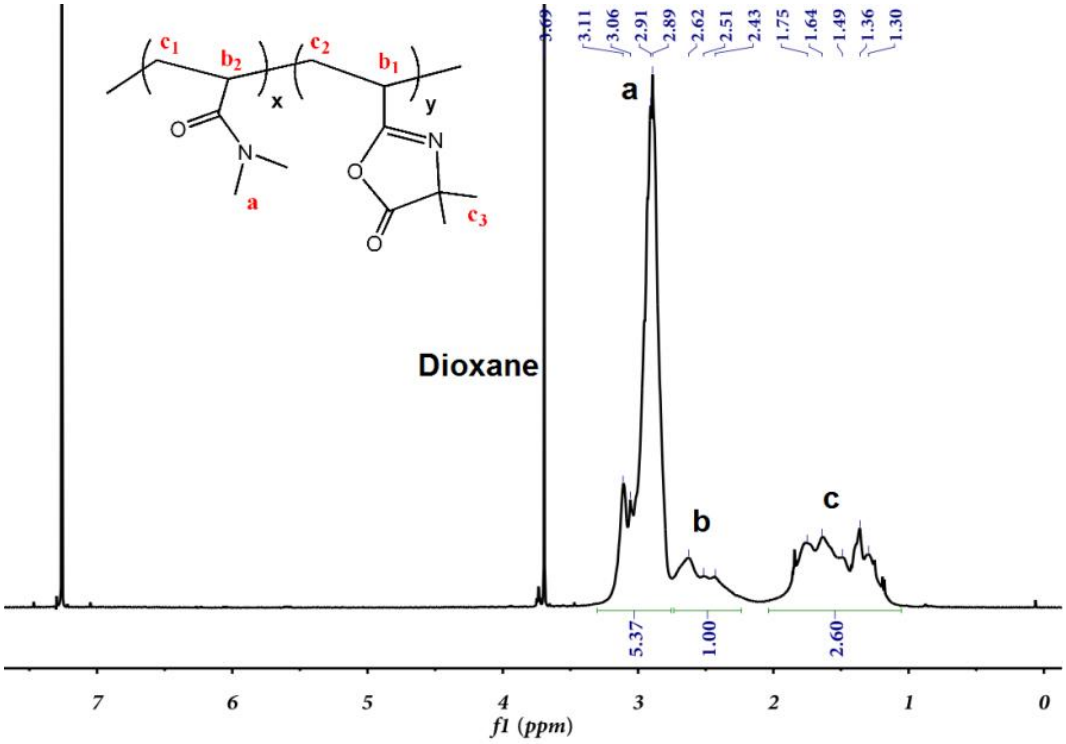

Figure 4.2. ^{1}H NMR spectrum of P(DMAAm-*co*-VDMA)-2 in $CDCl_3$.

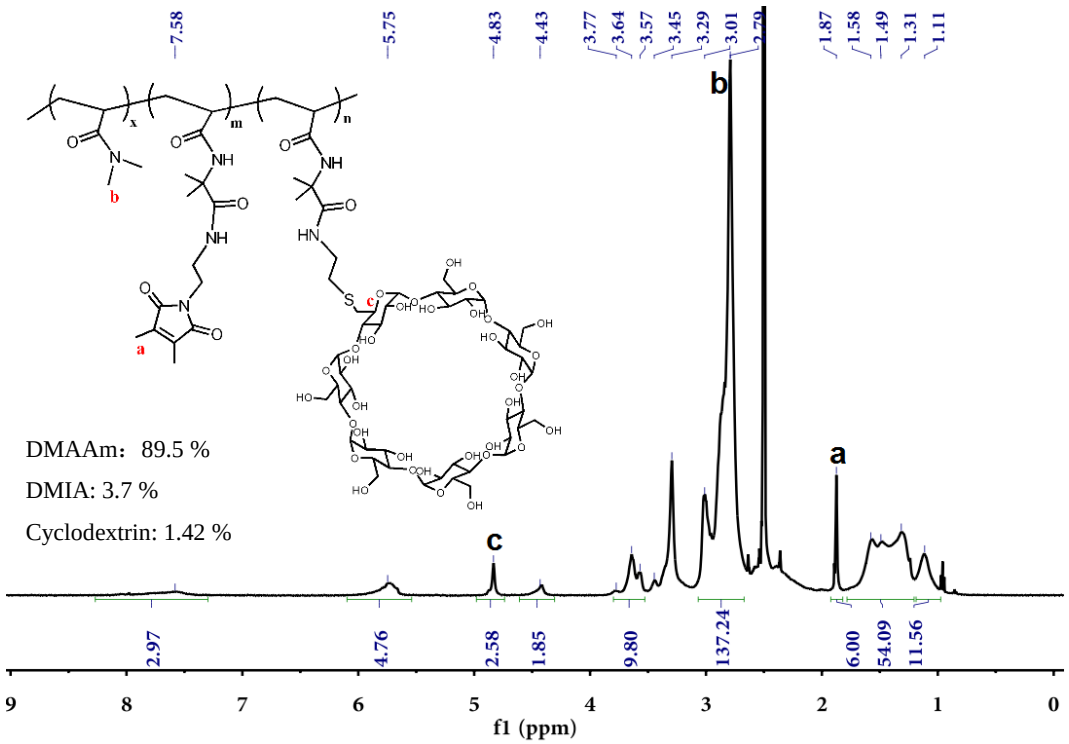

Figure 4.3. ^{1}H NMR spectrum of **P2** in d_6-DMSO.

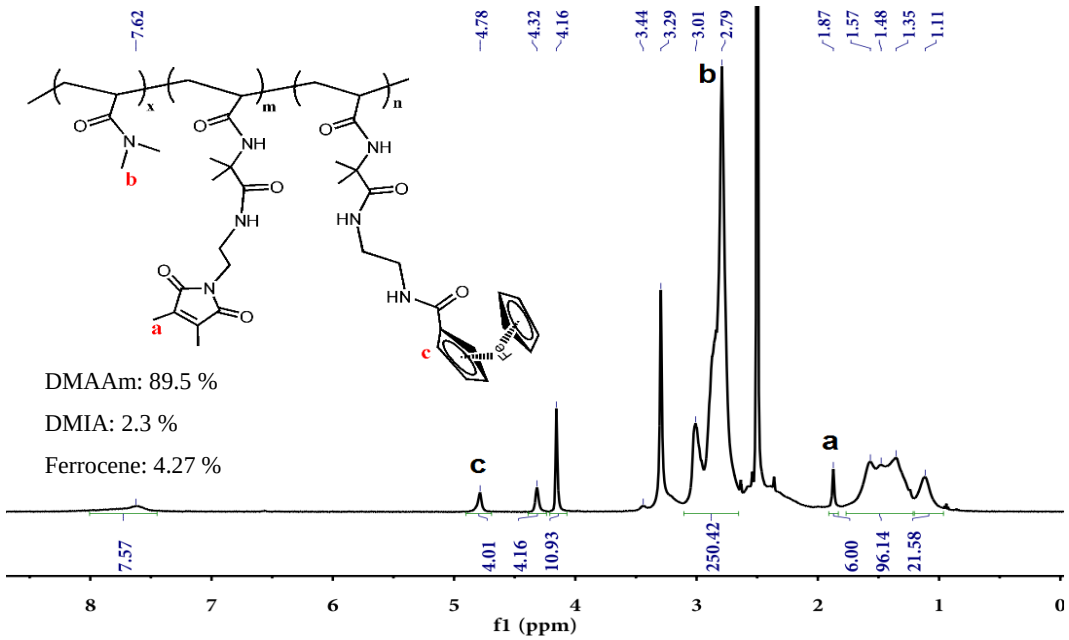

Figure 4.4. ^{1}H NMR spectrum of **P3** in d_6-DMSO.

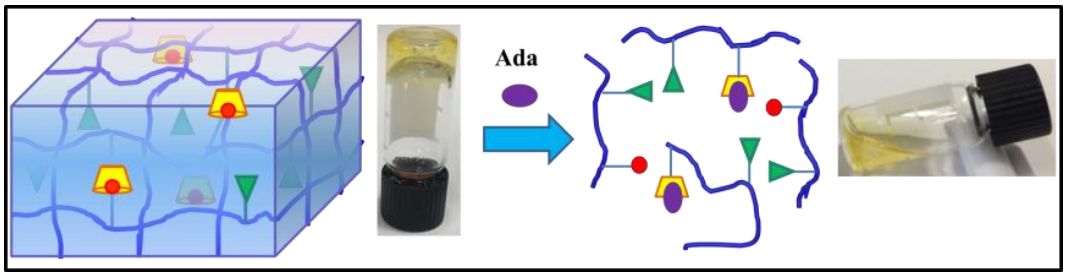

Figure 4.5. Sketch and photograph of gel-sol transformation in noncovalent bonded single cross-linked supramolecular polymer.

The host-guest complexation of β-CD and Fc drives supramolecular assemblies to form a physically cross-linked hydrogel by mixing the **P2** and **P3** in water (***Figure 4.5***). As expected, the mixture could form a hydrogel by equilibrating the mixture (10 wt%) for 2 h at room temperature. After the target molecule Ada was added in equivalent molar ratio with the Fc, the gel transformed to the sol. It was demonstrated that the host-guest interaction between β-CD and Fc was broken as the Ada was added, proving that the binding affinity between Ada and β-CD was higher than that of Fc and β-CD. Hence, this supramolecular pair can act as switchable cross-linker to detect small molecules.

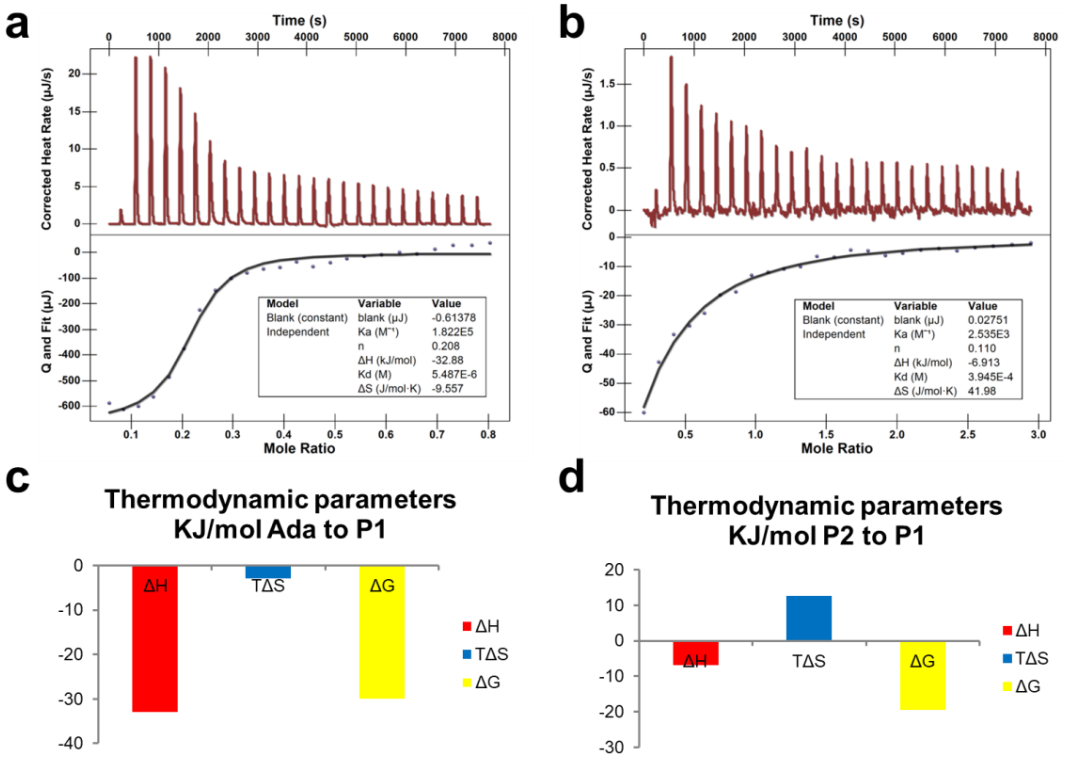

Figure 4.6. ITC titration curves obtained by injecting an Ada solution (a) and **P3** solution (b) (2.50 mM in pure water; the volume of each injection: 10 μL) to a **P2** solution (0.163 mM in pure water). **P2** was placed in the reaction cell of ITC instrument at 298.15 K. The thermodynamic parameters obtained from the fitting of ITC titration curve, Ada to **P2**(c) and **P3** to **P2** (d).

For confirmation, isothermal titration calorimetry (ITC) was employed to quantitatively compare the competitive interaction of Ada/**P2** and **P3**/**P2** (***Figure 4.6a and b***). The binding constant (K_a) of Ada/**P2** was 1.8×10^5 M^{-1}, [148,149] which was two orders of magnitude higher than that of **P3**/**P2** (2.5×10^3 M^{-1}).[150,151] The stronger interaction between Ada and β-CD ensured the quick replacement of Fc, resulting in the decross-linking of **P2** and **P3**. To further understand this competitive substitution process, the thermodynamic parameters were measured (***Figure 4.6c and d***). Both of the host-guest interactions were driven by favorable enthalpic changes ($\Delta H < 0$). However, entropic changes of **P3**/**P2** binding was favorable ($T\Delta S > 0$) while entropic changes of Ada/**P2** binding was unfavorable ($T\Delta S < 0$). According to literature,[152] the entropy changes are synergistic effects of complexation leading to a loss of conformation freedom and desolvation leading to an increased disorder of solvent. Overall, the Ada molecule has a better size effect than that of Fc, which loss more conformation freedom getting into the cavity of β-CD and leads to the entropy changes towards the unfavorable side. Therefore, Ada could serve as a competitive guest molecule to break the non-covalent cross-linking of **P2** and **P3**. Thus, on the basis of competitive complexation, sensors of specific molecular recognition could be developed.

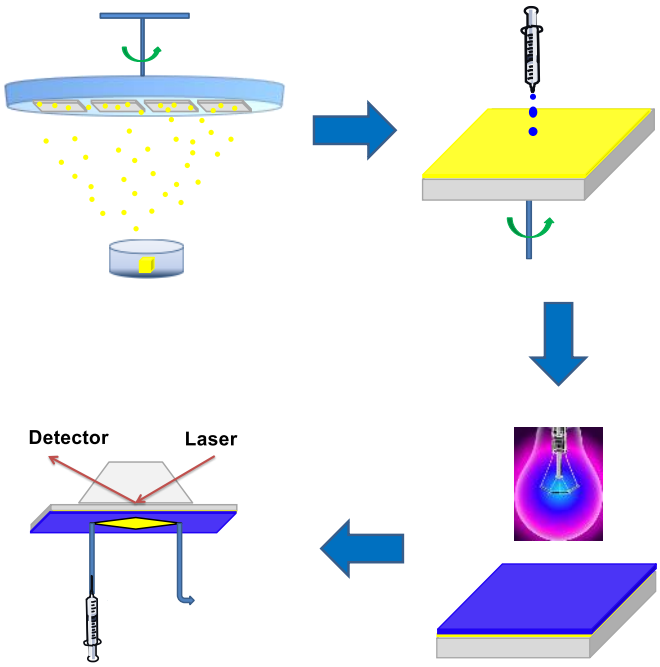

Figure 4.7. The preparation processes of DCSH onto a gold surface

Next, the **DCSH** system was prepared as a thin hydrogel layer, which could be used as a sensor to quantitatively detect target small molecules (Ada). The thin hydrogel layer was obtained after spin-coating onto a gold surface with the polymer mixture **P2**/**P3** in methanol that does not lead to the complex formation, photo cross-linking of DMIEA via [2+2] cyclization[116,118] and equilibrating in water (***Figure 4.7***). The competitive host-guest interaction of **DCSH** was evaluated by SPR-OWS, which provide information of both refractive index and layer thickness of the hydrogel within one measurement.[114,115] Hydrogel layers in different states were measured and characterized to obtain the angular reflectivity spectra R(θ) with both optical waveguide (OW) and surface plasma (SP) modes (***Figure 4.8a***). By fitting the

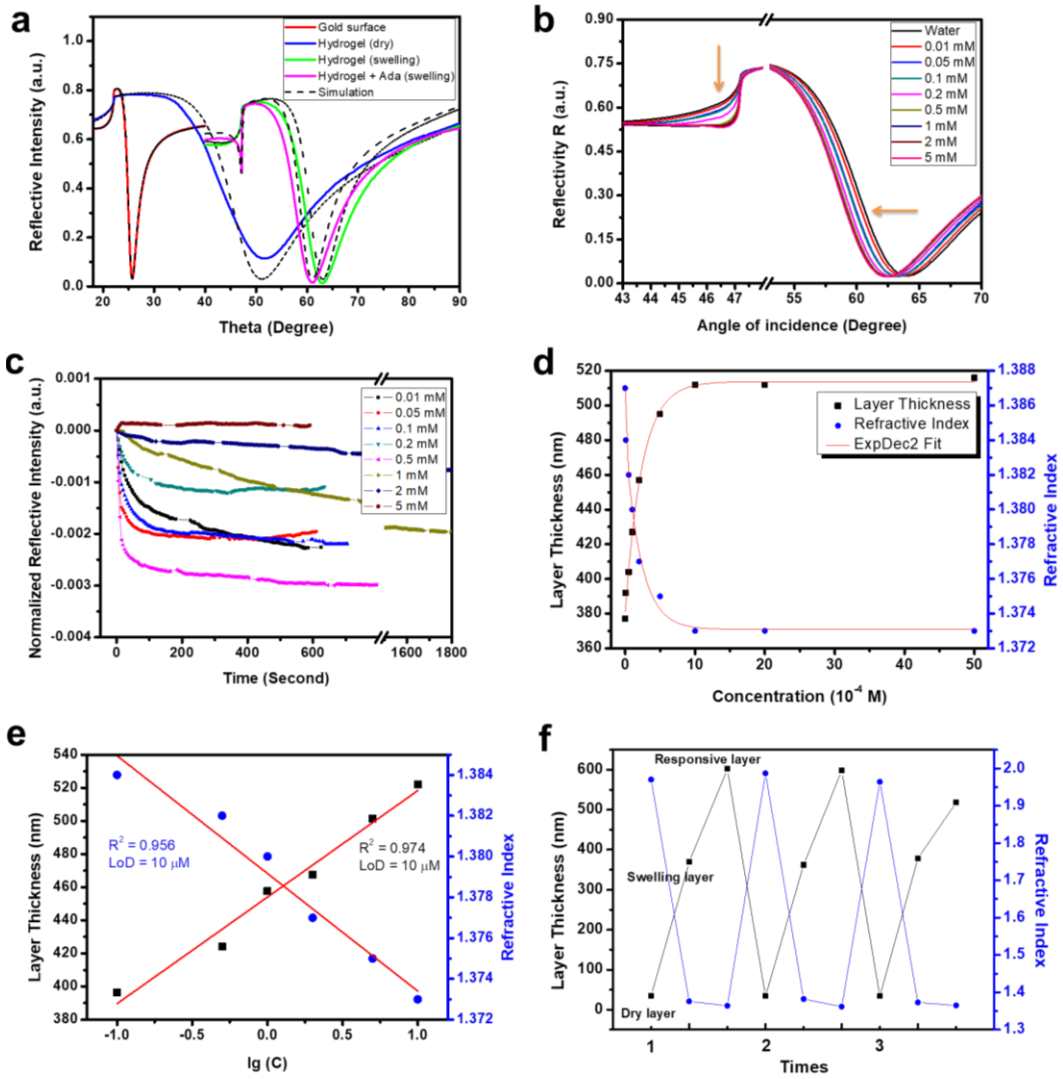

Figure 4.8. SPR-OWS measurements for target small molecules detection. a) Representative SPR-OWS curves with gold layer, hydrogel layer in dry state, hydrogel layer in swollen state and swollen hydrogel layer after adding Ada，respectively. b) Concentration dependent measurements of **DCSH** against diverse amounts of Ada, angle of incidence drop from 48° to 53°. c) Kinetics of reflectivity changes after injecting diverse concentrations of Ada solutions at a certain incidence angle of 59.3°. d) Plot of layer thickness and refractive index against concentration of Ada from simulated parameters of SPR-OWS and their nonlinear fitting. e) After logarithmizing the concentration value of Ada, the plot of the concentration from 1×10^{-5} to 1×10^{-3} M to layer thickness and refractive index were fitted linearly. f) Reversibility of the sensor chip tested by measuring layer thickness and refractive index in different states after washing off Ada with Methanol/Acetone (V/V = 7:3).

two distinct resonances at θ_{OW} and θ_{SP} corresponding to the excitation of OW and SP modes, respectively, the layer thickness d_h and refractive index n_h of the hydrogel were determined (***Table 4.2***). After swelling in water, the corresponding layer thickness of swollen hydrogel was 375 nm with a swelling ratio of 11.3, indicating the formation of the **DCSH**. The high swelling ratio of the DCSH in water benefits the diffusion of target molecule throughout the hydrogel. When treated with Ada solution, the d_h of the hydrogel significantly increased to 528 nm and the n_h decreased to 1.362. This demonstrated that Ada acted as a target molecule to break the interaction between Fc and β-CD in the thin hydrogel layer. Thus, the sensor chip could be used to detect small molecule (Ada) by SPR-OWS measurements.

Table 4.2. Characteristics of the hydrogel film upon its different states.

Materials	**Layer Thickness d_n (nm)**	**Refractive Index n_h**
Gold layer	41	-3.466
Dried Hydrogel	33	2.156
Hydrogel swelling in water	375	1.387
Hydrogel swelling in Ada solution	528	1.362

As the competitive interaction behavior was concentration dependent, the responsive behavior of the sensor with diverse amounts of Ada was investigated. The Ada targeting to the β-CD was studied upon injecting a series of Ada solutions at concentrations ranging from 10 μM to 5 mM. The reflection point of the plasmon mode decreased as the concentration of Ada increased (***Figure 4.8b***). An additional feature is observed below the critical angle ($\theta < \theta_c$) with appearance of a dip indicating that the first optical waveguide comes out.[114] The hydrogel film gradually swells as the concentration of Ada increases, which leads to a decrease in its n_h and an increase in its d_h. Swelling kinetics of the **DCSH** was studied by measuring the reflectivity variations at a certain incidence angle of 59.3° where the curve has a sharp dip showing the most sensitivity towards Ada. As shown in ***Figure 4.8c***, the competitive interaction between Ada and β-CD mostly took place within 100 S, indicating the Ada could replace Fc to

form a new host-guest pair with β-CD quickly. ***Figure 4.8d*** shows plots of layer thickness and refractive index of the **DCSH** from concentration dependent measurements. Both of the plots were fitted with exponential equation to yield standard curves. Further, the linear fitting was carried out by utilizing logarithmic values of concentration of Ada in the range from 1×10^{-5} to 1×10^{-3} M (***Figure 4.8e***). It was shown that in this responsive range, both the layer thickness and refractive index have the linear relationship with concentration of Ada. Also, the limit of detection[153] of the target molecule (Ada) was 2.43×10^{-5} M. Therefore, the d_n and n_h could be used as parameters to quantitatively calculate the concentration of Ada in the responsive range.

Further, reversibility of the sensor chip was checked with SPR-OWS measurements. The interactions of β-CD/Ada or β-CD/Fc were inherently hydrophobic interaction, which could be broken in organic solvent like methanol, acetone, DMSO and so on. The disassembly between **P2** and **P3** was checked by dynamic light scattering in different solvents (***Figure 4.9***). It could be seen that the mixture of **P2** and **P3** disassembled in the mixed solvent of methanol/acetone (V:V = 7/3) being able to recover the **DCSH** system. ***Figure 4.8f*** shows the layer thickness and refractive index of the same chip in dry, swollen and responsive states within three cycles. The dry layer thickness of the chip remained the same after 3 cycles and the swollen layer thickness negligibly increased from 370 nm to 380 nm. The thickness of the responsive layer decreased from 600 nm to 520 nm, indicating a density decrease of noncovalent bonding between β-CD and Fc. Also, the refractive index shows similar results with that of layer thickness changes. Nevertheless, the **DCSH** system repeatedly used to detect the Ada after the noncovalent bonding recovering demonstrated that the sensor has good reversibility for small molecules detection.

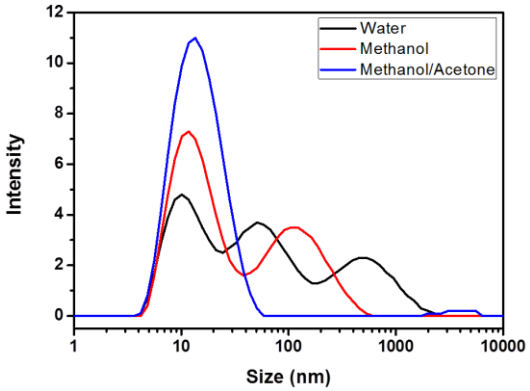

Figure 4.9. DLS measurements of mixed solution of **P1** and **P2** in different solvents.

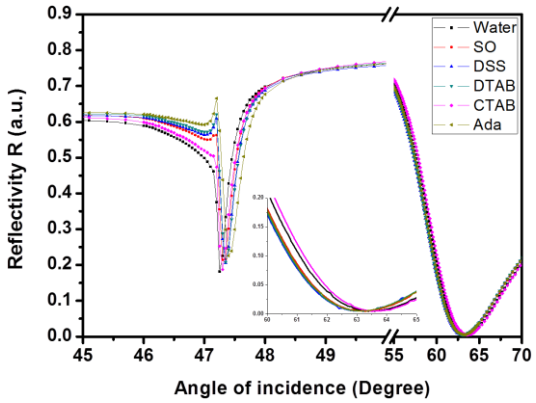

Figure 4.10. SPR-OWS measurements with different surfactants at a concentration of 0.1 mM, SO: sodium octanoate, DSS: dioctyl sodium sulfosuccinate, DTAB: dodecyl trimethyl ammonium bromide, CTAB: cetyltrimethylammonium bromide; angle of incidence breaks from 50° to 55°; inset graph was shown the amplifying totally reflective point of all the spectra at the angle between 60 ° and 65 °.

Finally, to confirm the **DCSH** system as a generalist, a series of surfactants as other target small molecules with different binding affinities to β-CD were measured via SPR-OWS. Comparing the binding affinity of Fc to β-CD (2.5×10^3 M^{-1}), the binding affinity of sodium octanoate (SO) to β-CD (370 M^{-1}) is weaker; the binding affinity of dioctyl sodium sulfosuccinate (DSS) to β-CD (2.8×10^3 M^{-1}) and dodecyl trimethyl ammonium bromide (DTAB) to β-CD (1.5×10^3 M^{-1}) are comparable; the binding affinity of cetyltrimethylammonium bromide (CTAB) to β-CD (2×10^4 M^{-1}) is stronger.[154–156] The SPR-OWS measurements (***Figure 4.10***) showed that, the chip could respond to all of the surfactants (0.1 mM) with diverse responsive ratio according

to their binding affinities. The responsive ratios were defined as $(d_s-d_w)/d_w$ (***Figure 4.11***) where ds is the layer thickness in surfactant solution and d_w (as the standard value) is the layer thickness in water. The responsive ratio of SO was around 0.02, which may attribute to the lower binding affinity of SO to β-CD than that of Fc to β-CD. The responsive ratio increased to around 0.06 by using DSS or DTAB that has a comparable binding affinity against Fc. When the target molecule has a higher binding affinity than Fc, the responsive ratio could be increased to around 0.12 like Ada. It is interesting that CTAB could trigger a deswelling effect owing to the 1:2 complexation of CTAB with β-CD. Due to the high binding affinity of CTAB, it can break the interaction between Fc and β-CD and reform a noncovalent cross-linking structure with closer distance of two polymer chain. Thus, taking the binding affinity of Fc to β-CD as a valve, the sensor responds to the target small molecules with higher binding affinity while does not respond to those with lower binding affinity. Therefore, The **DCSH** could be used as a general sensor chip to detect the small molecules owing high binding affinity with the β-CD. Additionally, as a side evidence here, the nonspecific adsorption could be avoided due to this selective responsive behavior in the **DCSH**.

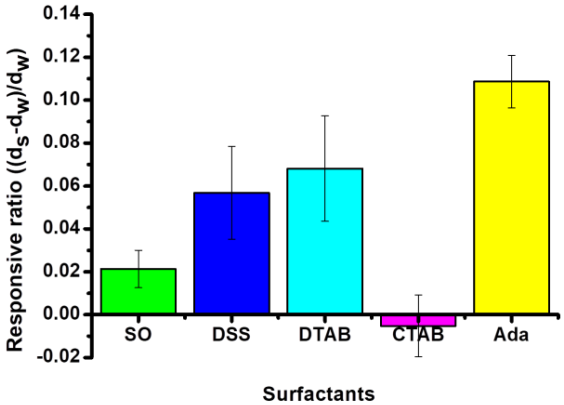

Figure 4.11. Responsive ratio of **DCSH** against various surfactants, where the layer thickness of the **DCSH** in water d_w as the standard. The concentrations of surfactants were 0.1 mM.

4.4 Conclusions

In summary, a template copolymer based **DCSH** was designed and a supramolecular hydrogel based sensor for target small molecules detection was developed. The **DCSH** structure was built by introducing DMIEA as the covalent bonding via [2+2] cyclization and ferrocene and β-cyclodextrin as the noncovalent bonding via host-guest interaction. Adamantane with higher binding affinity to β-CD was used as the competitive guest to replace Fc, verifying that the noncovalent bonding of the **DCSH** could be broken, which results in the swelling of the **DCSH**. Further, the **DCSH** was immobilized on a gold surface to obtain a sensor chip. The n_h and d_h of the **DCSH** were determined independently by using SPR-OWS measurements. The sensitivity, reversibility and universality of the sensor chip to several analytes were investigated, demonstrating the **DCSH** could be used as a SPR-OWS sensor for target small molecules detection. Our method opens a new strategy to build a **DCSH** based SPR-OWS sensor for target small molecules detection. The **DCSH** is thought to be easily modified with other molecular recognition pairs to be used potentially as a SPR biosensor for target small biomolecule detection.

Chapter Five: Dually cross-linked supramolecular hydrogel for cancer biomarker sensing

5.1 Introduction

Early-stage diagnosis for cancer and other diseases relies largely on biomarkers in body fluids.[157–159] In principle, the biomarker candidates, normally, from genetic, proteomic and metabolic products are still great challenges for sensitive and specific detection with modern detection methods.[160,161] Ovarian cancer has no obvious symptoms before it turns to advanced stages, which could be the reason for the lowest survival rate of this cancer type.[162] The biomarkers cancer antigen 125 (CA125) in genetic level[163] and lysophosphatidic acid (LPA) in metabolic level[164] were able to distinguish ovarian cancer in early-stage. LPA was thought to be better candidate as the ovarian cancer biomarker because is shows significant different between cancer samples and normal samples and crucial role in tumor progression and metastasis.[165] However, LPA, a kind of phospholipid molecule, shows poor binding site compared with other kind of biomarkers like proteins and nucleic acids.[166,167]

The analytical methods developed for LPA detection include enzymatic cycling,[168] immunoassays,[169] surface-enhanced Raman scattering[170] and other optical spectroscopies.[171–173] Surface plasmon resonance (SPR) based analytical method, which has already achieved commercial exploitation in biomolecules detection,[174–176] shows a great challenge to detect molecules like LPA with the normal strategy due to its small molecular weight (< 500 Da) and poor specific binding.[137,177–182] Moreover, the detection scope of SPR based on a single assembled monolayer approach normally range from pg/mL to ng/mL, which is far beyond the cutoff value of LPA (2.42 μM).[135,157,183,184] Therefore, a new strategy of SPR based sensor for small molecular detection within the physiological range would significantly expand the application

areas.

Recently, SPR combining optical waveguide spectrum (SPR-OWS) was developed by using a hydrogel layer instead of single assembled monolayer, resulting in a wider detection range.[185] However, the limitation for small molecule detection was still a problem.[186] Ultimately, small molecule with lower polarizability decreased the resonance of the sensor, which would be limited without amplifying or transforming the signal during binding process.[187] Here, a dually cross-linked supramolecular hydrogel (**DCSH**) come into view because of its responsiveness to low molecular weight compounds with volume expansion or shrinking as well as high stability. Therefore, a new SPR-OWS sensor based on **DCSH** could be a candidate for LPA detection in the physiological range.

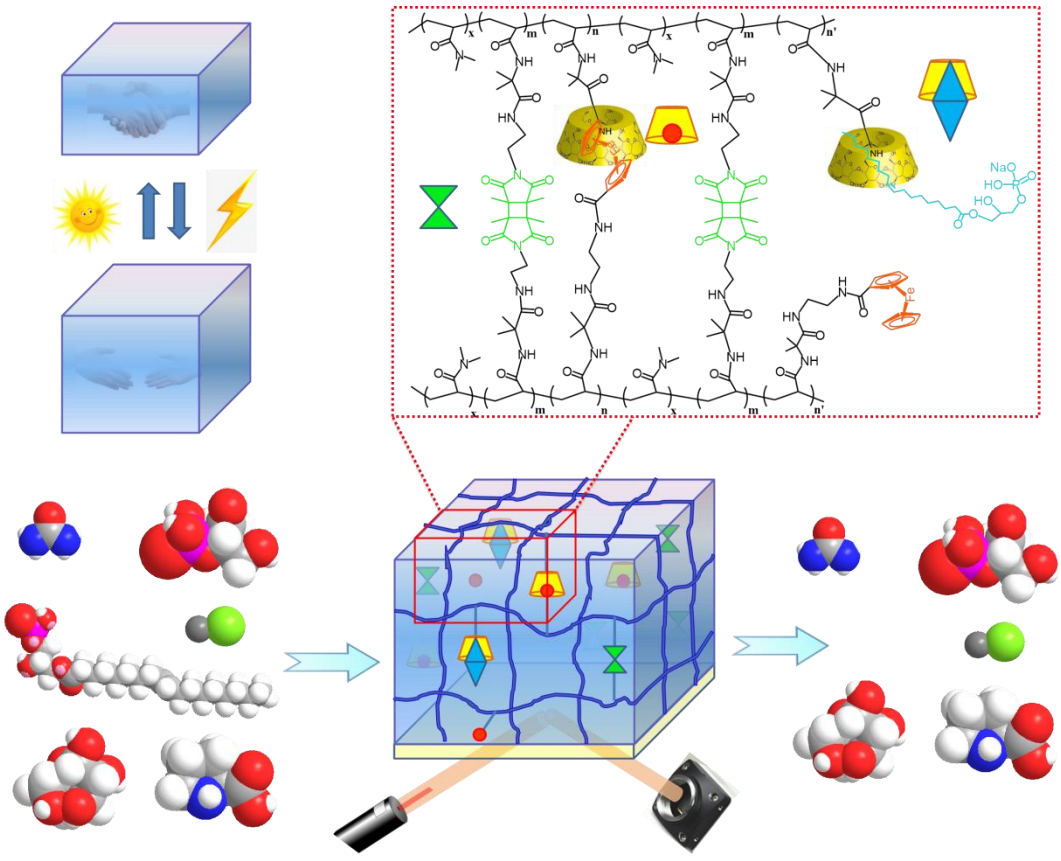

Figure 5.1. Schematic illustration of SPR-OWS sensor based on dually cross-linked supramolecular hydrogel towards specific detection of LPA in mimic plasm conditions.

Herein, a **DCSH** based SPR-OWS sensor was developed, which could specifically

respond to LPA in mimic plasm conditions (***Figure 5.1***). The **DCSH** was constructed by simultaneously introducing host-guest pairs of β-cyclodextrin (β-CD) and ferrocene (Fc), providing noncovalent bonding, and photo cross-linker 2-(dimethylmaleimido)-N-ethylamine (DMIEA), providing covalent bonding. LPA, the target molecule, was introduced into **DCSH** to break the host-guest interaction via competitive guest interaction. Thus, the signal of LPA binding could be transformed into swelling signal of **DCSH**, resulting in increase of the hydrogel layer thickness and decrease of the refractive index. The binding signal enhancement was monitored by SPR-OWS measurements, thus, achieving small molecule detection.

5.2 Experimental section

5.2.1 Reagents and Instruments

N,N-Dimethylacrylamide (> 99.0 %, TCI) was vacuum distillation before used. The following chemicals were purchased from commercial sources and used as received. 1,2-diaminoethane (98 %, Acros Organics), 1-hydroxybenzotriazole hydrate (HOBt) (> 97.0 %, Sigma Aldrich), 2-methylalanine (> 98.0 %, TCI), 2-aminoethanethiol hydrochloride (> 95.0 %, TCI), 2,6-Di-tert-butyl-p-cresol (BHT) (> 99 %, Fluka), acryloyl chloride (96 %, Alfa Aesar), allylamine (98+ %, Alfa Aesar), dimethymaleic anhydride (97 %, Acros Organics), D-glycerate 3-phosphate disodium salt (Chem Cruz), di-*tert*-butyl-dicarbonate (99 %, Acros Organics), ethyl chloroformate (99 %, Fluka), ferrocene carboxylic acid (98 %, Alfa Aesar), L-α-lysophosphatidylcholine (from egg yolk) (Chem Cruz), *N*-(3-dimethylaminopropyl)-*N'*-ethylcarbodiimide hydrochloride (EDC) (> 98.0 %, Sigma Aldrich), *N,N*-diisopropylethylamine (97 %, Alfa Aesar), oleoyl-L-α-lysophosphatidic acid sodium salt (≥ 98 %, Chem Cruz), tosylchloride (98 %, Alfa Aesar), trifluoroacetic acid (>99.0 %, TCI), thioacetic acid (> 97 %, Fluka). All other normal chemicals and solvents were of analytical grade and were used without further purification.

^{1}H and ^{13}C NMR spectra were recorded on a Bruker AV-500 spectrometer (500 MHz for ^{1}H and 125 MHz for ^{13}C), with chemical shifts (d) reported in ppm relative to solvent

peak (7.26 ppm for $CDCl_3$ and 2.50 ppm for DMSO) standards and coupling constants (*J*) reported in Hz. High-resolution mass spectra (HRMS) were recorded by electrospray ionization (ESI) on a Waters SYNAPT™ G2 HDMS™ mass spectra. The molar masses and molar mass distribution (M_w/M_n) were performed on a gel permeation chromatography (GPC) at a flow rate of 1 mL/min on a Merck Hitachi 655A-11 Liquid Chromatograph connected to a Knauer Smartline RI Detector 2300 and a Merck Hitachi L-4200 UVVIS Detector. The instrument was equipped with a PSS-GRAM 10^3 Å and PSS-GRAM 10^2 Å column and all samples were calibrated by poly(methylmethacrylate) standards. Supramolecular polymer size was carried out on a dynamic light scattering (DLS) apparatus of Malvern Nano-ZS at an angle of incidence of 15º. Photo cross-linking process was performed by an OmniCure® S1500 spot UV curing lamp with a unique and patented 200 Watt Intelli-Lamp.

5.2.2 Synthesis of 2-Vinyl-4,4-dimethylazlactone (VDMA)

See 3.2.5

5.2.3 Synthesis of additional promotor and photo cross-linker

See 3.2.3 and 3.2.4

5.2.4 Synthesis of primary amine modified cyclodextrin

See 4.2.4

5.2.5 Synthesis of primary amine modified ferrocene

See 4.2.5

5.2.6 Copolymerization of P(DMAAm-*co*-VDMA)

See 4.2.6

5.2.7 Synthesis of P2

See 4.2.7

5.2.8 Synthesis of P3

See 4.2.8

5.2.9 Determination of layer thickness of SN supramolecular gel with SPR measurements

See 3.2.8

5.3 Results and discussion

To prepare **DCSH**, an azlactone based template copolymer was prepared through reversible addition-fragmentation chain transfer (RAFT) polymerization and then the covalent and noncovalent cross-linkers were introduced (***Scheme 4.1***). Initially, *N*, *N'*-dimethylacrylamide (DMAAm) was copolymerized with 2-vinyl-4,4-dimethylazlactone (VDMA) through RAFT polymerization to obtain P(DMAAm-*co*-VDMA) with a relatively uniform distribution in polymer composition. The number average molecular weight of P(DMAAm-*co*-VDMA) at high conversions reached 38600 g/mol with a polydispersity of 1.6. The polymer composition was confirmed by evaluating characteristic peaks in ^{1}H NMR spectrum. The VDMA content was 10.5%, which was consistent with its original composition (***Figure 4.2***). Next, the template copolymer was modified with covalent cross-linker DMIEA and non-covalent cross-linker (β-CD for **P2**, Fc for **P3**) under mild conditions to give rise to **P2** and **P3**. Cross-linker contents in **P2** and **P3** were calculated by ^{1}H NMR spectra (***Figure 4.3*** and ***Figure 4.4***). 1.4% of β-CD and 3.7% of DMIEA were introduced in **P2**, meanwhile, 4.3% of Fc and 2.3% of DMIEA were introduced in **P3**.

Next, the **DCSH** system was constructed to form a thin hydrogel layer, which could be used as a sensor to quantitatively detect target molecule LPA. The thin hydrogel layer based on **DCSH** was obtained after spin-coating of the polymer mixture **P2**/**P3** in

methanol onto a gold surface modified with adhesion promoter, photo cross-linking of DMIEA via [2+2] cyclization and equilibrating in water (***Figure 4.7***). What should be noted is that the mixture **P2**/**P3** shows no host-guest complex in methanol (***Figure 4.9***), which is crucial for preparing a uniform thin film. Specially, the SPR-OWS was used to monitor the responsive behaviors of DCSH in different states with both layer thickness and refractive index with one measurement (***Figure 5.2a***). By fitting the two distinct resonances at θ_{OW} and θ_{SP} corresponding to the excitation of OW and SP modes respectively, the layer thickness d_h and refractive index n_h of the hydrogel were determined (***Table 5.1***). After swelling in water, the corresponding layer thickness of swollen hydrogel was 734 nm with a swelling ratio of 16.3, indicating the formation of DCSH. The high swelling ratio of the DCSH in water benefits the diffusion of target molecule throughout the hydrogel. When treated with LPA solution (50 μM), d_h of the hydrogel significantly increased to 946 nm and n_h decreased to 1.346. This demonstrated that LPA, as a competitive guest, could break the interaction between Fc and β-CD in the hydrogel thin layer. Thus, the sensor chip could be used to detect LPA by SPR-OWS measurements.

Swelling kinetics of the DCSH was studied by measuring the reflectivity variations at a certain incidence angle of 56.5° where the curve has a sharp dip, showing the most sensitivity towards LPA. As shown in ***Figure 5.2b***, the competitive interaction between β-CD and LPA mostly took place within 300 S, indicating that LPA could replace Fc to form a new host-guest pair with β-CD quickly. On the other hand, the quick recovery of the reflective intensity under the flow of water within a comparative time as the binding process indicating that the elution was also very efficient and the DCSH was rebuilt. Then, two verification experiments were carried out to confirm this specially responsive behavior with both fast binding and recovery (***Figure 5.3***). Both of the hydrogels constructed by P(DMAAm-*co*-DMIAAm) and **P2** show no swelling behaviors upon adding 10 μM LPA, indicating that the special responsive behavior was caused by the host-guest interaction between Fc and β-CD rather than the moiety of DMAAm or β-CD.

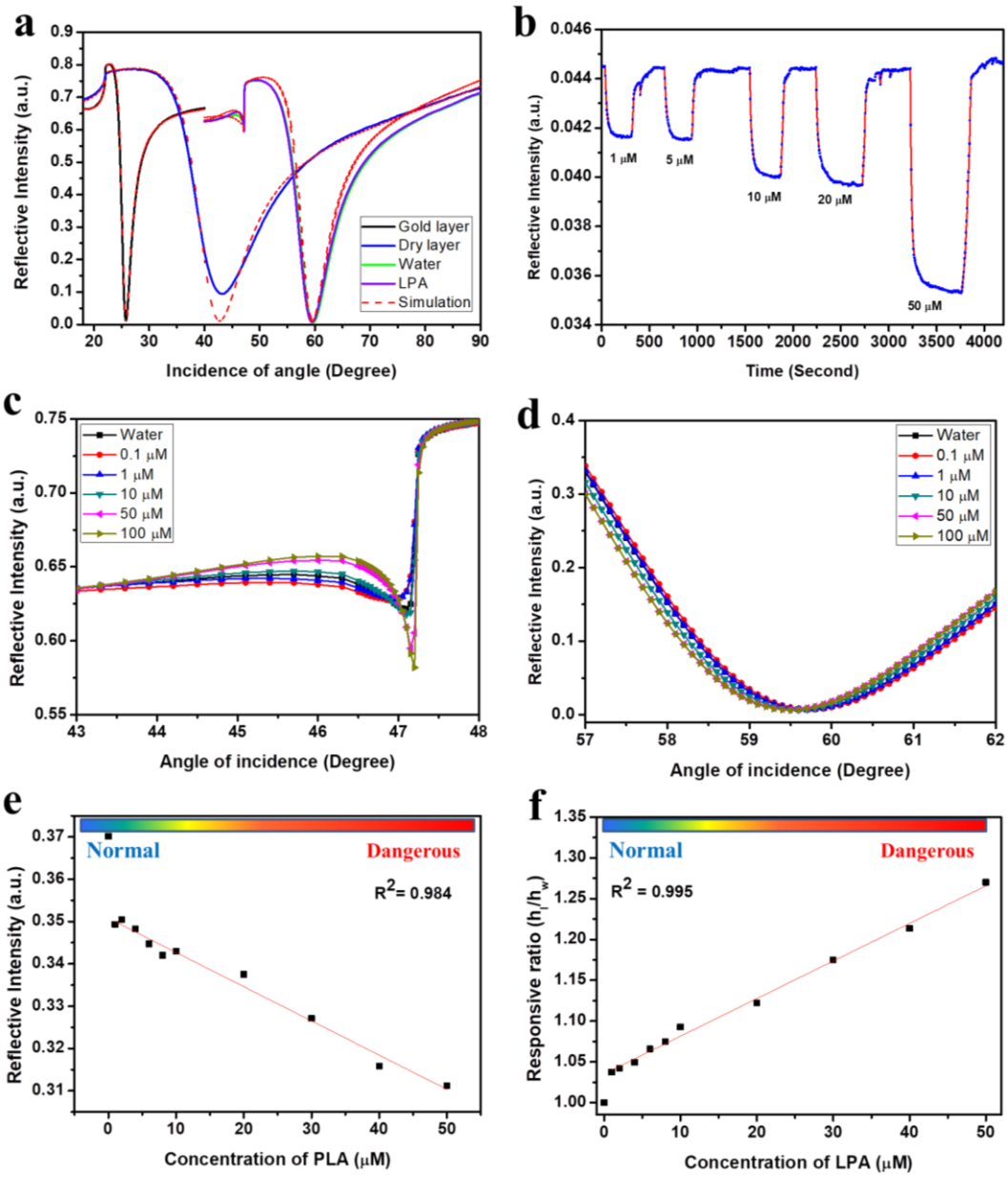

Figure 5.2. SPR-OWS measurements for LPA detection. a) Representative SPR-OWS curves with gold layer, hydrogel layer in dry state, hydrogel layer in swollen state and hydrogel layer in responsive state with LPA，respectively. b) Kinetics of reflectivity changes after injecting diverse concentrations of LPA solutions at a certain angle of incidence at 56.5°. Concentration dependent measurements of DCSH against diverse amount of LPA in magnified regions (c) from 43° to 48° and (d) from 57° to 62°. e) Plot of reflective intensity against concentration of LPA from measured dates of SPR-OWS at angle of incidence at 57° and its linear fitting. f) Plot of layer thickness against concentration of LPA from simulated parameters of SPR-OWS and its linear fitting.

Table 5.1. Characteristics of the hydrogel film upon its different states.

Materials	**Layer Thickness d_n (nm)**	**Refractive Index n_h**
Gold layer	44	-3.389
Dried Hydrogel	45	1.5942
Hydrogel swelling in water	734	1.3477
Hydrogel swelling in LPA solution	988	1.3461

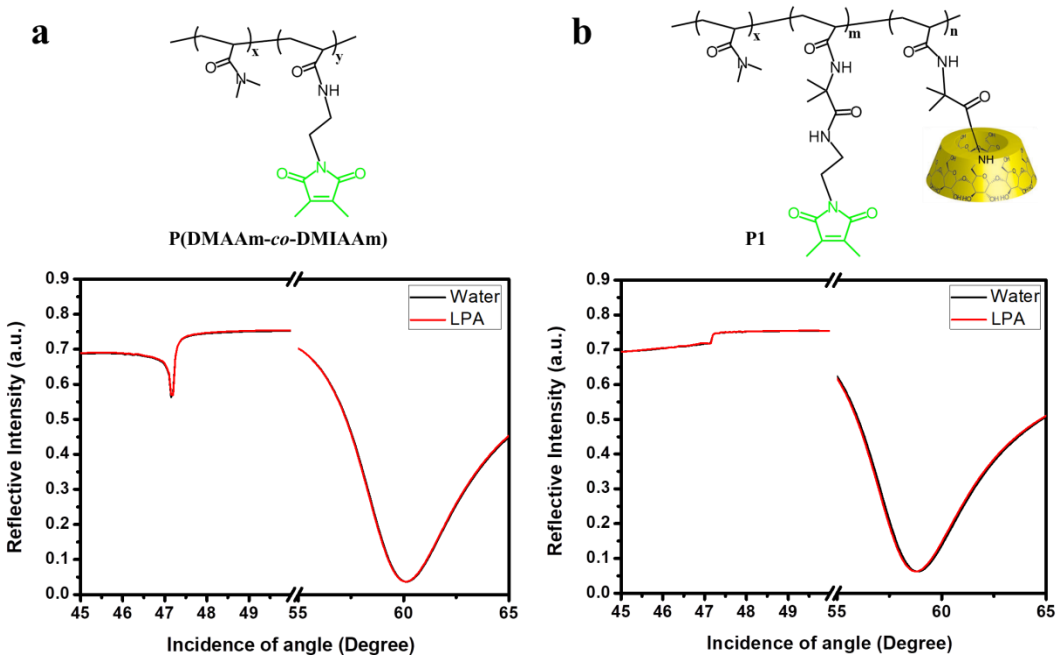

Figure 5.3. a) Chemical structure of P(DMAAm-*co*-DMIAAm) and the SPR-OWS measurements upon adding LPA solution (10 μM); b) Chemical structure of **P2** and the SPR-OWS measurements upon adding LPA solution (10 μM).

As the competitive interaction behavior was concentration dependent, responsive behavior of the sensor with diverse amount of LPA within physiological concentrations was investigated to check the sensitivity of **DCSH** towards LPA in water (***Figure 5.2c, d***). The total reflection point (***Figure 5.2d***) decreased as the concentration of LPA increase from 1 μM to 50 μM, indicating a decrease of refractive index n_h caused by the swelling of **DCSH**. Further, the first optical waveguide mode (***Figure 5.2c***) observed at around 47.2° appeared with a gradual dip along with the increase of LPA concentration, revealing an increase of layer thickness d_h. The reflective intensity,

which could directly be read from the measuring curve and has an intrinsically squared relationship to the n_h was collected according to the concentration dependent measurements (***Figure 5.2f***). Additionally, the layer thickness plot of **DCSH** was obtained from the simulation curves of concentration dependent measurements (***Figure 5.2e***). Both of the plots were fitted well by linear equation with a standard deviation above 0.98. Typically, the concentration of LPA in physiological levels is from 1.4 to 43.3 μM with a cutoff value for early stage ovarian cancer of 2.42 μM.[162,165] It was shown that in the concentration range from 1 μM to 50 μM, **DCSH** has great sensitivity to LPA with a limit of detection (LoD) at 0.122 μM, where the value was calculated from the linear regression by using the formula LoD = F × SD/b (F: factor of 3.3; SD: residual standard deviation of the linear regression; b: slope of the linear regression).[188] Therefore, the reflective intensity and layer thickness could be used as parameters to quantitatively calculate the concentration of LPA within the responsive range.

The excellent responsive behaviors of **DCSH** towards LPA show that LPA could replace Fc successfully. This was encouraged to further compare their inherent binding affinity with β-CD. Firstly, ^{1}H NMR spectrometry was carried out to observe the inclusion complexes formation of LPA with β-CD (***Figure 5.4a***). Alkyl chain protons of LPA marked from H_a to H_d show significant downfield shifts upon addition of increasing amount of β-CD to 2 mole equivalents. This variation shows that the complex of LPA and β-CD was formed with a 1:2 manner. To get further insight in atomic-level information on the inclusion geometry, 1D NOESY experiments were also carried out (***Figure 5.4b***). Deep immersion of the long alkyl chain from LPA into β-CD cavity was confirmed by strong NOE between the alkyl chain (H_a to H_d) and the protons in β-CD cavity (3.56 ppm and 3.80 ppm) with selective irradiation signals of both 1.312 ppm and 3.566 ppm. What should be noted is that all the NOE signals show a negative effect, indicating a large complex formation. Electrospray ionization mass spectrometry in positive mode was used to investigate the complex of LPA and β-CD as well.

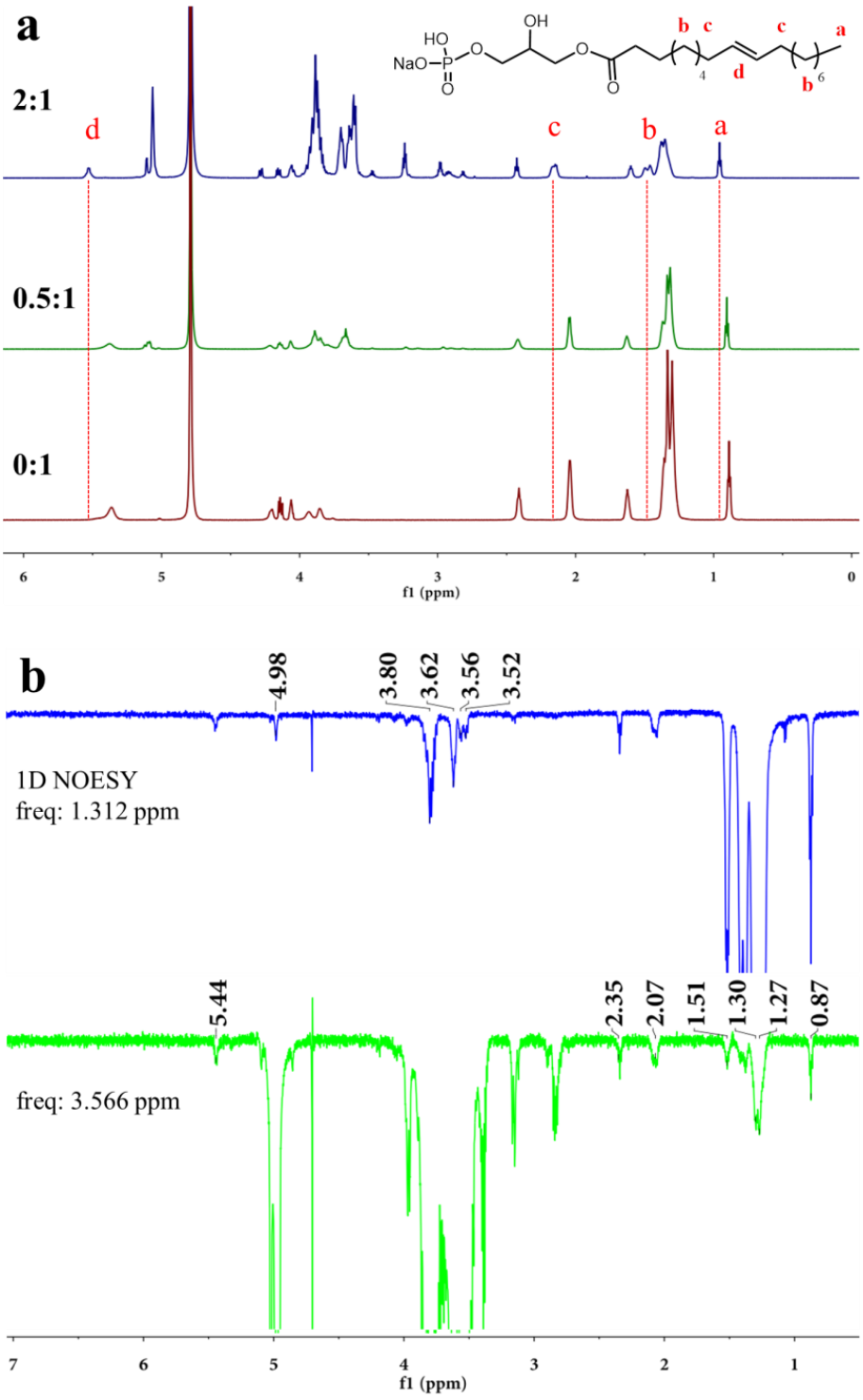

Figure 5.4. a) ^{1}H NMR experiments for the LPA and β-CD system in D_2O upon addition of increasing amounts of β-CD at 298 K. b) DPFGSENOE (1D NOSEY) spectra of the mixture of LPA and β-CD (1:2) with signal irradiation at 1.312 ppm and 3.566 ppm, respectively. Selectively excited proton resonances are shown by dashed arrows.

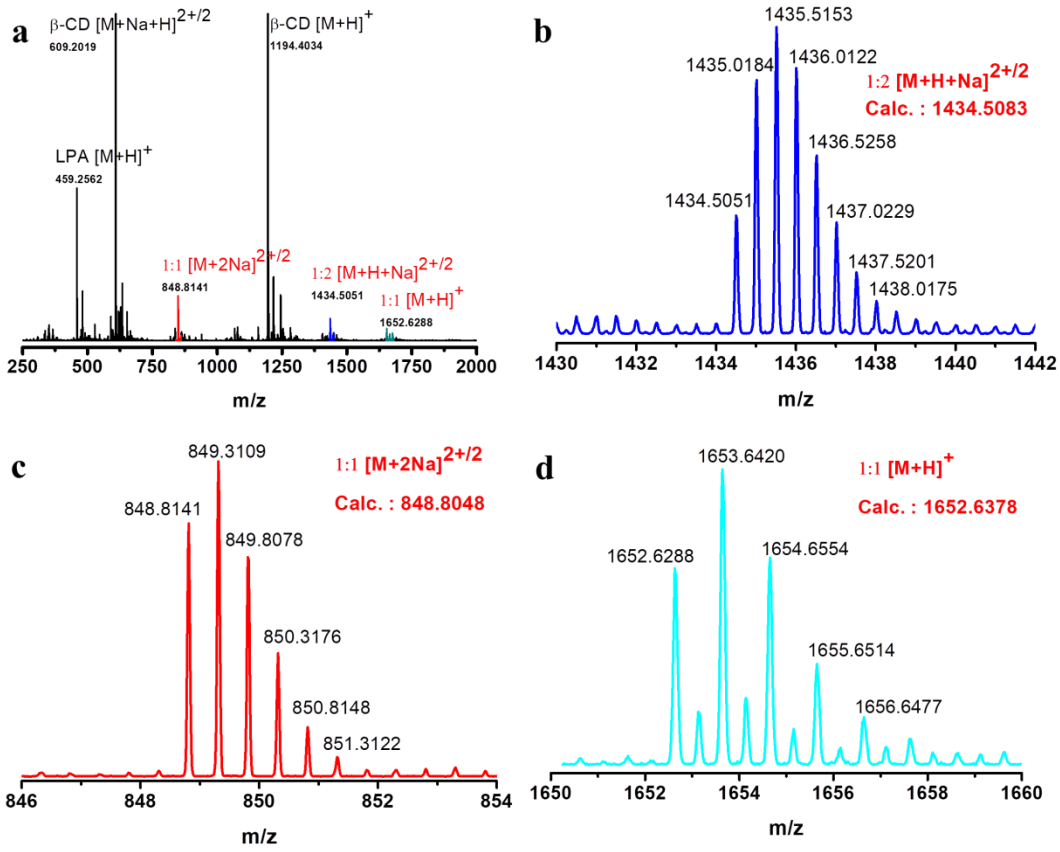

Figure 5.5. a) ESI-HRMS for the mixture of host-guest pairs of LPA and β-CD; b) the selective range from 1430 to 1442 m/z with 1:2 complex of doubly charged ion; c) selective range from 846 to 854 m/z with 1:1 complex of doubly charged ion; d) selective range from 1650 to 1660 m/z with 1:1 complex of singly charged ion.

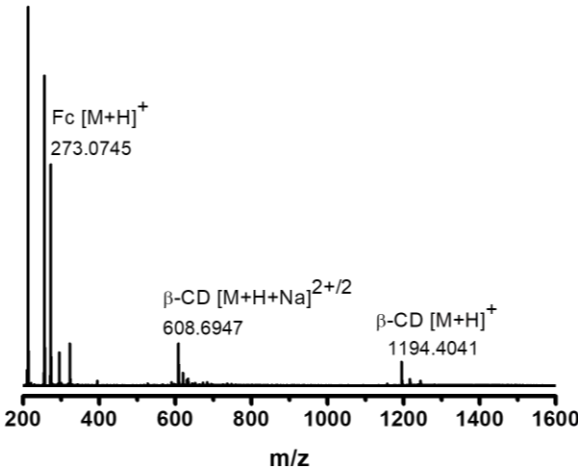

Figure 5.6. ESI-HRMS for the mixture of host-guest pair of Fc and β-CD.

The mass spectra yield mainly singly and doubly charged ions for each component as well as their complex (***Figure 5.5a***). The complexes of LPA and β-CD with 1:2

composition was found with doubly charged ion at 1434.5051 Da that has a difference to calculation value (1434.5083 Da) of 3.2 mDa (accuracy 2.2 ppm) (***Figure 5.5b***). The 1:1 complex with both singly and doubly charged ion were found as well at 1652.6288 Da (calculation: 1652.6378 Da, accuracy 5.4 ppm) (***Figure 5.5d***) and 848.8141 Da (calculation: 848.8048 Da, accuracy 10.9 ppm) (***Figure 5.5c***), respectively. These results indicated that the LPA and β-CD complex has a sufficiently strong binding affinity. As a comparison, the mass spectrum of the mixture of Fc and β-CD shows no complex signal (***Figure 5.6***), indicating that the binding affinity between Fc and β-CD was lower than that of LPA and β-CD.

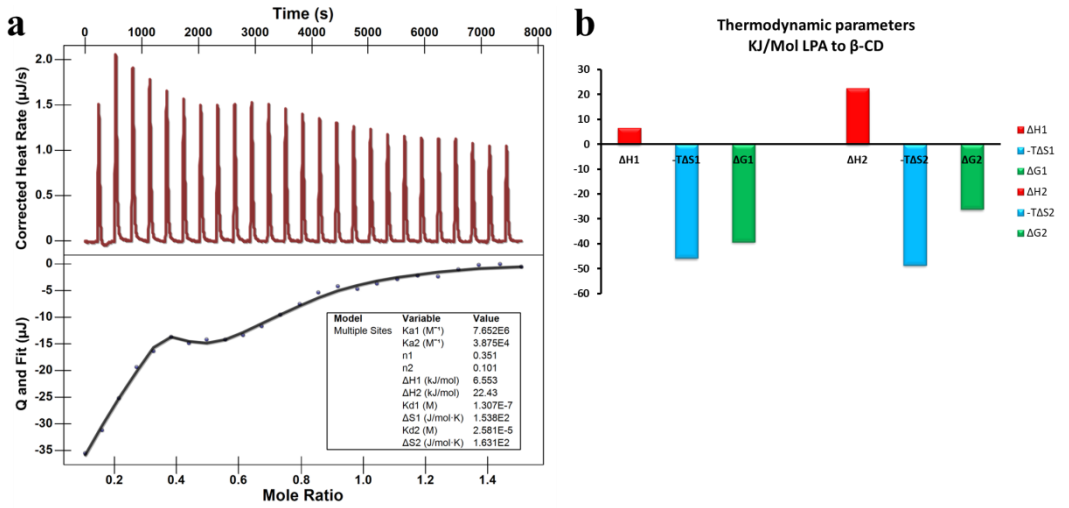

Figure 5.7. a) ITC titration and simulation curves obtained by injecting LPA solution (0.5 mM in pure water; the volume of each injection: 10 µL) to a β-CD solution (0.1 mM in pure water). β-CD was placed in the reaction cell of ITC instrument at 298.15 K. b) The thermodynamic parameters obtained from the fitting of ITC titration curve.

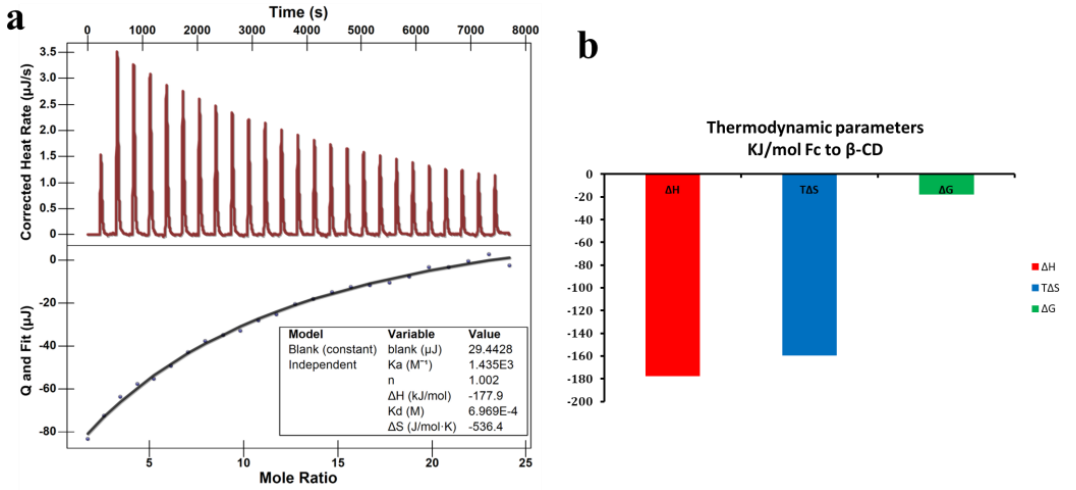

Figure 5.8. a) The ITC titration and simulation curves obtained by injecting an Ferrocene solution (2.50 mM in pure water; the volume of each injection: 10μL) to a β-CD solution (0.163 mM in pure water) placed in the reaction cell of ITC instrument at 298.15K; b) The thermodynamic parameters obtained from the simulation of ITC titration curve: Ferrocene to β-CD.

For further quantification of the binding affinity between LPA and β-CD, isothermal titration calorimetry (ITC) was employed to measure the binding affinity of LPA/β-CD (***Figure 5.7a***). The modulation process was carried out by two binding site mode according to the complex 1:2 of PLA and β-CD observing from NMR and HRMS. It shows that the first binding constant K_{a1} (7.65×10^6 M^{-1}) was two orders of magnitude higher than that of the second binding constant K_{a2} (3.88×10^4 M^{-1}) indicating that the 1:1 complex mode was more favorable than the 1:2 complex mode. Additionally, the K_{a1} was three orders of magnitude higher than that of Fc/β-CD (1.43×10^3 M^{-1} in ***Figure 5.8a***). The stronger interaction between LPA and β-CD ensured quick replacement of Fc by LPA, resulting in the decross-linking of **P2** and **P3**. To further understand this competitive substitution process, the thermodynamic parameters were calculated from the ITC measurements (***Figure 5.7b*** and ***Figure 5.8b***). The interaction of LPA/β-CD was driven by favorable entropic changes ($T\Delta S > 0$) with the unfavorable enthalpic changes ($\Delta H > 0$) that are more like to the thermodynamic parameter of traditional hydrophobic interaction.[189] While the interaction of Fc/β-CD undergoing favorable enthalpic ($\Delta H < 0$) and unfavorable entropic ($T\Delta S < 0$) changes shows characteristic of

the thermodynamic parameter of untraditional host-guest interaction.[190] Therefore, LPA could serve as a competitive guest molecule to break the non-covalent cross-linking between Fc and β-CD in the DCSH.

Finally, the concentration dependent measurements of the **DCSH** sensor upon LPA addition in mimic plasma condition were investigated to test the responsibility and selectivity. Considering the complexity of plasma, only the major compounds in plasma (including NaCl, glucose, urea, Glycerophosphoric acid (GPA), and lysophosphatidylcholine (LPC)) were selected to measure the SPR-OWS of **DCSH** with physiological concentrations (***Figure 5.9***). It was shown that glucose and LPC, besides LPA, also caused responsive behavior of the **DCSH** sensor due to their special structures that would interact with β-CD at a sufficiently high concentration. In the vitro samples of blood plasma, LPC was thought to be transformed to LPA within short time and would not exist for later detection. Nevertheless, it was assumed that the high binding affinity between LPA and β-CD would be beneficial for this competitive guest interaction even though the interferential composition like glucose in plasma has much higher concentrations. Therefore, taking all of the interferential compositions together with different amount of LPA, the concentration dependent SPR-OWS were measured (***Figure 5.10a***) and plots of reflective intensity as well as layer thickness were obtained (***Figure 5.10b and c***). An exponential correlation ($R^2 = 0.89$ for reflective intensity and $R^2 = 0.99$ for layer thickness) were obtained over a LPA concentration range from 2 to 30 μM in mimic plasma conditions. This approach was highly sensitive with the limit of detection at 1.36 μM,[194] which is thought to be below the cutoff value of LPA in early-state ovarian cancer.

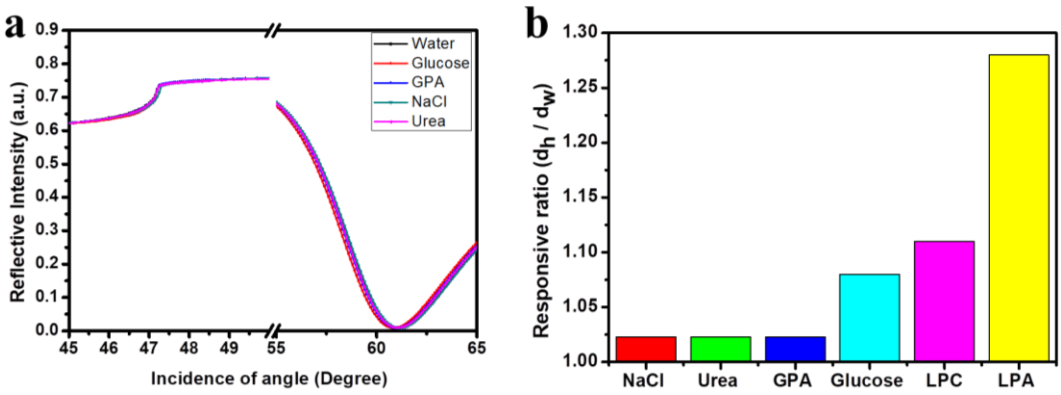

Figure 5.9. a) SPR-OWS curves of the **DCSH** with different chemical agents in mimic plasma concentrations: Glucose (3 mM), GPA (10 μM), NaCl (100 mM) and Urea (5 mM). b) Responsive ratio (where d_h is the layer thickness of hydrogel in diverse components and d_w is the layer thickness of hydrogel in water) of **DCSH** in the presence of major blood plasma components. NaCl (100 mM), Urea (5 mM), Glucose (3 mM), GPA (10 μM), LPC (10μM), LPA (50μM).

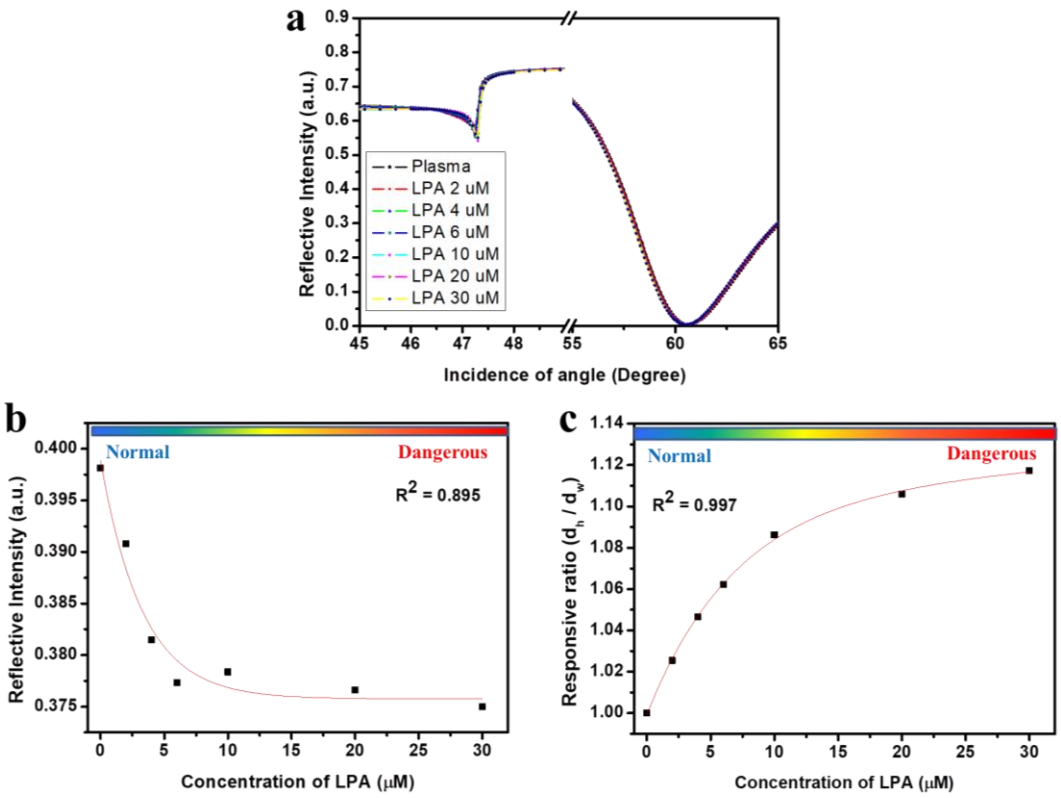

Figure 5.10. a) Concentration dependent measurements of **DCSH** with different concentrations of LPA in mimic plasma by using SPR-OWS method. The spectrum was break from 49° to 55°. b) Plot of reflective intensity against concentration of LPA in mimic plasma from measured SPR-OWS at a certain angle of incidence at 57° and its

nonlinear fitting. c) Plot of layer thickness against concentration of LPA from simulated parameters of SPR-OWS and its nonlinear fitting.

5.4 Conclusions

In summary, a template copolymer based **DCSH** was designed and a supramolecular hydrogel based sensor for cancer biomarker detection was developed. The **DCSH** structure was built by introducing DMIEA as the covalent bonding via [2+2] cyclization and ferrocene and β-cyclodextrin as the noncovalent bonding via host-guest interaction. LPA with higher binding affinity to β-CD was used as the competitive guest to replace Fc, verifying that the noncovalent bonding of the **DCSH** could be broken resulting in the swelling of the **DCSH**. Further, the **DCSH** was immobilized on a gold surface to obtain a sensor chip. The n_h and d_h of the **DCSH** were determined independently by using SPR-OWS measurements. The sensitivity, reversibility and universality of the sensor chip to LPA were investigated, demonstrating the **DCSH** could be used as a SPR-OWS sensor for LPA detection under mimic plasma condition. This method opens a new strategy to build a **DCSH** based SPR-OWS sensor for cancer biomarker detection. The **DCSH** is thought to be easily modified with other molecular recognition pairs to be used potentially as a SPR biosensor for other cancer biomarkers detection.

Chapter Six: Dually cross-linked supramolecular gel for barbiturates detection

6.1 Introduction

Gels from either covalent cross-linking or noncovalent cross-linking could form soft materials, which has been widely investigated for long time from its constructions to its applications.[191,192] Such gels could use organic as well as aqueous solvents according to their hydrophobicity or hydrophilicity.[193] Among them, supramolecular polymers based gels were more considered because of their reversible interactions, responsive behaviors and easy formation.[195,196] Organogels, which formed a gel in organic solvents are usually derived from weak forces such as hydrogen bonding and π-stacking interactions, and are used e.g. as organic electronic devices and sensors.[193] Therefore, developing such kind of organogel sensor based on supramolecular polymers was important especially in detection of hydrophobic analytes.

Thymine as one of the basic group to form base pair with adenine in DNA has been widely known as a multiple hydrogen bonding system and was also used as supramolecular polymer building block.[197–202] Another multiple hydrogen bonding host called Hamilton receptor, which was firstly reported in 1990 was also widely reported owing to its high binding affinity to barbiturates and cyanuric acid.[203,204] Later, this multiple hydrogen bonding pair was used in diverse areas such as nanoparticles loading onto surface,[205,206] separation of single-walled carbon nanotubes,[207] multiblock copolymer building blocks[208–210] and self-assembled dendrimers.[211] From the structure point of view, thymine has the similar imide group as cyanuric acid or barbiturate, which could also interact with Hamilton receptor. But this interaction maximum could form three hydrogen bonds less than that of barbiturate (six hydrogen bonds). It could be expected that the binding affinity between thymine and Hamilton

receptor would be much lower compared with barbiturates. Based on this, it was assumed that the interaction pair of Hamilton receptor and thymine can form reversible cross-links that can be broken by addition of barbiturates. Thus, according to this principle supramolecular polymers can be used as a sensor to detect hydrophobic barbiturates.

Herein, Hamilton receptor and thymine as a partly multiple hydrogen bonding pair was introduced to detect barbiturates. The principle was confirmed by ^{1}H NMR showing that the binding affinity between Hamilton receptor and thymine was three orders of magnitude lower than that of Hamilton receptor and barbiturates. Then, dually cross-linked supramolecular gels (**DCSG**) were prepared after spin coating onto a gold surface in chloroform solution, UV-Vis irradiating and equilibrating in chloroform. SPR-OWS was used to detect the responsive behavior towards addition of barbiturates. However, the layer thickness as well as the refractive index was not changed during the responsive process. It was speculated that the hydrogen binding between Hamilton receptor and thymine was broken during the swelling process owing to their really low binding affinity. Therefore, the molecular recognition pair should be optimized further.

6.2 Experimental section

6.2.1 Materials and Instruments

Methyl acrylate (> 99.0 %, TCI), thionyl chloride (> 99.0 %, Sigma Aldrich) were distilled before used. 2,2'-azobis(2-methylpropionitrile) (AIBN) (98 %, Sigma Aldrich) was recrystallized from methanol before used. The following chemicals were purchased from commercial sources and used as received. 2, 6-diaminopyridine (98 %, Acros Organics), 3-bromo-1-propanol (97 %, Sigma Aldrich), 5-hydroxyisophthalic acid (99 %, Acros Organics), 18-crown-6 (99 %, Acros Organics), acryloyl chloride (96 %, Alfa Aesar), dimethymaleic anhydride (97 %, Acros Organics), ethanolamine (98 + %, Alfa Aesar), triethylamine (TEA) (99.7 %, Acros Organics), benzoyl chloride (99 + %, Alfa Aesar), butyryl chloride (99 %, Acros Organics), HCl in dioxane (3 M, Alfa Aesar), *tert*-butylchlorodimethylsilane (98 %, Acros Organics), thymine (> 98 %, TCI), TBAF

in THF (1 M, Acros Organics), *tert*-butyl (2-bromoethyl)carbamate (≥ 97 %, Sigma Aldrich). All other normal chemicals and solvents were of analytical grade and were used without further purification. Chain transfer agent (CTA): 2-(dodecylthiocarbonothioylthio)-2-methylpropionic acid (DDMAT) was Lab produced according to the literature.[212]

^{1}H and ^{13}C NMR spectra were recorded on a Bruker AV-500 spectrometer (500 MHz for ^{1}H and 125 MHz for ^{13}C), with chemical shifts (δ) reported in ppm relative to the solvent peak (7.26 ppm for $CDCl_3$ and 2.50 ppm for DMSO) and coupling constants (*J*) reported in Hz. High-resolution mass spectra (HRMS) were recorded by electrospray ionization (ESI) on a Waters SYNAPT™ G2 HDMS™. Determination of molar mass distributions was performed by modular gel permeation chromatography (GPC) system at a flow rate of 1 mL/min with a Knauer Smartline RI Detector 2300 and a Merck Hitachi L-4200 UVVIS Detector. The instrument was equipped with a PSS-SDV 10^5 Å and PSS-SDV 10^3 Å column and all samples were calibrated by poly(methylmethacrylate) standards. Photo cross-linking process was performed by an OmniCure® S1500 spot UV curing lamp with a unique and patented 200 Watt Intelli-Lamp.

6.2.2 Synthesis of photo cross-linker[213]

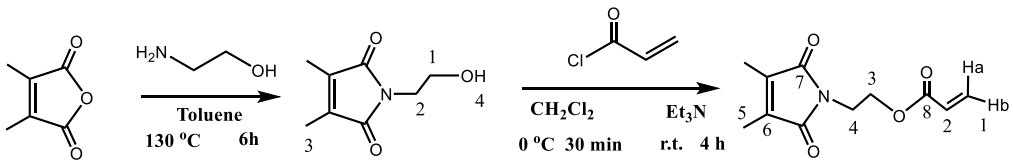

1 2

Synthesis of 1-(2-hydroxyethyl)-3,4-dimethyl-1H-pyrrole-2,5-dione (1)

Dimethylmaleic anhydride (12.67 g, 100 mmol) was added into a flask followed by adding toluene (300 mL) with stirring under argon atmosphere. The mixture was then turned into oil bath at 130 °C followed by adding ethanolamine (12.1 mL, 200 mmol) dropwise within 1 h. After refluxing at 130 °C for 4 h, the mixture was evaporated to remove the solvent. The residue was purified with short column chromatography with 100 mL EtOAc and evaporated the solvent to give rise the final product as a colorless

oil (15.95 g, 94.3 %). ^{1}H NMR (500 MHz, $CDCl_3$) δ (ppm) = 3.70 – 3.64 (m, 2H, H1), 3.61 (t, ^{2}J = 5.3 Hz, 2H, H2), 2.47 (s, 1H, H4), 1.90 (s, 6H, H3).

Synthesis of 2-(3,4-dimethyl-2,5-dioxo-2,5-dihydro-1H-pyrrol-1-yl)ethyl acrylate (2)

Compound **1** (3.656 g, 21.6 mmol) was dissolved in DCM (40 mL) and added into a flask followed by adding Et_3N (6 mL) under stirring. Acryloyl chloride (3.55 mL, 43.3 mmol) was mixed with DCM (10 mL) and added into the flask dropwise within 30 min at 0 ºC. After stirring for another 4 h at room temperature, the mixture was filtered to remove the solid. The solution was washed with saturated brine (3 × 50 mL), dried with $MgSO_4$ and concentrated by evaporation. The final product was obtained after purification by column chromatography (n-hexane/ EtOAc = 2/1) as a light yellow oil (2.881g, 59.7%). ^{1}H NMR (500 MHz, $CDCl_3$) δ (ppm) = 6.37 (dd, ^{2}J = 17.3, ^{3}J = 1.4 Hz, 1H, H1a), 6.07 (dd, ^{2}J = 17.3, ^{3}J = 10.5 Hz, 1H, H1b), 5.82 (dd, ^{3}J = 10.5, ^{3}J = 1.4 Hz, 1H, H2), 4.33 – 4.25 (m, 2H, H3), 3.86 – 3.76 (m, 2H, H4), 1.96 (s, 6H, H5). ^{13}C NMR (126 MHz, $CDCl_3$) δ (ppm) = 171.79 (C7), 165.79 (C8), 137.37 (C2), 131.23 (C1), 128.02 (C6), 61.81 (C4), 36.84 (C3), 8.68 (C5). HRMS (ESI-TOF: *m/z* (%)): $[M+Na]^{+}$: Calc. 246.0742, Found 246.0748 (99.5).

6.2.3 Synthesis of primary amine modified Hamilton receptor[209]

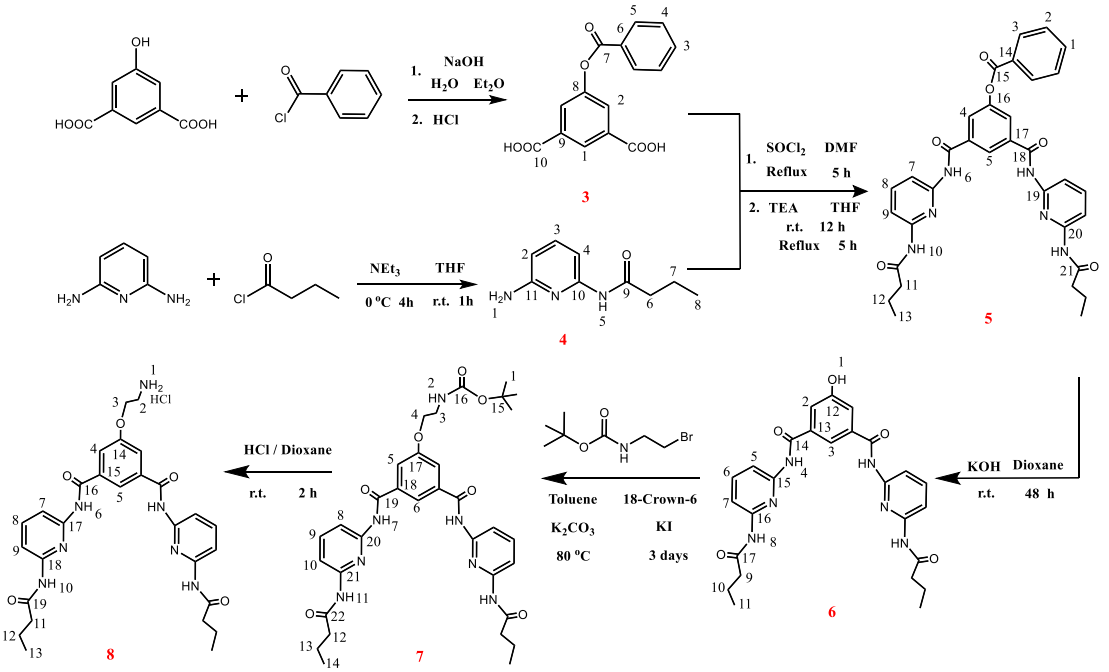

Synthesis of 5-(benzoyloxy)isophthalic acid (3)

5-hydroxyisophthalic acid (13.9g, 75 mmol) and NaOH (9.21g, 230 mmol) were mixed and added into a flask followed by adding distilled water (100 mL) in ice bath under argon atmosphere. Benzoyl chloride (8.6 mL, 75 mmol) was dissolved in Et_2O (50 mL) and added into the flask dropwise within 4 h followed by stirring for another 4 h at room temperature. After that, the water phase was collected and the organic phase was extracted with water (3 × 50 mL). Then the water phase was added hydrochloric acid (saturated) to adjust pH of the water till 2 followed by filtration to collect the solid. The solid was dried to obtain the final product as a white solid (20.22 g, 94.1%). ^{1}H NMR (500 MHz, DMSO-d_6) δ (ppm) = 8.41 (t, ^4J = 1.4 Hz, 1H, H1), 8.19 – 8.15 (m, 2H, H2), 8.04 (d, ^4J = 1.4 Hz, 2H, H3), 7.76 (t, ^3J = 7.5 Hz, 1H, H3), 7.62 (t, ^3J = 7.6 Hz, 2H, H4). ^{13}C NMR (126 MHz, DMSO-d_6) δ (ppm) = 166.49 (C10), 164.91 (C7), 151.13 (C9), 134.65 (C8), 133.96 (C6), 130.43 (C1), 129.42 (C2), 129.13 (C3), 127.85 (C5), 126.95 (C4).

Synthesis of N-(6-aminopyridin-2-yl)butyramide (4)

2, 6-diaminopyridine (10.02g, 64 mmol) was added into a flask followed by adding THF (200 mL) and TEA (12.6 mL, 64 mmol) with stirring under argon atmosphere. Butyryl chloride (9.6 mL, 64 mmol) was dissolved in of THF (20 mL) and then added into the flask dropwise within 1 h in ice bath. Next, the mixture was stirred at 0 ^{o}C for 3 h and at room temperature for 1 h. After that, the solvent was removed by evaporation and the residue was suspended in EtOAc (200 mL). The solution was collected after filtration to remove insoluble solid and evaporated to remove the solvent. The residue was recrystallized in MeOH to give rise to the final product as a light yellow needle (9g, yield: 81.8%). ^{1}H NMR (500 MHz, DMSO-d_6) δ (ppm) = 9.72 (s, 1H, H5), 7.31 (t, ^3J = 7.9 Hz, 1H, H3), 7.23 (d, ^3J = 7.8 Hz, 1H, H4), 6.15 (d, ^3J = 7.9 Hz, 1H, H2), 5.66 (s, 2H, H1), 2.29 (t, ^3J = 7.3 Hz, 2H, H6), 1.56 (m, 2H, H7), 0.88 (t, ^3J = 7.4 Hz, 3H, H8). ^{13}C NMR (126 MHz, DMSO-d_6) δ (ppm) = 171.56 (C9), 158.40 (C10), 150.47 (C11), 138.75 (C2), 103.16 (C4), 100.89 (C3), 38.00 (C6), 18.46 (C7), 13.55 (C8).

Synthesis of 3,5-bis((6-butyramidopyridin-2-yl)carbamoyl)phenyl benzoate (5)

Compound **3** (5.48 g, 11.47 mmol) was suspended in thionyl chloride (75 mL) in a flask followed by adding DMF (0.73 mL) with stirring under argon atmosphere. Then the mixture was refluxed at 80 ºC for 5 h. After that, the excess thionyl chloride was removed by reduced pressure distillation (55 ºC, 170 mbar). The residue was used without any further purification and was dissolved in THF (15 mL) for the next step. Next, compound **4** (4.53 g, 23 mmol) was dissolved in THF (60 mL) and added into a flask followed by adding the THF solution (15 mL) dropwise with stirring under argon atmosphere at 0 ºC (ice bath). The mixture was stirred at room temperature overnight and then the solvent was removed by evaporation. Then, to the residue DCM (200 mL) and water (100 mL) were added followed by collecting the organic phase. The water phase was extracted with DCM (3 × 100 mL). All the organic phase was washed with water (pH =1 and pH = 11) and dried with $MgSO_4$, concentrated by evaporation and precipitated in Et_2O to obtain the final product as a light brown solid (3.02 g, 43.3 %). ^{1}H NMR (500 MHz, $CDCl_3$) δ (ppm) = 8.63 (s, 2H, H6), 8.27 (s, 2H, H10), 8.19 (s, 1H, H5), 8.08 (d, ^3J = 7.3 Hz, 2H, H3), 7.89 (m, 4H, H4 and H8), 7.83 (d, ^3J = 8.0 Hz, 2H, H7), 7.63-7.57 (m, 3H, H1 and H2), 7.46 (t, ^3J = 7.8 Hz, 2H, H9), 2.33 (t, ^3J = 7.4 Hz, 4H, H11), 1.77 – 1.69 (m, 4H, H12), 0.97 (t, ^3J = 7.4 Hz, 6H, H13). ^{13}C NMR (126 MHz, $CDCl_3$) δ (ppm) = 172.01 (C18), 165.10 (C21), 163.66 (C15), 151.50 (C17), 149.87 (C19), 149.00 (C20), 140.85 (C14), 136.03 (C16), 134.30 (C5), 130.31 (C7), 128.75 (C9), 128.33 (C4), 124.89 (C8), 122.97 (C3), 110.29 (C2), 109.74 (C1), 39.47 (C11), 18.78 (C12), 13.70 (C13).

Synthesis of N^1,N^3-bis(6-butyramidopyridin-2-yl)-5-hydroxyisophthalamide (6)

Compound **5** (1 g, 1.64 mmol) was added into a flask followed by adding dioxane (400 mL) with stirring. KOH (1.84 g) was dissolved in water (200 mL) and added dropwise into the flask with stirring. The mixture was stirred at room temperature for 48 h. Then the solvent of dioxane was evaporated to give a water solution followed by adding HCl (saturated) to adjust the pH to 2. The solution was then concentrated to 25 mL to obtain a suspension followed by collected the solid and washed it with cooled water and cooled

EtOAc to give the final product as a brown solid (369 mg, 44.5%). ^{1}H NMR (500 MHz, DMSO-d_6) δ (ppm) = 11.07 (s, 2H, H4), 10.98 (s, 2H, H8), 8.16 (s, 1H, H3), 7.99 (t, ^{3}J = 8.1 Hz, 2H, H6), 7.72 (d, ^{3}J = 7.9 Hz, 2H, H5), 7.67 (d, ^{3}J = 8.1 Hz, 2H, H7), 7.61 (d, ^{34}J = 1.3 Hz, 2H, H2), 6.38 (s, 1H, H1), 2.45 (t, ^{3}J = 7.3 Hz, 4H, H8), 1.72 – 1.53 (m, 4H, H9), 0.92 (t, ^{3}J = 7.4 Hz, 6H, H10). ^{13}C NMR (126 MHz, DMSO-d_6) δ (ppm) = 173.72 (C14), 166.40 (C17), 158.35 (C15), 149.88 (C16), 149.12 (C13), 142.66 (C12), 135.34 (C3), 119.21 (C5), 118.66 (C7), 110.37 (C2), 109.89 (C6), 38.46 (C9), 18.66 (C10), 13.99 (C11). HRMS (ESI-TOF: *m/z* (%)): $[M-H]^-$: Calc. 503.2043, Found 503.2039 (85.8).

Synthesis of tert-butyl (2-(3,5-bis((6-butyramidopyridin-2-yl)carbamoyl)phenoxy) ethyl)carbamate (7)

Compound **6** (403 mg, 0.8 mmol), *tert*-butyl (2-bromoethyl)carbamate (224 mg, 1 mmol), K_2CO_3 (448 mg, 3.2 mmol) and KI (16 mg, 0.08 mmol) were mixed and added into a flask followed by adding toluene (20 mL) with stirring under argon atmosphere. Then, 18-crown-6 (212 mg, 0.8 mmol) was added into the mixture followed by stirring at 80 ºC for 48 h. After that, the solvent was removed by evaporation followed by adding 50 mL water and extracted with EtOAc (3 × 50 mL). The organic phase was washed with saturated ammonium chloride (3 × 20 mL) and brine (3 × 20 mL), dried with $MgSO_4$, concentrated to 5 mL by evaporation and precipitated in hexane to give the final product as a yellow solid (426 mg, 82.2 %). ^{1}H NMR (500 MHz, DMSO-d_6) δ (ppm) = 10.46 (s, 2H, H7), 10.07 (s, 2H, H11), 8.13 (s, 1H, H6), 7.86 – 7.81 (m, 4H, H8 and H9), 7.77 (m, 2H, H10), 7.71 (d, ^{4}J = 1.4 Hz, 2H, H5), 7.05 (t, ^{3}J = 5.2 Hz, 1H, H2), 4.14 (t, ^{3}J = 5.7 Hz, 2H, H4), 3.36 (m, 2H, H3), 2.39 (t, ^{3}J = 7.3 Hz, 4H, H12), 1.61 (dt, ^{2}J = 14.7, ^{3}J = 7.4 Hz, 4H, H13), 1.39 (s, 9H, H1), 0.91 (t, ^{3}J = 7.4 Hz, 6H, H14). ^{13}C NMR (126 MHz, DMSO-d_6) δ (ppm) = 172.54 (C19), 165.33 (C16), 158.94 (C22), 156.19 (C20), 151.07 (C21), 150.55 (C18), 140.46 (C17), 136.09 (C6), 120.36 (C8), 117.77 (C10), 111.03 (C5), 110.46 (C9), 78.33 (C15), 61.94 (C3), 43.78 (C4), 38.48 (C12), 28.71 (C1), 18.89 (C13), 14.03 (C14).

Synthesis of 5-(2-aminoethoxy)-N^1,N^3-bis(6-butyramidopyridin-2-yl)isophthalamide hydrochloride (8)

Compound **7** (426 mg, 0.56 mmol) was added into a flask followed by adding HCl in dioxane (10 mL, 3 M) with stirring under argon atmosphere. The mixture was stirred for 2 h at room temperature followed by centrifugation and washed with Et_2O to obtain the finals product as a yellow solid (362 mg, 94.3 %). ^{1}H NMR (500 MHz, DMSO-d_6) δ (ppm) = 11.27 (s, 2H, H6), 10.96 (s, 2H, H10), 8.42 (s, 3H, H1), 8.36 (s, 1H, H5), 7.99 (t, ^3J = 8.1 Hz, 2H, H8), 7.88 (d, ^4J = 1.0 Hz, 2H, H4), 7.78 (d, ^3J = 7.9 Hz, 2H, H7), 7.70 (d, ^3J = 8.1 Hz, 2H, H9), 4.43 (t, ^3J = 5.1 Hz, 2H, H3), 3.27 (dd, ^2J = 10.4, ^3J = 5.3 Hz, 2H, H2), 2.45 (t, ^3J = 7.3 Hz, 4H, H11), 1.63 (m, 4H, H12), 0.92 (t, ^3J = 7.4 Hz, 6H, H13). ^{13}C NMR (126 MHz, DMSO-d_6) δ (ppm) = 173.64 (C16), 165.94 (C19), 158.47 (C17), 149.50 (C18), 149.01 (C15), 142.47 (C14), 135.44 (C5), 121.15 (C7), 118.76 (C9), 110.56 (C4), 110.07 (C8), 65.63 (C2), 38.67 (C3), 38.45 (C11), 18.68 (C12), 14.00 (C13). HRMS (ESI-TOF: *m/z* (%)): $[M+H]^+$: Calc. 548.2621, Found 548.2639 (100).

6.2.4 Synthesis of primary amine modified thymine[214]

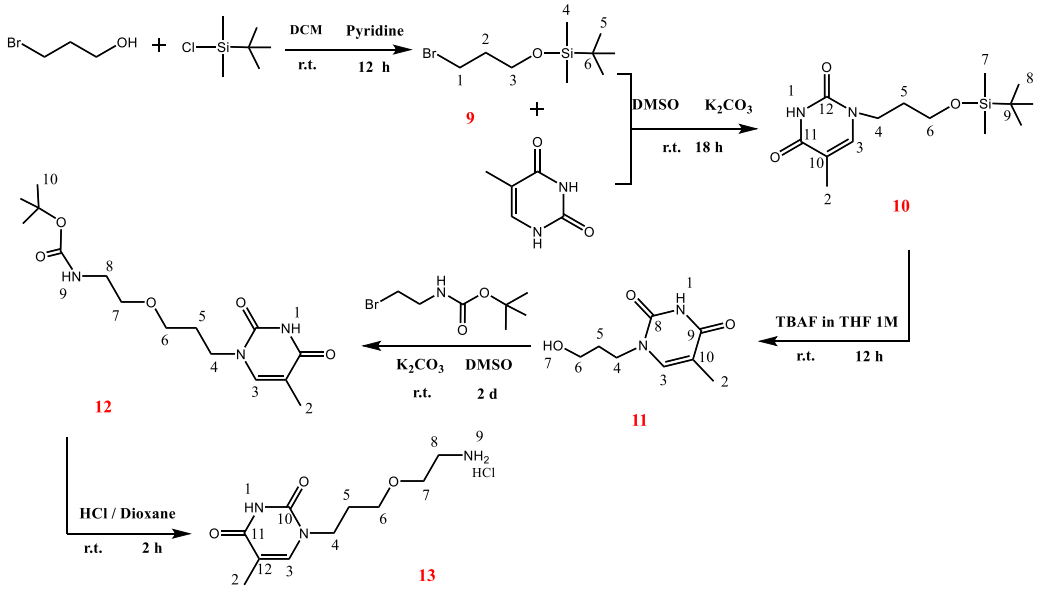

Synthesis of (3-bromopropoxy)(tert-butyl)dimethylsilane (9)

tert-Butylchlorodimethylsilane (15.2 g, 0.1 mol) was dissolved in 100 mL DCM and

added into a flask followed by adding 3-bromo-1-propanol (8.9 mL, 0.1 mol) with stirring under argon atmosphere. Then the system was poured into an ice bath followed by adding pyridine (9.66 mL) and stirring for 10 m. Next, the mixture was stirred at room temperature overnight followed by filtration to remove the solid. The organic phase was washed with water (2 × 50 mL) and the water phase extracted with DCM (50 mL). Then, the combined organic phase was collected, dried with $MgSO_4$ and evaporated to remove the solvent to obtain the final product as colorless oil (20.28 g, 80.1 %). ^{1}H NMR (500 MHz, $CDCl_3$) δ (ppm) = 3.73 (t, ^3J = 5.7 Hz, 2H, H1), 3.51 (t, ^3J = 6.5 Hz, 2H, H3), 2.07 – 1.99 (m, 2H, H2), 0.90 (s, 9H, H5), 0.07 (s, 6H, H4). ^{13}C NMR (126 MHz, $CDCl_3$) δ (ppm) = 60.44 (C6), 35.59 (C1), 30.59 (C3), 25.89 (C2), 18.28 (C5), -5.39 (C4).

Synthesis of 1-(3-((tert-butyldimethylsilyl)oxy)propyl)-5-methylpyrimidine-2,4(1H, 3H)-dione (10)

Compound **9** (3.8 g, 15 mmol), thymine (5 g, 40 mmol) and K_2CO_3 (5.5 g, 44 mmol) were mixed and added into a flask followed by adding DMSO (130 mL) with stirring under argon atmosphere. Then, the mixture was stirred at room temperature for 2 d followed by filtrating to remove the solid. After that, the solvent was removed by reduced pressure distillation. The residue was suspended in water (300 mL) and extracted with chloroform (4 × 100 mL). The organic phase was dried with $MgSO_4$ and evaporated the solvent to give the final product as a white solid (1.72 g, 76.8 %). ^{1}H NMR (500 MHz, $CDCl_3$) δ (ppm) = 9.00 (s, 1H, H1), 7.05 (s, 1H, H3), 3.82 (t, ^3J = 6.7 Hz, 2H, H4), 3.64 (t, ^3J = 5.7 Hz, 2H, H6), 1.90 (d, ^4J = 1.2 Hz, 3H, H2), 1.88-1.85 (m, 2H, H5), 0.90 (s, 9H, H8), 0.05 (s, 6H, H7). ^{13}C NMR (126 MHz, $CDCl_3$) δ (ppm) = 164.52 (C12), 151.02 (C11), 141.58 (C10), 110.12 (C3), 59.24 (C9), 45.97 (C4), 31.33 (C6), 26.01 (C5), 18.35 (C8), 12.38 (C2), -5.30 (C7).

Synthesis of 1-(3-hydroxypropyl)-5-methylpyrimidine-2,4(1H,3H)-dione (11)

Compound **10** (2.4 g, 8 mmol) was added into a flask followed by adding TBAF in THF (40 mL, 1 M) with stirring under argon atmosphere. The mixture was stirred for 12 h at

room temperature followed by evaporation to remove the solvent. The residue was purified by short column chromatography with THF as a solvent to obtain a light yellow solid. The final product was obtained via recrystallization in iso-propanol (1.306 g, 87.9 %). ^{1}H NMR (500 MHz, DMSO-d_6) δ (ppm) = 11.15 (s, 1H, H1), 7.47 (s, 1H, H3), 4.53 (t, ^{3}J = 5.1 Hz, 1H, H7), 3.67 (t, ^{3}J = 8.1 Hz, 2H, H4), 3.41 (dd, ^{3}J = 11.3, ^{3}J = 6.1 Hz, 2H, H6), 1.75 (d, ^{4}J = 1.0 Hz, 3H, H2), 1.73–1.69 (m, 2H, H5). ^{13}C NMR (126 MHz, DMSO-d_6) δ (ppm) = 164.77 (C8), 151.34 (C9), 142.12 (C10), 108.74 (C3), 58.22 (C4), 45.38 (C6), 31.99 (C5), 12.37 (C2). HRMS (ESI-TOF: *m/z* (%)): $[M-H]^-$: Calc. 183.0770, Found 183.0772 (100).

Synthesis of tert-butyl(2-(3-(5-methyl-2,4-dioxo-3,4-dihydropyrimidin-1(2H)-yl) propoxy)ethyl)carbamate (12)

Compound **11** (370 mg, 2 mmol), *tert*-butyl (2-bromoethyl)carbamate (500 mg, 2.5 mmol) and K_2CO_3 (2.76 g) were mixed and added into a flask followed by adding DMSO (30 mL) under argon atmosphere. The mixture was then stirred for 2 d at room temperature followed by evaporating the solvent by reduced pressure distillation to remove the solvent. After that, to the residue DCM (20 mL) was added and all was filtrated to remove the insoluble solid. The solution was precipitated in Et_2O to obtain the final product as a white solid. ^{1}H NMR (500 MHz, $CDCl_3$) δ (ppm) = 7.02 (d, ^{4}J = 1.2 Hz, 1H, H3), 4.96 (s, 1H, H9), 4.13 – 4.11 (m, 2H, H8), 3.89 (t, ^{3}J = 6.3 Hz, 2H, H4), 3.64 – 3.62 (m, 2H, H6), 1.91 (d, ^{4}J = 1.4 Hz, 3H, H2), 1.91–1.87 (m, 2H, H5), 1.38 (s, 9H, H10), 1.13–1.11 (m, 2H, H7). HRMS (ESI-TOF: *m/z* (%)): $[M+Na]^+$: Calc. 350.1692, Found 350.1701; $[M+K]^+$: Calc. 366.1431, Found 366.1443.

Synthesis of 1-(3-(2-aminoethoxy)propyl)-5-methylpyrimidine-2,4(1H,3H)-dione hydrochloride (13)

Compound **12** (100 mg) was added into a flask followed by adding HCl in Dioxane (5 mL, 3 M) under argon atmosphere. The mixture was stirred for 2 h followed by precipitation in Et_2O. The solid was washed with Et_2O for 3 times to give the final product as a white solid. ^{1}H NMR (500 MHz, DMSO-d_6) δ (ppm) = 8.00 (s, 3H, H9),

7.61 (d, ^{4}J = 1.2 Hz, 1H, H3), 4.62 (s, 1H, H1), 4.07 (t, ^{3}J = 6.1 Hz, 2H, H4), 3.76 (t, ^{3}J = 7.1 Hz, 2H, H7), 3.45 (t, ^{3}J = 6.1 Hz, 2H, H6), 3.00 (m, 2H, H8), 1.83 (d, ^{4}J = 1.0 Hz, 3H, H2), 1.79 – 1.74 (m, 2H, H5). ^{13}C NMR (126 MHz, DMSO-d_6) δ (ppm) = 164.02 (C10), 151.71 (C11), 141.14 (C12), 108.09 (C3), 58.23 (C4), 46.65 (C8), 38.83 (C6), 37.71 (C7), 31.84 (C5), 12.98 (C2).

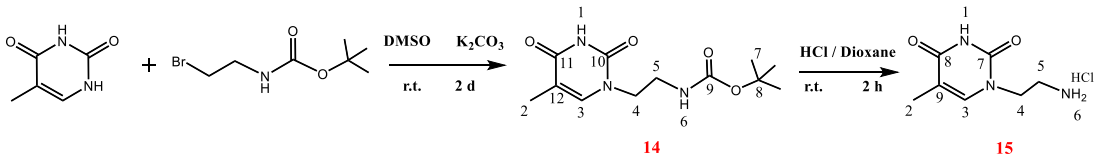

Synthesis of tert-butyl (2-(5-methyl-2,4-dioxo-3,4-dihydropyrimidin-1(2H)-yl)ethyl) carbamate (14)

Thymine (1.26 g, 10 mmol) and *tert*-butyl (2-bromoethyl)carbamate (900 mg, 4 mmol) were mixed and added into a flask followed by adding K_2CO_3 (1.12 g) and DMSO (50 mL) with stirring under argon atmosphere. The mixture was then stirred for 2 d at room temperature. After that, the solvent was removed by reduced vacuum followed by adding water (100 mL) and extracting with chloroform (3 × 50 mL). The organic phase was dried with $MgSO_4$ and the solvent was evaporated followed by precipitating in Et_2O/n-hexane (V:V = 1:1) (100 mL) to give the final product as a white solid (369 mg, 34.2 %). ^{1}H NMR (500 MHz, DMSO-d_6) δ (ppm) = 11.11 (s, 1H, H1), 7.29 (s, 1H, H3), 6.87 (s, 1H, H6), 3.63 (t, ^{3}J = 5.3 Hz, 2H, H4), 3.15 (m, 2H, H5), 1.73 (s, 3H, H2), 1.33 (s, 9H, H7). ^{13}C NMR (126 MHz, DMSO-d_6) δ (ppm) = 164.50 (C10), 151.52 (C11), 141.89 (C12), 136.24 (C9), 107.86 (C3), 77.86 (C8), 47.85 (C5), 37.75 (C4), 28.27 (C7), 12.57 (C2). HRMS (ESI-TOF: *m/z* (%)): $[M+Na]^+$: Calc. 292.1273, Found 292.1268 (100).

Synthesis of 1-(2-aminoethyl)-5-methylpyrimidine-2,4(1H,3H)-dione hydrochloride (15)

Compound **14** (135 mg, 0.5 mmol) was added into a flask followed by adding HCl in dioxane (5 mL, 3 M) under stirring at room temperature. The mixture was stirred for 2 h followed by evaporated the solvent. The residue was washed with Et_2O to obtain the

final product as a white solid (91mg, 83 %). ^{1}H NMR (500 MHz, DMSO-d_6) δ (ppm) = 11.25 (s, 1H, H1), 8.19 (s, 3H, H6), 7.55 (s, 1H, H3), 3.91 (t, ^{3}J = 5.8 Hz, 2H, H4), 3.08–3.05 (m, 2H, H5), 1.75 (s, 3H, H2). ^{13}C NMR (126 MHz, DMSO-d_6) δ (ppm) = 164.54 (C7), 151.49 (C8), 141.37 (C9), 108.91 (C3), 45.26 (C5), 37.80 (C4), 12.11 (C2). HRMS (ESI-TOF: *m/z* (%)): $[M+H]^{+}$: Calc. 170.0930, Found 170.0926 (100).

6.2.5 Copolymerization of P(MA-*co*-DMIA-*co*-VDMA)

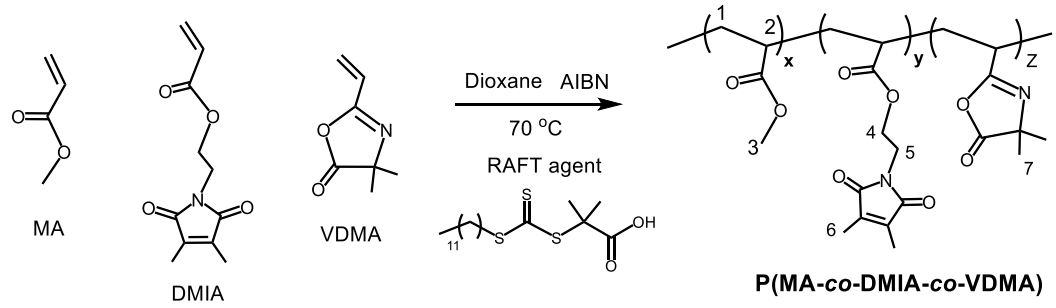

MA (3.5g, 36 mmol), DMIA (0.45g, 2 mmol) and VDMA (0.28g, 2 mmol) were mixed and added into a flask followed by adding RAFT agent (14.4 mg, 0.04 mmol), AIBN (3.3 mg, 0.02 mmol) and dioxane (13.5 mL). The mixture was stirred under argon atmosphere for 30 min at room temperature and then turned into the oil bath at 70 °C for 24 h. After the reaction was cooled to room temperature, the mixture was precipitated in cooled n-hexane and dissolved in DCM to repeat this process for 2 times to give the final product P(MA-*co*-DMIA-*co*-VDMA) as a white solid (3.6 g, 85.1 %). ^{1}H NMR (500 MHz, $CDCl_3$) δ (ppm) = 4.15 (s, 2H, H4), 3.8 –3.43 (m, 78H, H5 and H3), 2.30 (s, 27H, H2), 1.96-1.92 (m, 18H, H6 and H1), 1.75–1.59 (m, 26H, H1), 1.51–1.48 (m, 10H, H1), 1.40 (s, 8H, H7).

6.2.6 Post polymerization of P(MA-*co*-DMIA-*co*-VDMA) with Hamilton receptor and thymine

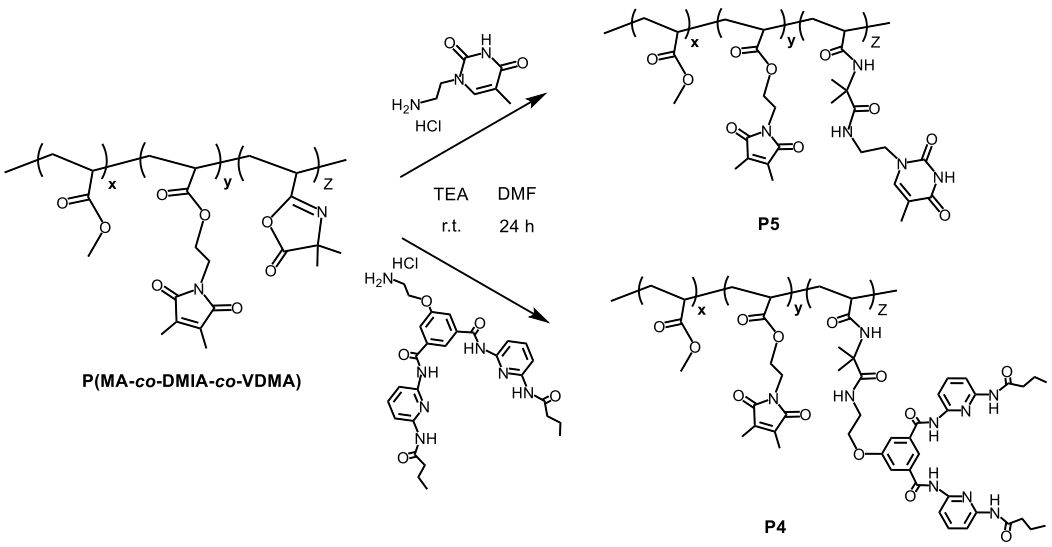

P4

Copolymer P(MA-*co*-DMIA-*co*-VDMA) (300 mg) was added into a flask followed by adding compound **8** (60 mg), DMF (5 mL) and TEA (0.1 mL). The mixture was stirred for 24 h followed precipitated in cooled hexane/Et_2O (V:V = 2:1) to give the solid. After that, the solid was dissolved in chloroform and filtrated to remove insoluble solid. The solution was precipitated in cool hexane/Et_2O again to obtain the final product as a light yellow solid (235 mg, 78.3 %). ^{1}H NMR (500 MHz, DMSO-d_6) δ (ppm) = 10.43 (s, 0.45H), 10.04 (s, 0.57H), 9.65 (s, 1.12H), 8.22 – 7.42 (m, 4.72H), 4.20 – 3.98 (m, 2.15H), 3.57 (s, 60.24H,), 2.36–2.02 (m, 22.97H,), 1.90 (s, 6H,), 1.76 (s, 9.24H,), 1.60 (s, 20.69H,), 1.46 (s, 10.11H,), 1.32 (s, 7.1H,), 0.91 (s, 2H,).

P5

Copolymer P(MA-*co*-DMIA-*co*-VDMA) (300 mg) was added into a flask followed by adding compound **15** (30 mg), DMF (5 mL) and TEA (0.02 mL). Then, the mixture was stirred for 12 h at room temperature followed by precipitated in cooled hexane/Et_2O (V:V = 2:1) to obtain a solid. After that, the solid was dissolved in chloroform and filtrated to remove the insoluble solid. The final product was collected by precipitated the solution in cooled hexane/Et_2O as a light yellow solid (253 mg, 85.7 %). ^{1}H NMR

(500 MHz, DMSO-d_6) δ (ppm) = 7.83 (s, 3.89H), 7.52 (s, 1.1H), 7.30 (s, 1.35H), 4.57 (m, 2.71H), 3.92 (s, 2.24H), 3.58 (s, 59.74H), 2.21 (s, 22.36H), 1.91 (s, 6H), 1.84 (s, 5H), 1.83 – 1.72 (m, 19.52H), 1.62 (s, 17.92H), 1.47 (s, 10H), 1.28 (s, 7.16H).

6.2.7 Determination of layer thickness of SN supramolecular gel with SPR measurements

See 3.2.8

6.3 Results and discussion

6.3.1 Template copolymers P(MA-co-DMIA-co-VDMA) via RAFT polymerization

RAFT polymerization was used to control the uniform distribution of each polymer chain. Here, it was used a CTA 2-(dodecylthiocarbonothioylthio)-2-methylpropionic acid (DDMAT) (synthesized by Xiaoqian Yu). Before use, the ^{1}H and ^{13}C NMR spectra were measured as shown in ***Figure 6.1*** and ***Figure 6.2*** for ^{1}H and ^{13}C NMR spectrum, respectively. From the spectra, the structure was confirmed.

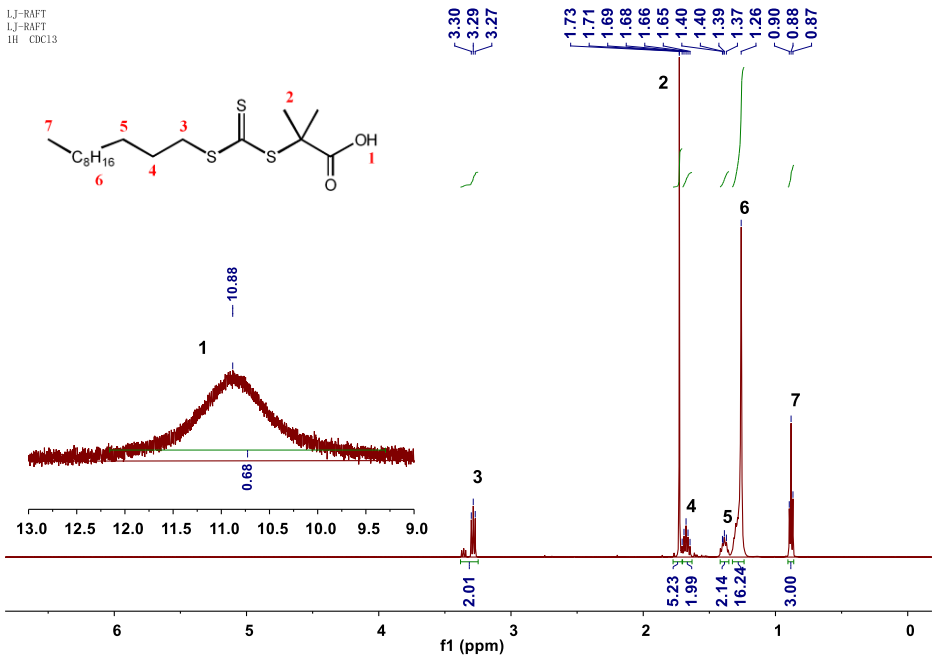

Figure 6.1. ^{1}H NMR spectrum of RAFT agent in $CDCl_3$.

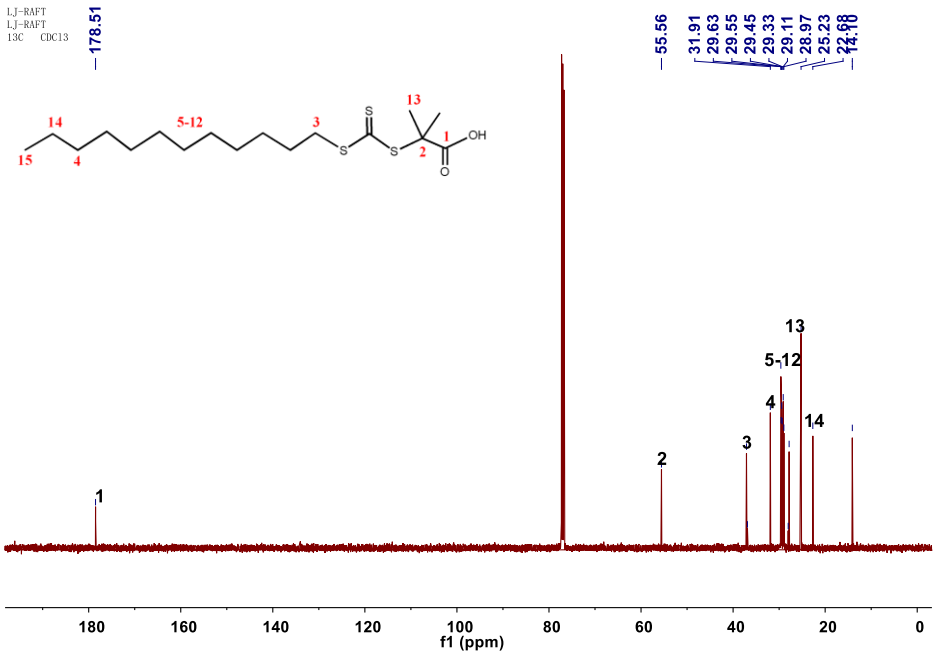

Figure 6.2. ^{13}C NMR spectrum of RAFT agent in $CDCl_3$.

Firstly, the homopolymer PMA was polymerized with the CTA to check the reactivity of monomer MA. ^{1}H NMR spectrum was used to check the conversion of CTA-mediated solution polymerization of methyl acrylate (MA) at 70 °C at a ratio of $[monomer]_0:[CTA]_0:[AIBN]_0 = 458:1:0.4$ for $[monomer]_0 = 3$ M in dioxane conditions. After polymerization, the proton of methyl group shifted from 3.74 ppm to 3.64 ppm that were marked as a and b, respectively. The conversion of monomer MA was calculated through the ratio of integral area a/(a+b). The conversion of MA reached 81.6% after polymerization for 4 h as shown in ***Figure 6.3***. The result shows that monomer MA has high reactivity under these conditions.

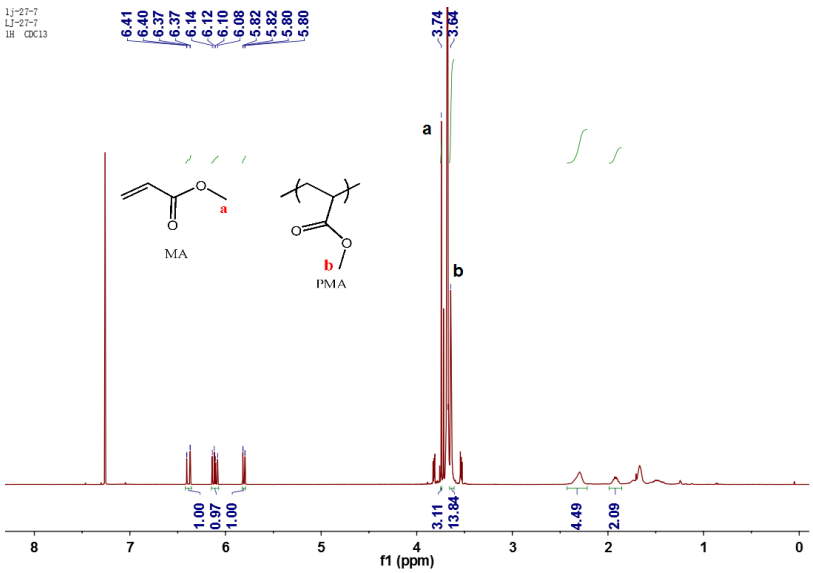

Figure 6.3. ^{1}H NMR spectrum of PMA in $CDCl_3$ after polymerization for 4 h.

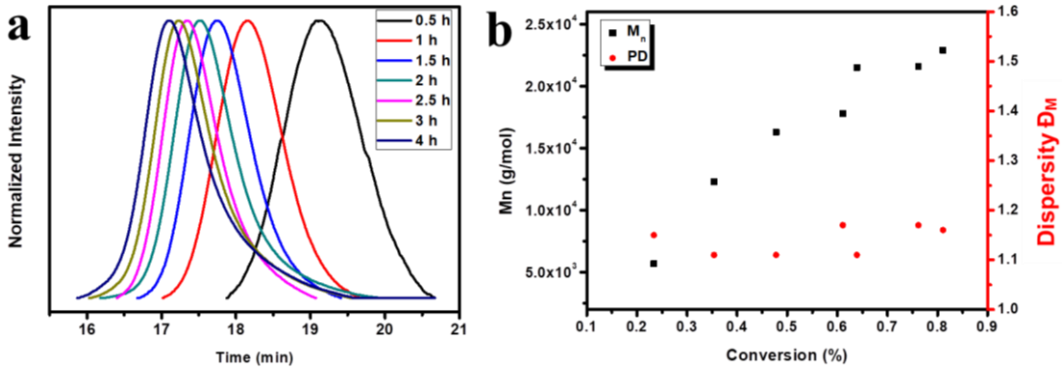

Figure 6.4. (a) Evolution of molecular weight as a function of monomer conversion. (b) Corresponding evolution of Mn and Đ with conversion for a CTA-mediated solution polymerization of methyl acrylate at 70 °C at a ratio of $[monomer]_0$:$[CTA]_0$:$[AIBN]_0$ = 458:1:0.4 for $[monomer]_0$ = 3 M under dioxane conditions. The conversion date was obtained from corresponding ^{1}H NMR spectra.

Size exclusion chromatography (SEC) was used to investigate the average molecular weight. As shown in ***Figure 6.4a***, the retention time was reduced as the reaction time increasing indicating an increasing of the average molecular weight along with increasing of reaction time. The resulting evolution of Mn and Đ against monomer conversion was illustrated in ***Figure 6.4b***. The Mn is observed to increase linearly along with increasing of the monomer conversion, which is characteristic of a controlled radical polymerization (CRP) process. The Đ values initially decreased with increasing

conversion till 65% and then increased in high conversion. However, the values of Đ remain still relatively low (<1.2) throughout the polymerization even in high conversion. These results indicated that the CTA well conducted to MA during the polymerization.

Next, the dipolymerization of MA and VDMA was investigated to check their reactivity with RAFT polymerization. As the same calculation for homopolymerization in PMA, the parameters from dipolymerization of P(MA-*co*-VDMA) was shown in ***Figure 6.5***. The results of SEC measurements show that the average molecular weight of P(MA-*co*-VDMA) increased linearly with increasing monomer conversion (***Figure6.5b***), which shows the characteristics of CRP. Also, at low conversion (< 30%), the polydispersity of P(MA-*co*-VDMA) was decreased with the increasing of conversion. At high conversion, the polydispersity of P(MA-*co*-VDMA) was increased along with the increasing of conversion due to a high viscosity and low monomer concentration of the system.

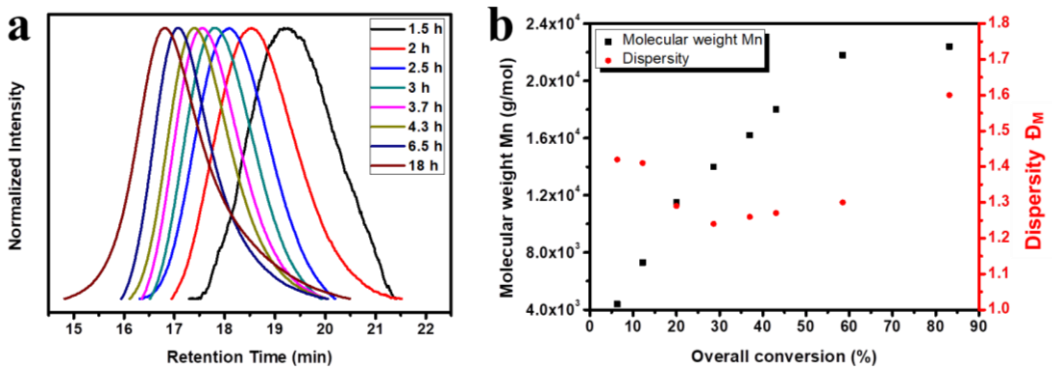

Figure 6.5. (a) Evolution of molecular weight as a function of overall monomer conversion. (b) Corresponding evolution of Mn and Đ with overall conversion for a CTA-mediated solution dipolymerization of methyl acrylate and 2-Vinyl-4,4-dimethylazlactone at 70 °C at a ratio of $[monomer]_0:[CTA]_0:[AIBN]_0$ = 500:1:0.4 for $[monomer]_0$ = 3 M under dioxane conditions. The conversion date was obtained from corresponding ^{1}H NMR spectra.

The dipolymerization of P(MA-*co*-DMIA) was also carried out with the same conditions as the copolymer of P(MA-*co*-VDMA) to compare the reactivity of monomer MA and DMIA. As shown in ***Table 6.1***, the monomer MA has higher

reactivity than that of DMIA.

Table 6.1. Conversion of dipolymerization of MA (M_1) and DMIA (M_2) in ^{1}H NMR spectra

Time (min)	$[M_1]/[M_2]$	$[P_1]/[P_2]$	Conversion M_1 (%)	Conversion M_2 (%)
0	90.0/10.0	-	-	-
30	87.3/12.7	95.5/4.5	3.5	1.2
60	87.4/12.6	90.5/9.5	27.4	21.6
120	87.0/13.0	89.7/10.3	56.5	50
180	85.5/14.5	89.7/10.3	74.7	66.7

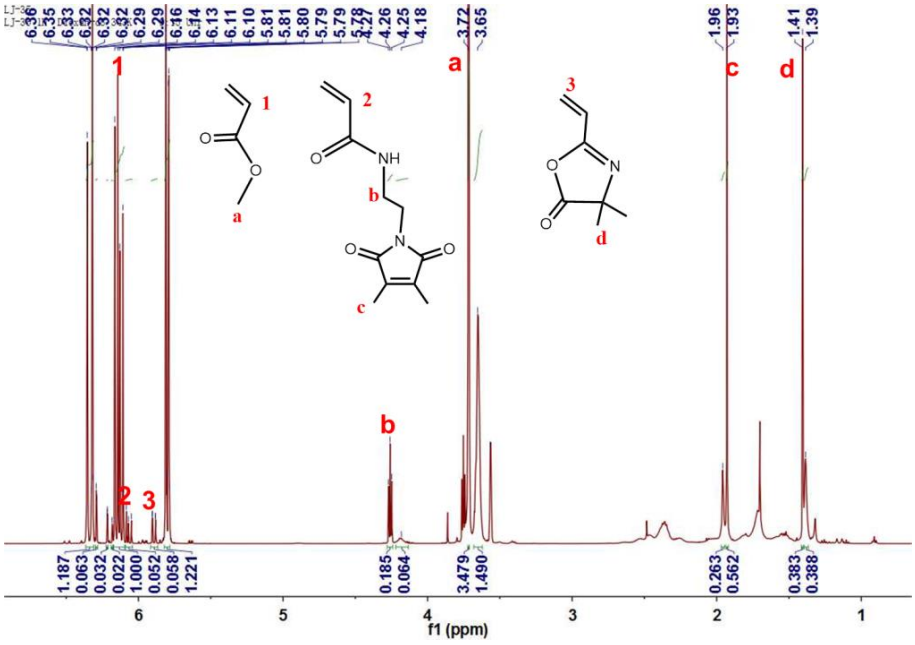

Figure 6.6. ^{1}H NMR spectrum of copolymerization in dioxane-d_8 at 70 ℃ after 40 min.

From the results of homopolymerization and dipolymerization, the monomer VDMA shows the highest reactivity and the monomer DMIA shows lower reactivity than that of MA. Then, the copolymerization of MA (M_1), DMIA (M_2) and VDMA (M_3) was carried out in NMR tubes to investigate the kinetics of copolymerization in situ. The polymerization was carried out with an overall monomer concentration of 3 M at a ratio of $[M_1]/[M_2]/[M_3]$ = 87.7/5.9/6.4 and [M]/[CTA]/[AIBN] = 300/1/0.5 in dioxane-d_8 at 70 ℃. The characteristic peaks of every monomer were monitored to

calculate their conversion and composition in the copolymer as shown in ***Figure 6.6*** for example. The peak marked as 1 and a belonged to MA, 2, b and c belonged to DMIA and 3 and c belonged to VDMA.

Table 6.2. Kinetics of ternary copolymerization of MA, DMIA and VDMA from situ ^{1}H NMR spectra

Time (min)	$[M_1]/[M_2]/[M_3]$	$[P_1]/[P_2]/[P_3]$	Conversion M_1 (%)	Conversion M_2 (%)	Conversion M_3 (%)
0	87.7/5.9/6.4	-	-	-	-
10	87.8/6.1/6.1	87.8/4.2/8.0	5.1	3.6	6.6
20	88.3/6.2/5.6	83.6/4.8/11.5	13.3	11.3	25.0
30	88.5/6.3/5.2	83.1/4.9/12.0	21.1	18.1	39.9
40	89.2/6.4/4.4	84.0/5.5/10.5	28.0	26.4	50.3
50	89.4/6.4/4.1	83.9/5.3/10.8	35.2	32.1	60.5
60	89.8/6.5/3.8	84.3/5.2/10.5	41.2	37.6	67.3
70	90.4/6.5/3.1	85.0/5.2/9.8	46.5	42.5	74.5
80	90.8/6.5/2.6	84.8/5.1/10.1	51.8	47.4	81.5
90	91.4/6.5/2.1	85.2/5.2/9.6	56.5	52.8	86.5
100	91.7/6.5/1.8	85.6/5.2/9.2	61.0	57.6	89.6
110	91.7/6.5/1.7	85.8/5.4/8.8	64.6	62.0	91.5
120	92.3/6.4/1.3	86.2/5.3/8.4	67.8	65.5	93.6
130	92.3/6.4/1.3	86.5/5.4/8.0	70.7	68.6	94.3
140	92.3/6.4/1.3	86.7/5.5/7.8	73.0	71.5	95.8
150	92.8/6.2/0.9	87.0/5.4/7.6	75.0	73.5	96.3

The integration of each peak was done every 10 minutes in 2.5 h to calculate the monomer ratio, copolymer composition and conversion as shown in ***Table 6.2***. It was shown that the monomer VDMA has the highest reactivity and monomer DMIA shows the lowest reactivity in this condition, which is the same situation as the dipolymerization. Therefore, the RAFT agent was also well conducted in the copolymerization to ensure a uniform distribution of each polymer chain. From the copolymer composition it shows that the VDMA moiety was more incorporated into the copolymer than the other two monomers at low conversion while decreased gradually along with the increasing of conversion due to the disproportionate expense of monomers. It could be expected that the VDMA has gradient distribution in the copolymer chain.

Table 6.3. Parameters of P(MA-*co*-DMIA-*co*-VDMA) with a monomer ratio of [M1]/[M2]/[M3] = 90/5/5 in dioxane at 70 ℃.

P(MA-*co*-DMIA-*co*-VDMA)	[M]/[CTA]/[AIBN]	t (h)	Overall Conv.[b] (%)	M_n [a] (g/mol)	$Đ_M$ [a]	Comp. [b] $[P_1]/[P_2]/[P_3]$ (%)
1	300/1/0.5	4	83.4	21000	1.36	89.2/3.8/7.2
2	1000/1/0.5	24	99.3	55100	3.14	90.0/4.5/5.5
3	1000/1/0.2	4	31.8	32100	1.22	87.1/3.8/9.1
4	1000/1/0.2	8	57.6	46700	1.50	87.4/4.9/7.7
5	1000/1/0.2	12	71.5	46100	1.87	89.0/4.3/6.7
6	1000/1/0.2	16	81.2	52500	2.25	89.7/4.5/5.8

[a] Determined by SEC (THF) using PMMA standards. [b] Determined using ^{1}H NMR spectroscopy as show in ***Figure 6.8***.

The copolymerization experiment was then carried out in a flask with the same condition. ***Table 6.3*** shows parameters for P(MA-*co*-DMIA-*co*-VDMA) with different CTA concentrations and polymerization time. As shown in this table, the ratio of [initiator]/[CTA] can influence the rate of polymerization and polydispersity. When the ratio of [initiator]/[CTA] was 0.5, the degree of polymerization reached to 83.4% after 4 h as a ratio of [monomer]/[CTA] = 300/1. The polydispersity was 1.36 indicating a good control of the copolymerization even reaching to high conversions. For the copolymer composition VDMA has the higher composition than what was designed due to its highest reactivity in this system that was discussed above. However, when the ratio of [monomer]/[CTA] increased to 1000/1, the copolymerization need more time to reach high conversion. It shows that after 24 h the degree of polymerization was 99.3% and $Đ_M$ was 3.14. In this situation, the copolymerization was not well controlled to high conversion due to a long reaction time and high viscosity in the system. In this case, the ratio of [initiator]/[CTA] was reduced to 0.2 to investigate the controllable capability of CTA in long time polymerization. It should be noted that the system has lower rate of polymerization than that of high initiator concentration. After 12 h, the degree of polymerization reached to 71.5% with a polydispersity of 1.87, which shows that the CTA could conduct the copolymerization in high conversion and longtime reaction.

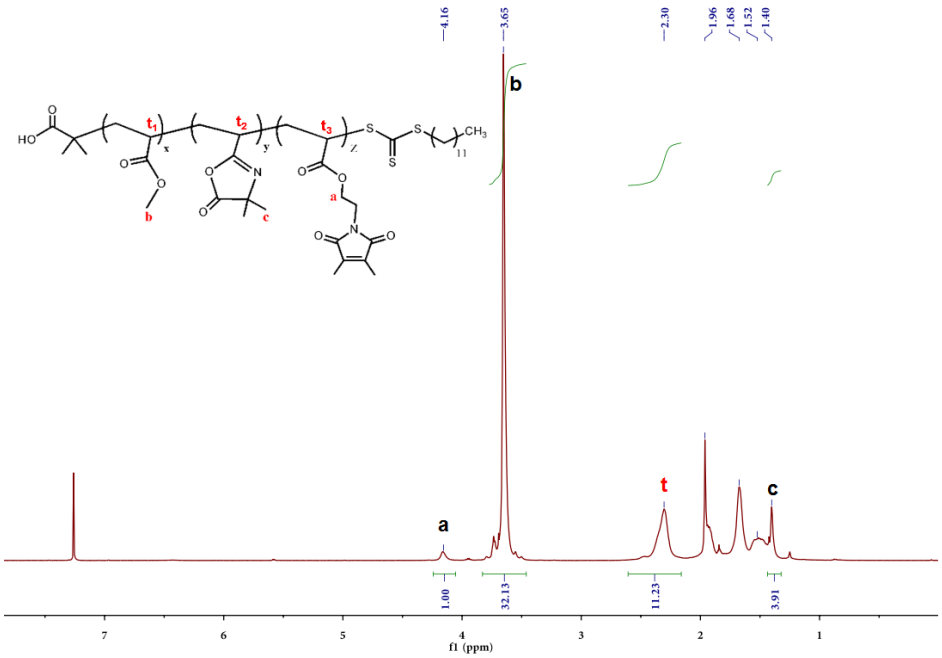

Figure 6.8. ^{1}H NMR of P(MA-DMIA-VDMA) in $CDCl_3$.

6.3.2 P4 and P5 modified from P(MA-*co*-DMIA-*co*-VDMA)

P(MA-*co*-DMIA-*co*-VDMA) containing azlactone moiety could be modified via ring open reaction under basic condition. Functional groups like hydroxyl groups and primary amine groups were selected to achieve this modification. Comparing to hydroxyl groups, primary amine groups are stronger nucleophiles that would be easier to trigger the ring open reaction. Thus, the primary amine group functionalized Hamilton receptor (compound **8**) and thymine (compound **15**) were introduced to modify the P(MA-*co*-DMIA-*co*-VDMA).

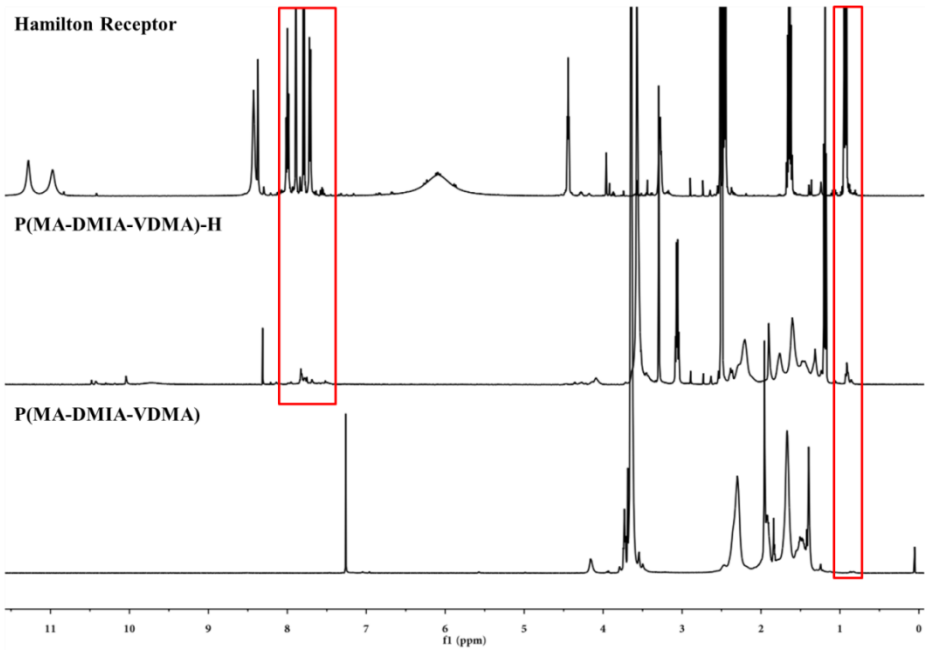

Figure 6.9. ^{1}H NMR spectra combination of Hamilton receptor, P(MA-*co*-DMIA-*co*-VDMA) and **P4**, respectively.

The post-polymerization was carried out in DMF as solvent with triethylamine (TEA) as an acid-binding agent. The **P4** and **P5** were obtained after modification. Taking **P4** as an example, the ring open efficiency of VDMA was calculated by using ^{1}H NMR spectrum. ***Figure 6.9*** shows that the characteristics peaks from Hamilton receptor appeared after modification indicating that the Hamilton receptor was grafted to the copolymer chain successfully. The methyl group from Hamilton receptor was used as reference peak to calculate the ratio with MA (d), DMIA (c) and VDMA (b) (***Figure 6.10***). Also, the methyne group from the backbone was marked as e, which can used to check the composition of each moiety of monomer. As a result, 33.2% of VDMA was modified with Hamilton receptor in **P4** where the polymer composition (MA/DMIA/VDMA) was 90.0/4.6/5.4. With the same method, the grafted efficiency of thymine was carried out. There was 92.4 % (VDMA as a standard) of thymine (***Figure 5.11***) grafted to **P5**, where the polymer composition (MA/DMIA/VDMA) was 90.1/4.5/5.4. What should be noted is that the copolymer compositions of both two samples analyzed from each ^{1}H NMR spectrum were well fitted to the composition of the copolymer P(MA-*co*-DMIA-*co*-VDMA) (90/4.5/5.5). The efficiency of Hamilton

receptor was lower than thymine because of its bigger structure resulting steric effects.

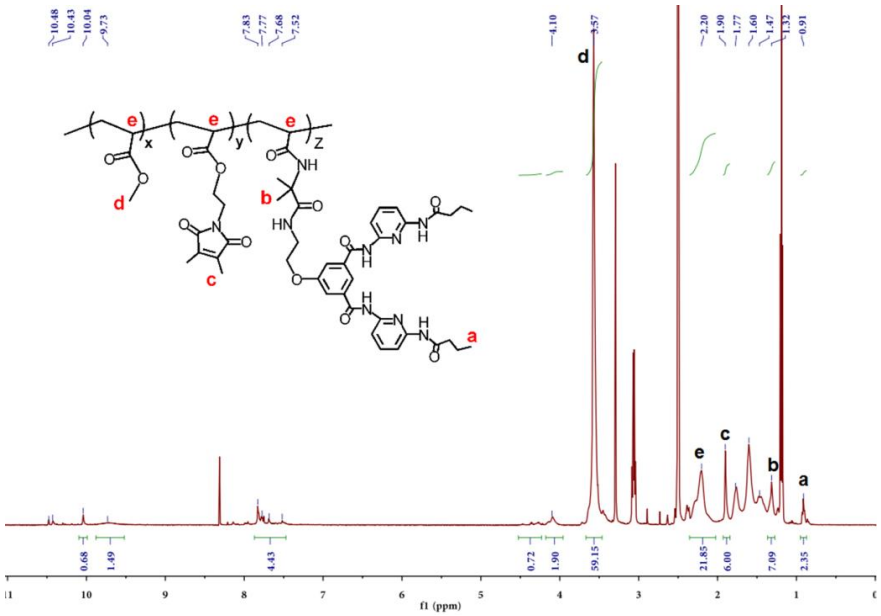

Figure 6.10. ^{1}H NMR spectrum of **P4** in DMSO-d_6.

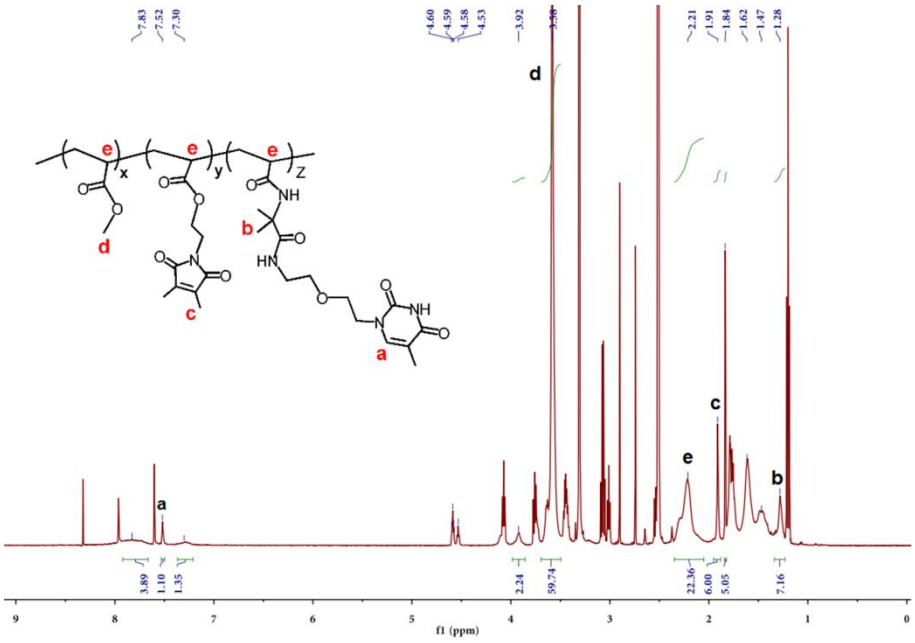

Figure 6.11. ^{1}H NMR spectrum of **P5** in DMSO-d_6.

6.3.3 Construction of supramolecular gel via non-covalent bonding[215–217]

As our design, the dually cross-linking supramolecular gel system was constructed by combining covalent bonding with noncovalent bonding to maintain the skeleton of

the gel as well as response to target molecules. Firstly, the supramolecular gel was constructed via noncovalent bonding to check their responsive ability. When the supramolecular gel was added the target molecule, the noncovalent bonding would be broken resulting a gel to sol transformation.

P4 and **P5** were introduced in building a competitive interaction with cyanuric acid or barbiturates. We assume that the thymine and Hamilton receptor could form a four hydrogen bonding complex. While the cyanuric acid and Hamilton receptor could form a six hydrogen bonding complex. Therefore, the binding affinity of thymine is lower than that of cyanuric acid. Here, we combined the **P4** with **P5** to form a supramolecular gel as shown in ***Figure 6.12***. The supramolecular gel was broken after adding cyanuric acid as a target molecule. This experiment shows that the cyanuric acid has higher binding affinity than that of thymine in macroscopic view.

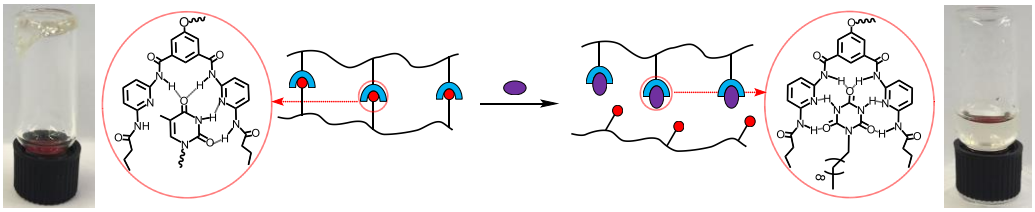

Figure 6.12. Mechanism of gel-sol transformation of **P4** and **P5** with cyanuric acid as a target molecule.

6.3.4 Binding affinity detection via ^{1}H NMR titration

Further, we investigated the binding constant of thymine and Hamilton receptor as well as the binding constant of cyanuric acid and Hamilton receptor by using ^{1}H NMR titration. The Hamilton receptor was collected as substrate with a constant concentration of 10 mM, and thymine and cyanuric acid were added gradually from 0 to 3 molar ratio, respectively. The molecules used for titration here were shown in ***Figure 6.13*** and their titration ^{1}H NMR spectra were recorded as shown in ***Figure 6.14***. The ^{1}H NMR titration was carried out the in dioxane because of the poor solubility of cyanuric acid in chloroform.

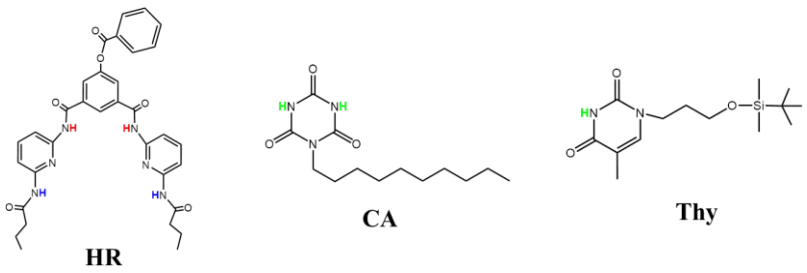

Figure 6.13. Molecular structures of Hamilton receptor, cyanuric acid and thymine for ^{1}H NMR titrations, protons marked with different colors corresponding to the NMR spectra with different colored boxes.

Here, the most significant shift was found consistently for the imide protons of the Hamilton receptor, which were marked as red and blue box. After adding guest molecules, the protons from host molecule (Hamilton receptor) were shift to lower field showing that the Hamilton receptor has interactions with guest molecules. The bonding constant (K) was obtained from chemical shift dates of imide protons by using the nonlinear regression method.

It was assumed that the system was simple as a host-guest system to form a complex by 1:1 molar ratio. The basic equations were shown below as (1)-(4):

$$G + H \overset{K}{\rightleftharpoons} C \qquad (1)$$

$$K = \frac{[c]}{[H]\times[G]} \qquad (2)$$

$$[H]_t = [H] + [C] \qquad (3)$$

$$[G]_t = [G] + [C] \qquad (4)$$

where G is guest molecule, H is host molecule and C is complex; $[H]_t$ is the total concentration of host molecule at initial state; $[G]_t$ is the total concentration of guest molecular at final stage; [H], [G] and [C], are concentrations of host, guest, and complex, respectively, at each equilibrium state; K is the binding constant.

Then the equation (5) was derived from equations (1)-(4):

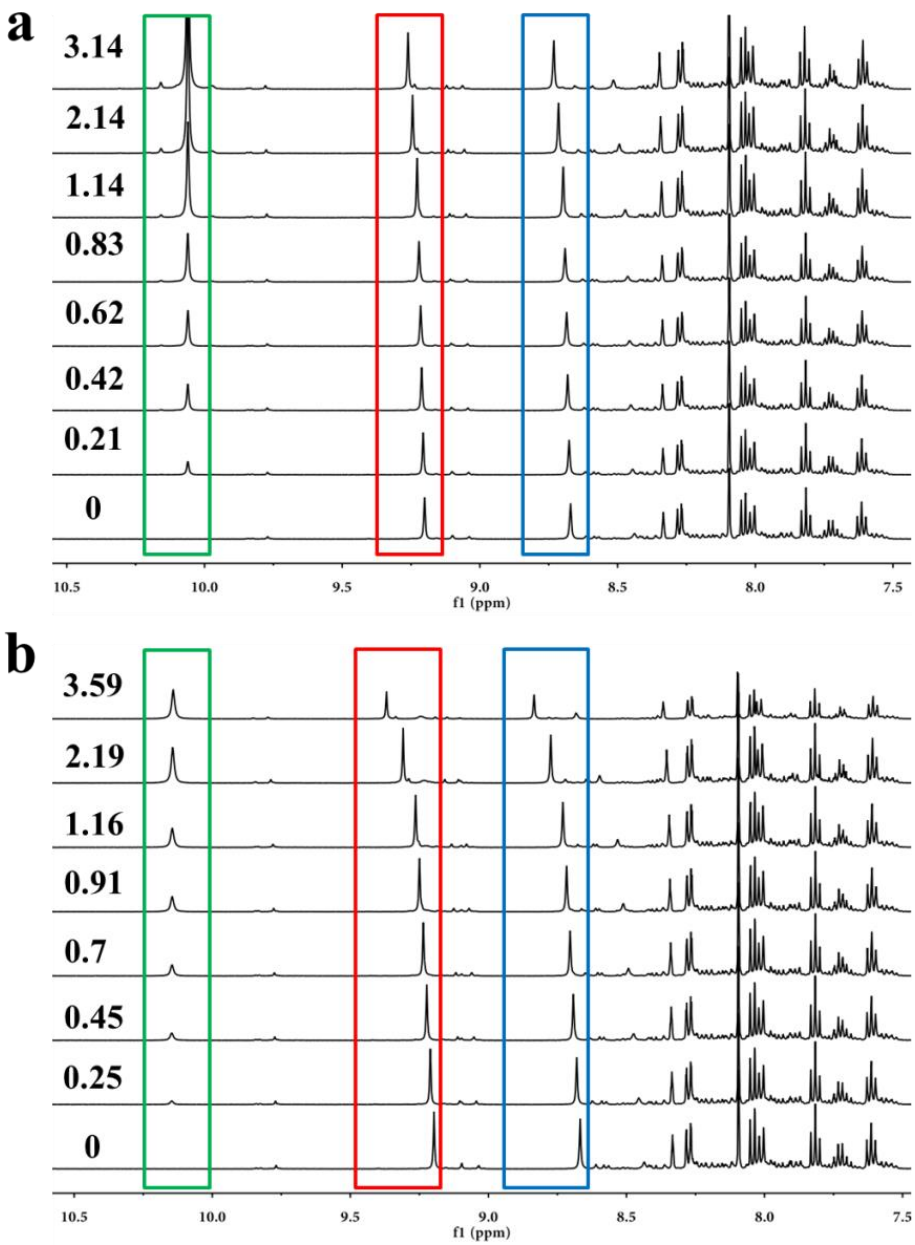

Figure 6.14. ^{1}H NMR titration spectra from 7.5 to 10.5 ppm with Hamilton receptor as a substrate (10 mM in dioxane-d_8), cyanuric acid (a) and thymine (b) were added from 0 to 3 molar ratio gradually.

$$K = \frac{[C]}{([H]_t - [C]) \times ([G]_t - [C])} \qquad (5)$$

For this equation (5), the concentration of complex [C] should be obtained that the value of K could be calculated. Here we also assume that the host-guest complexation equilibrium has a very fast exchange rate compared to the ^{1}H NMR time scale. The complex concentration could be simplified as the degree of chemical shift of the host proton as shown in equation (6).

$$[\mathrm{C}] = \frac{\delta - \delta_h}{\delta_c - \delta_h}[H]_t \qquad (6)$$

Where δ_h is the chemical shift of the proton from host molecule at initial state; δ_c is the chemical shift of the proton from host molecule at final state; δ is the chemical shift of the proton from host molecule at each titration state.

Then the ^{1}H NMR titration was carried out with a constant concentration of the total host molecule. The chemical shifts of δ_h and δ_c are constant. However, we can't get the value of δ_c directly from ^{1}H NMR spectrum because of the limitation to detection of the final state. Therefore, we name a contant $a = \delta_c - \delta_h$ (7). There are two values that we can obtain directly from the experimental dates. One is the difference of δ and δ_h, the other one is the ratio of $[G]_t/[H]_t$. Thus it could be named that $Y = \delta - \delta_h$ and $X = [G]_t/[H]_t$. Then the equation (5) could be derived as the equation (8).

$$\mathrm{K} \times [\mathrm{H}]_t = \frac{aY}{(a-Y)\times(aX-Y)} \qquad (8)$$

Also the value of $K \times [H]_t$ was a constant that be named as b. Then the equation (8) was transformed into

$$\mathrm{Y} = \frac{1}{2}a\left(\left(1 + X + \frac{1}{b}\right) - \left(\left(1 + X + \frac{1}{b}\right)^{\frac{1}{2}} - 4X\right)^{\frac{1}{2}}\right) \qquad (9)$$

From the equation (9), we can obtain the constants a and b by using nonlinear regression analysis with the different values of X and Y. ***Figure 6.15*** shows the simulation of the ^{1}H NMR titration with the proton of imide group on Hamilton receptor in the solvent of dioxane-d_8. It was shows that the binding affinity of thymine to Hamilton receptor is 8.5, while the binding affinity of cyanuric acid to Hamilton receptor is 13.4. The results showed that cyanuric acid has a higher binding affinity than that of thymine for interactions with Hamilton receptor, though the binding affinity is far low than the date from literature. This is because the polar solvent dioxane could break the hydrogen bonding, which would make the binding affinity lower than non-polar solvent like chloroform.

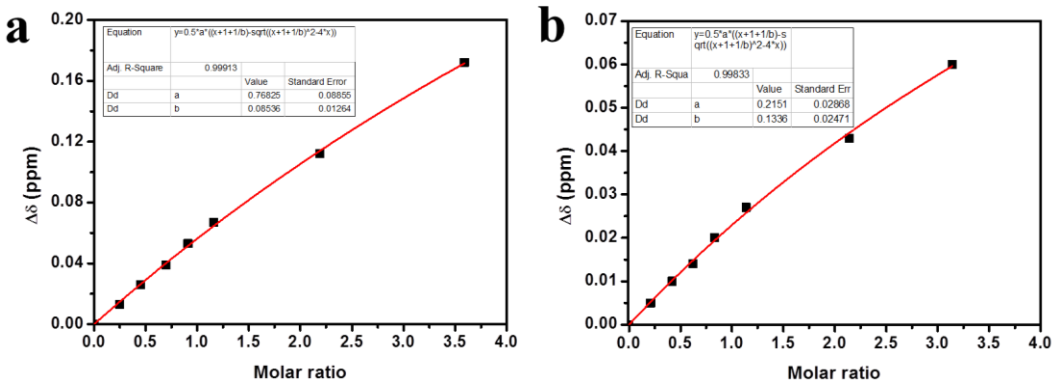

Figure 6.15. Experimental ^{1}H chemical shifts (black square) measured for imide group of Hamilton receptor in NMR titration with thymine (a) and cyanuric acid (b). Red lines represent the best fit curves for the stepwise binding (complex stoichiometry 1:1).

Therefore, the molecule 5,5'-dipropylbarbituric acid was introduced into the system instead of cyanuric acid due to its better solubility in chloroform. The process of the transformation from gel to sol was also done in chloroform as shown in ***Figure 6.16***. As expected, the 5,5'-dipropylbarbituric acid could also break the interaction between thymine and Hamilton receptor causing a gel to sol transformation. Next, the ^{1}H NMR titration was carried out with 5,5'-dipropylbarbituric acid and Hamilton receptor as well as thymine and Hamilton receptor in $CDCl_3$ to investigate binding affinities of these two hydrogen complex systems.

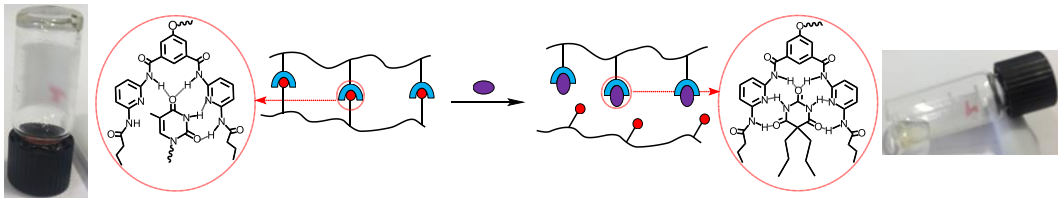

Figure 6.16. Scheme of gel-sol transformation of P(MA-*co*-DMIA-*co*-VDMA)-H and P(MA-*co*-DMIA-*co*-VDMA)-T with 5,5'-Dipropylbarbituric acid as a target molecule.

Hamilton receptor was selected as the titrand, in which 5,5'-dipropylbarbituric acid and thymine, as a titrant, were gradually added in to Hamilton receptor solution, respectively. As the ratio increased, the peaks from imide groups of Hamilton receptor were shifted to lower field as shown in ***Figure 6.17***. What should be noted is that the shifting of peaks in $CDCl_3$ is much more than that of in dioxane-d_8. This also

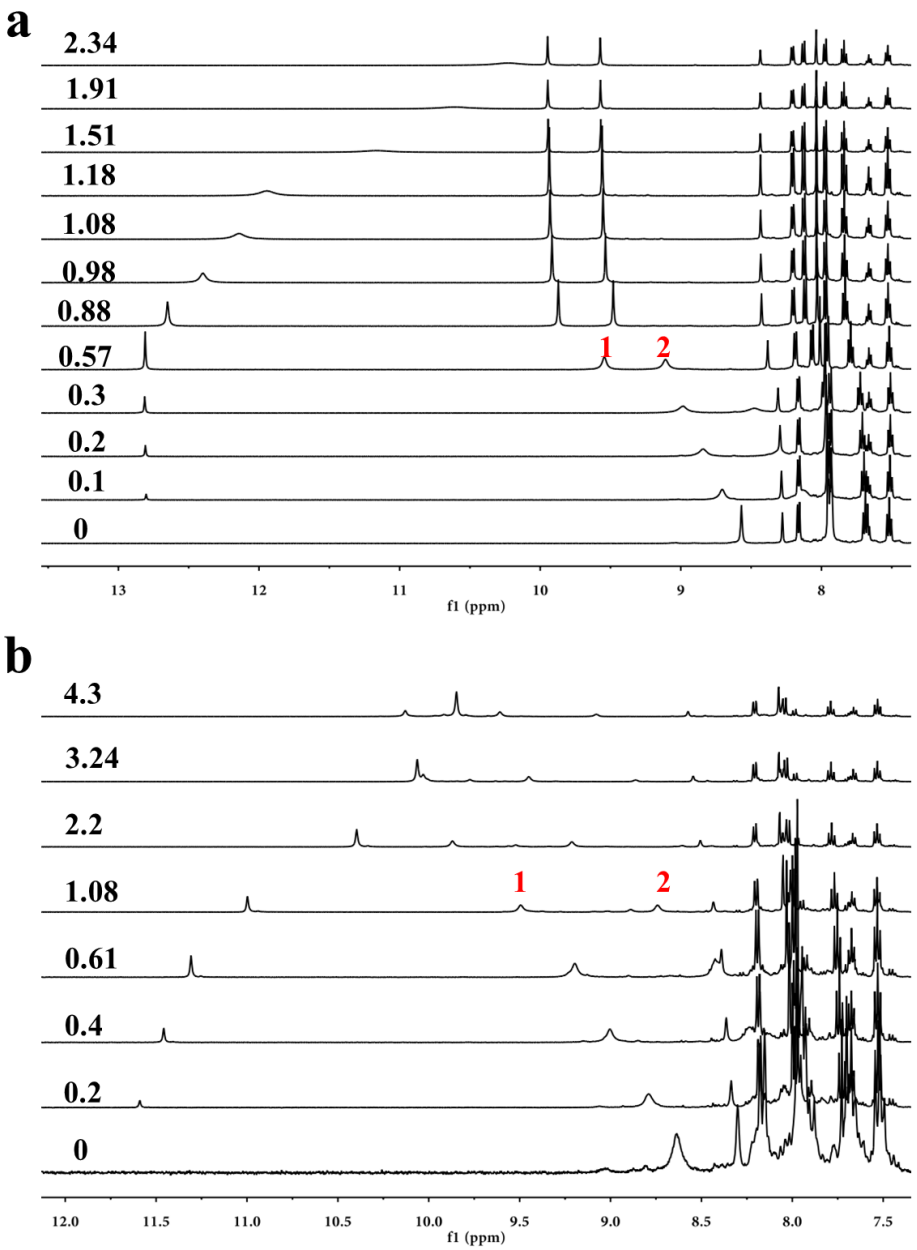

Figure 6.17. ^{1}H NMR titration spectra from 7.5 to 10.5 ppm with Hamilton receptor as a substrate (10 mM), 5, 5'-Dipropylbarbituric acid (a) and thymine (b) were added from 0 to 4 molar ratio gradually.

indicated that the hydrogen bonding was broken in polar solvents like dioxane. The chemical shifting of protons from imide groups both Hamilton receptor and guest molecules were recorded in ***Figure 6.18***. It clearly showed that the protons of Hamilton receptor interaction with 5,5'-dipropylbarbituric acid were changed faster than that of thymine. There is an inflection point around ratio 1 for 5, 5'-dipropylbarbituric acid and then nearly no changes further. While, there is no inflection point for thymine

interaction with Hamilton receptor, though the chemical shift changes higher than that of 5,5'-dipropylbarbituric acid in the end. The chemical shift of imide group from 5,5'-dipropylbarbituric acid occurred also faster than that of thymine, when they are titration with Hamilton receptor (***Figure 6.18b***).

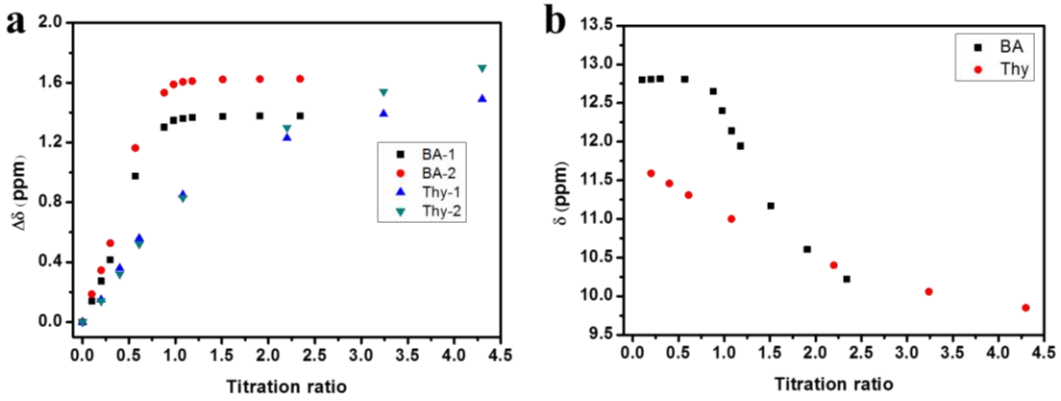

Figure 6.18. (a) Difference of chemical shifts measured for imide group of Hamilton receptor in ^{1}H NMR titration with 5,5'-dipropylbarbituric acid and thymine; (b) Chemical shifts measured for imide group of 5, 5'-Dipropylbarbituric acid and thymine in ^{1}H NMR titration.

The next step, the Equation (9) was use to simulate the binding affinity between 5,5'-dipropylbarbituric acid and Hamilton receptor as well as thymine and Hamilton receptor, which we used above for analyzing the binding affinity of 1:1 complex model. As shown in ***Figure 6.19***, the binding affinity between Hamilton receptor and 5,5'-dipropylbarbituric acid, calculating from proton **1**, was 1.24×10^{5} M^{-1}, while the binding affinity between Hamilton receptor and thymine was 144 M^{-1}. Also the binding affinity calculated from proton **2** was showing that the 5,5'-dipropylbarbituric acid was three orders of magnitude higher than that of thymine. The results demonstrated that the guest molecule 5,5'-dipropylbarbituric acid has stronger binding affinity with Hamilton receptor than that of thymine, which caused a competitive guest interaction when 5,5'-dipropylbarbituric acid as a target molecule added into the system. Therefore, the 5,5'-dipropylbarbituric acid was used as a target molecule for the next sensor investigation. What should be noted was that the binding affinity of the multi hydrogen bonding operated in chloroform was much higher than that in dioxane. Because of the polar

solvent dioxane the binding affinity of hydrogen bond was not suitable for simulating bonding strength between guest molecules and Hamilton receptor.

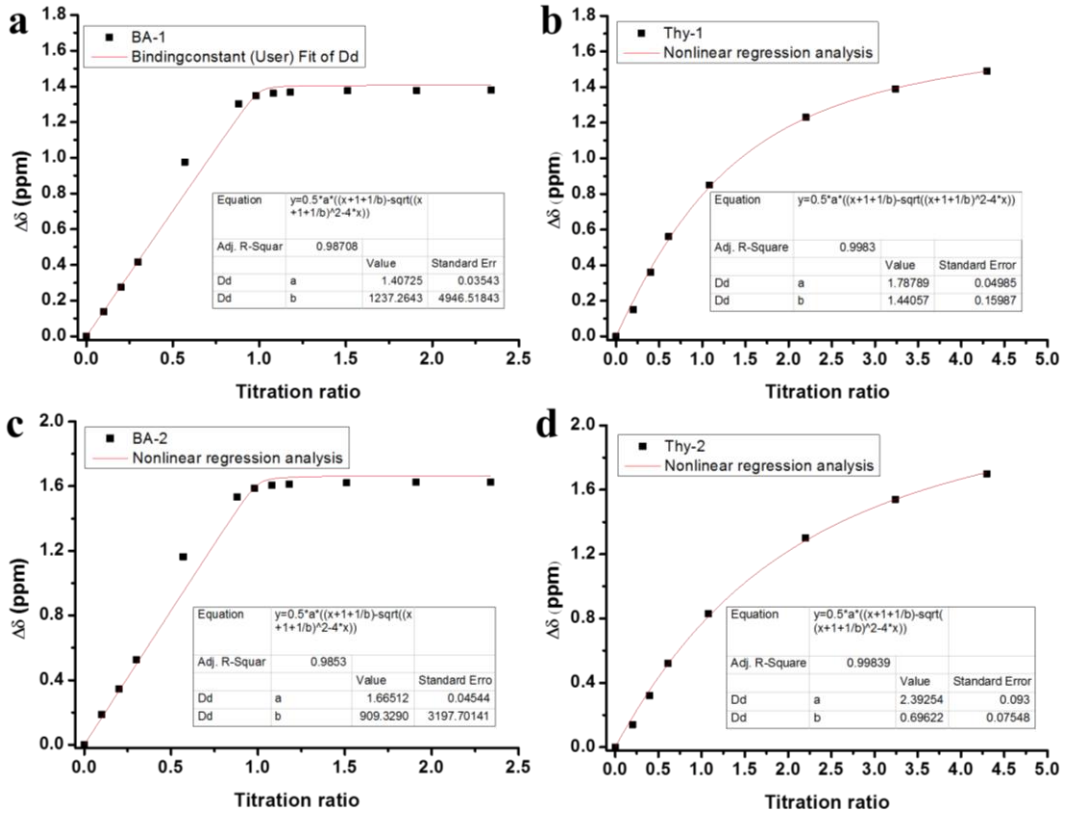

Figure 6.19. Experimental ^{1}H chemical shifts (black square) measured for imide group of Hamilton receptor in NMR titration with 5,5'-dipropylbarbituric acid (a and c) and thymine (b and d). Red lines represent the best fit curves for the stepwise binding (complex stoichiometry 1:1).

Further, the temperature dependent ^{1}H NMR spectra were investigated because the hydrogen bond is also sensitive to temperature changes. The measurements were operated in $CDCl_3$ from 30 ℃ to 55 ℃ in situ as shown in ***Figure 6.20***. ***Figure 6.20a*** shows the temperature dependent ^{1}H NMR spectrum of 5,5'-dipropylbarbituric acid and Hamilton receptor. The protons **1** and **2** (the imide groups from Hamilton receptor) shifted to higher field around 0.08 ppm when the temperature increasing from 30 ℃ to 55 ℃. However, the protons **1** and **2** (imide groups from Hamilton receptor) in thymine system (***Figure 6.20b***) shifted to higher field around 0.31 ppm at the same conditions. These results show that both of the complexes were disassembled when the temperature

increase indicating a hydrogen bonding interaction. What's more, the hydrogen bonding between 5,5'-dipropylbarbituric acid and Hamilton receptor was higher than that of thymine and Hamilton receptor, which makes the former more difficult to be broken when it suffered from temperature increase.

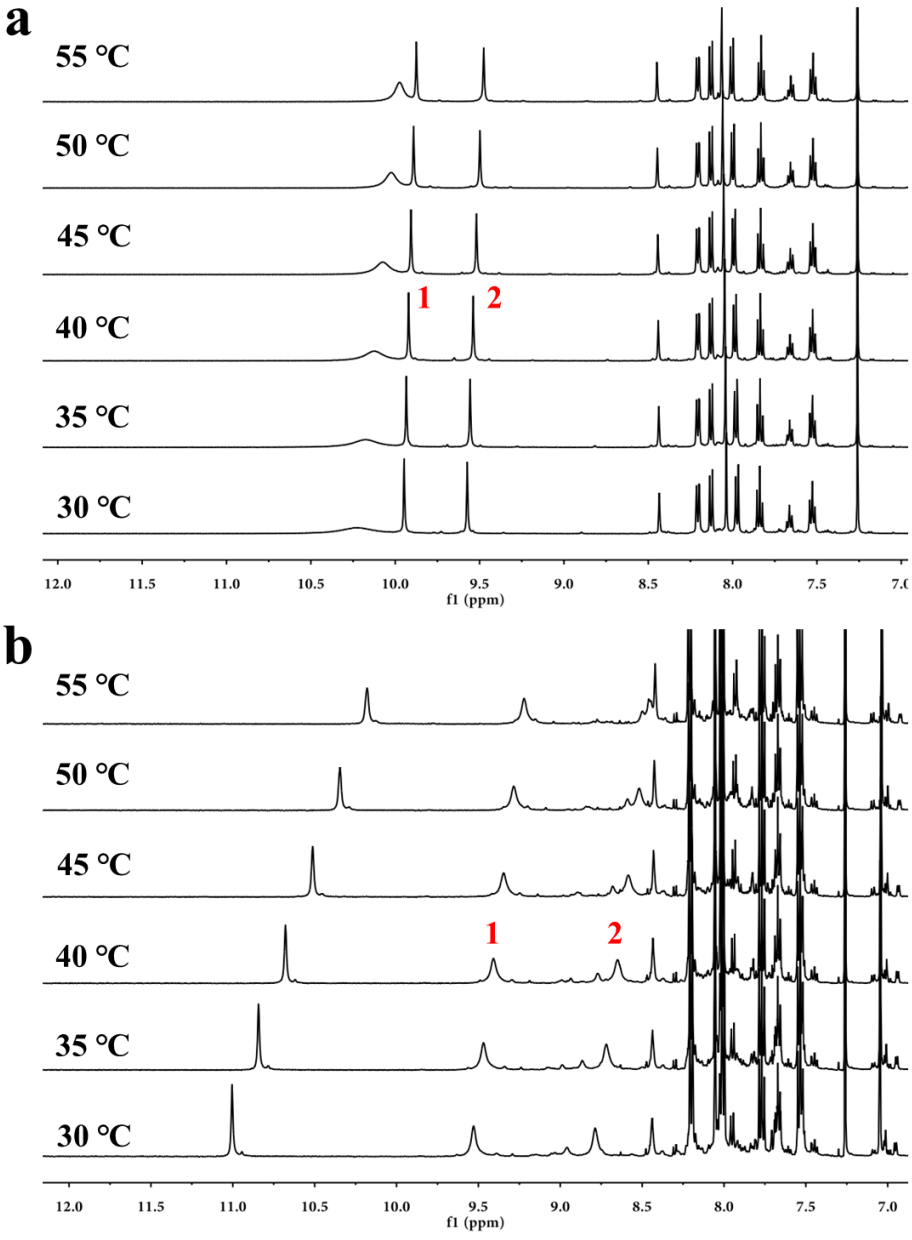

Figure 6.20. Temperature dependent ^{1}H NMR spectra from 7 to 12 ppm with host molecule of Hamilton receptor (10 mM) and guest molecule of 5,5'-Dipropylbarbituric acid (23.4 mM) (a) and thymine (45 mM) (b), respectively.

6.3.5 Construction of dually cross-linked supramolecular gel and barbiturates detection

The dually cross-linked supramolecular gel (**DCSG**) was constructed after spin coating onto a gold surface, photo cross-linking via UV-Vis irradiation and equilibrating in chloroform. The detail process was shown in ***Figure 4.7***. After the **DCSG** was prepared, the sensor was then evaluated to detect 5,5'-dipropylbarbituric acid by SPR-OWS measurements. The **DCSG** layer in different states were measured and characterized to obtain the angular reflectivity spectra R(θ) with both optical waveguide (OW) and surface plasma (SP) modes (***Figure 6.21a***). By fitting the two distinct resonances at θ_{OW} and θ_{SP} corresponding to the excitation of OW and SP modes, respectively, the layer thickness d_h and refractive index n_h of the gel were determined. After swelling in chloroform, the corresponding layer thickness of swollen hydrogel was increasing from 43 nm to 445 nm with a swelling ratio of 10.1, indicating the formation of the **DCSG**. The high swelling ratio of the **DCSG** in chloroform benefits the diffusion of target molecule throughout the gel. When treated with 5,5'-dipropylbarbituric acid solution, however, the d_h and the n_h of the gel does almost no change. This unexpected result suggested that there is no responsive behavior during the binding process. In order to investigate the reasons the failure for responsive behavior, the SPR-OWS of the **DCSG** in mixture solvent of chloroform/methanol (V:V = 9/1) was measured (***Figure 6.21b***). It was shown that the layer thickness was increasing and the refractive index was decreasing in the mixture solvent due to the breakage of the hydrogen bonding or solvent induced swelling. Then, the system was measured in different solvents (***Figure 6.21c***) and different composition of the mixture of chloroform/methanol (***Figure 6.21d***). The layer thickness of the **DCSG** in different solvents showed that the **DCSG** was significantly influenced by the polarity of the solvent (***Table 6.4***). Therefore, it was speculated that the noncovalent bonding between Hamilton receptor and thymine was broken during the swelling process due to their week binding affinity.

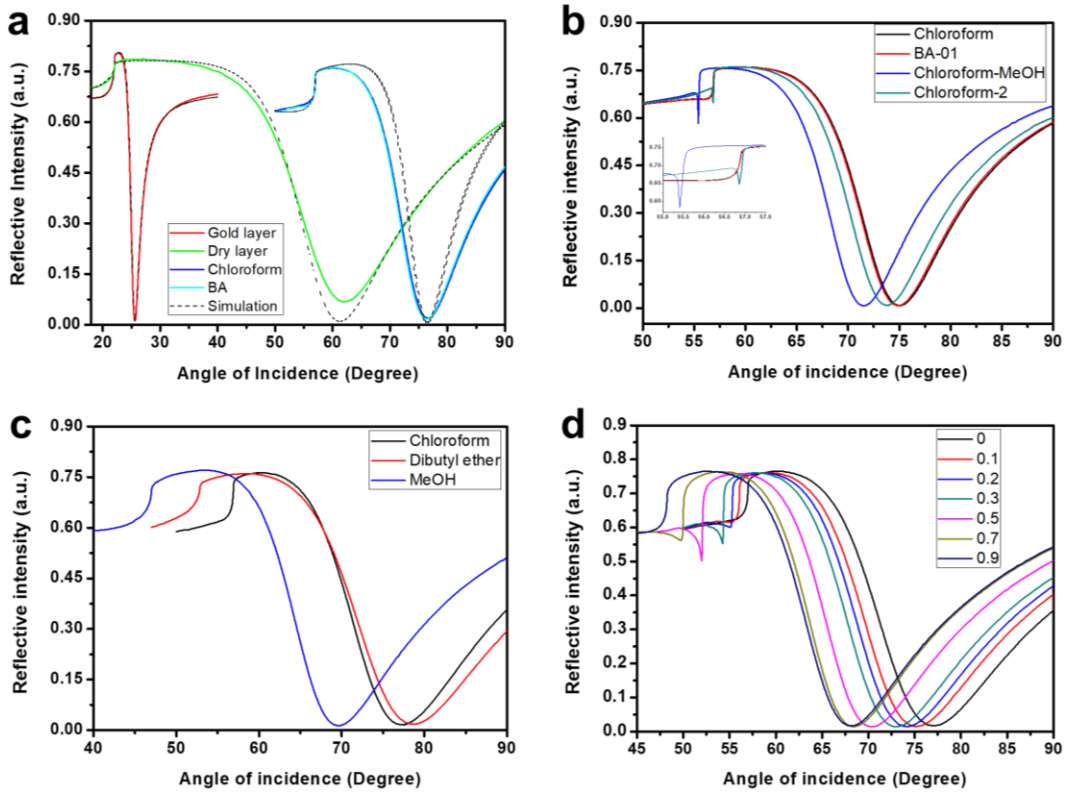

Figure 6.21. SPR-OWS measurements for 5,5'-dipropylbarbituric acid detection. a) Representative SPR-OWS curves with gold layer, gel layer in dry state, gel layer in swollen state and swollen gel layer after adding 5,5'-dipropylbarbituric acid , respectively. b) SPR-OWS measurements with 5,5'-dipropylbarbituric acid and methanol in chloroform. c) Solvent dependent measurements of **DCSG**. d) SPR-OWS measurements with diverse amounts of methanol.

Table 6.4. Characteristics of the gel film in different solvents.

Solvent (n_s)	**d_n (nm)**	**n_h**
Chloroform (1.4436)	424	1.4744
Dibutyl ether (1.3975)	234	1.4862
Methonal (1.3294)	254	1.4310
Chloroform/Methanol = 9/1 (1.4328)	498	1.4632
Chloroform/Methanol = 8/2 (1.4258)	524	1.4574
Chloroform/Methanol = 7/3 (1.4153)	564	1.4498
Chloroform/Methanol = 5/5 (1.3903)	535	1.4324
Chloroform/Methanol = 3/7 (1.3667)	454	1.4188
Chloroform/Methanol = 1/9 (1.3461)	336	1.4177

6.4 Conclusions

A template copolymer based **DCSG** was designed by introducing photo cross-linkable DMIAA as a covalent bond and Hamilton receptor and thymine as a noncovalent bond. The binding affinity of the hydrogen bonds between Hamilton receptor and thymine was determined by ^{1}H NMR titration as well as Hamilton receptor and cyanuric acid or barbiturate. The results show that the binding affinity of Hamilton receptor and barbiturate is much stronger than that of Hamilton receptor and thymine. Further, the **DCSG** was immobilized on a gold surface to obtain a sensor chip. The n_h and d_h of the **DCSG** were determined independently by using SPR-OWS measurements. However, the **DCSG** did not respond to the addition of barbiturate, which showed that the dually cross-linking system was not formed during the swelling process of the **DCSG**. Nevertheless, the strategy for building a **DCSG** system was proved to be able achieving by using this method. What should be noted is that the noncovalent interaction pair needs to be carefully choices. As an outlook, the guest molecules with higher binding affinity than thymine were checked. Urea derivates were excepted to be a stronger binding moiety when they interact with Hamilton receptor. Both the heterocyclic and linear urea derivates are commercial available such as *N,N'*-trimethyleneurea and 1,3-diethylurea, respectively, which could be synthesized and used to construct **DCSG** for barbiturates detection.

SUMMARY

Template copolymer P(DMAAm-*co*-DMIAAm-*co*-VDMA), P(DMAAm-*co*-VDMA) and P(MA-*co*-DMIA-*co*-VDMA) were successfully synthesized by RAFT polymerization and subsequently modified with amine groups bearing functional molecules via ring opening of the azlactone moieties in copolymers to obtain **P1**-**P5**. The dually cross-linked supramolecular gels were built by introducing DMIEA as the covalent bonding via [2+2] cyclization and host-guest interactions like ferrocene and β-cyclodextrin as noncovalent bonding. The **DCSG** was immobilized on a gold surface after spin coating of the copolymer mixture solution, photo cross-linking of the 2,3-dimethylmaleimde groups in the copolymer and equilibrating in solvents to obtain a sensor chip.

The responsive hydrogel layer based on **P1** was achieved via exposure of the sensor chip to SAV solution monitored by using SPR-OWS measurements. The biosensor showed an excellent concentration dependent linear detection range for SAV concentration between 0.5 μM and 200 μM. It was demonstrated that the hydrogel can be used as a binding matrix for biomolecules that can diffuse and selectively bind to the immobilized docking molecules.

The n_h and d_h of the **DCSH** based on **P2** and **P3** towards responding to Ada were determined independently by using SPR-OWS measurements. the linear fitting was carried out by utilizing logarithmic values of concentration of Ada in the range from 1×10^{-5} to 1×10^{-3} M with a limit of detection[153] of 24.3 μM. Further, the sensor chip based on **DCSH** of **P2** and **P3** was also investigated the sensitivity, reversibility and universality upon LPA. An exponential correlation (R^2 = 0.89 for reflective intensity and R^2 = 0.99 for layer thickness) were obtained over a concentration of LPA range from 2 to 30 μM in mimic plasma conditions, demonstrating the **DCSH** could be used as a SPR-OWS sensor for LPA detection in a mimic plasma condition.

The binding affinity of the hydrogen bonds between Hamilton receptor and

thymine as well as Hamilton receptor and cyanuric acid or barbiturate was determined by ^{1}H NMR titration. The results show that the binding affinity of Hamilton receptor and barbiturate is three orders of magnitude higher than that of Hamilton receptor and thymine. However, the **DCSG** based on **P4** and **P5** did not respond to the addition of barbiturate, which showed that the dually cross-linking system was not formed during the swelling process of the **DCSG**. What should be noted is that the noncovalent interaction pair needs to be carefully choices according to their binding affinity. Nevertheless, the principle of the competitive guest molecule interaction was confirmed before incorporated into the **DCSG**. Urea derivates were excepted to be a stronger binding moiety when they interact with Hamilton receptor. Both the heterocyclic and linear urea derivates are commercial available such as *N,N'*-trimethyleneurea and 1,3-diethylurea, respectively, which could be synthesized and used to construct **DCSG** for barbiturates detection.

This method opens a new strategy to build a **DCSG** based SPR-OWS sensor for target small molecules detection. The **DCSG** is thought to be easily modified with other molecular recognition pairs to be used potentially as a SPR biosensor for target small biomolecule detection. As an outlook, the template copolymer could be modified with molecular recognition pair of dopamine and boronic acid, which would be expected to quantitatively detect glucose by using **SPR-OWS**.

REFERENCE

[1] C. Löwenberg, M. Balk, C. Wischke, M. Behl, A. Lendlein, *Acc. Chem. Res.* **2017**, *50*, 723.

[2] S. E. Bakarich, G. C. Pidcock, P. Balding, L. Stevens, P. Calvert, M. in het Panhuis, *Soft matter* **2012**, *8*, 9985.

[3] Ducrot, E., Chen, Y., Bulters, M., Sijbesma, R. P., Creton, C., *Science* **2014**, *344*, 186.

[4] S. Li, J. Wang, L. Song, Y. Zhou, J. Zhao, X. Hou, X. Yuan, *Biomed. Mater.* **2016**, *12*, 15012.

[5] S. Azevedo, A. M. S. Costa, A. Andersen, I. S. Choi, H. Birkedal, J. F. Mano, *Adv. Mater.* **2017**, *29*.

[6] C. Shao, H. Chang, M. Wang, F. Xu, J. Yang, *ACS Appl. Mater. Interfaces* **2017**, *9*, 28305.

[7] M. K. Jaiswal, J. R. Xavier, J. K. Carrow, P. Desai, D. Alge, A. K. Gaharwar, *ACS nano* **2016**, *10*, 246.

[8] M. Noack, R. Merindol, B. Zhu, A. Benitez, S. Hackelbusch, F. Beckert, S. Seiffert, R. Mülhaupt, A. Walther, *Adv. Funct. Mater.* **2017**, *27*, 1700767.

[9] K. Zhang, Q. Feng, J. Xu, X. Xu, F. Tian, K. W. K. Yeung, L. Bian, *Adv. Funct. Mater.* **2017**, *27*, 1701642.

[10] W. Lu, X. Le, J. Zhang, Y. Huang, T. Chen, *Chem. Soc. Rev.* **2017**, *46*, 1284.

[11] D. Buenger, F. Topuz, J. Groll, *Prog. Ploym. Sci.* **2012**, *37*, 1678.

[12] S. Strandman, X. X. Zhu, *Gels* **2016**, *2*, 16.

[13] E. Cho, S. Jung, *Molecules* **2015**, *20*, 19620.

[14] J. M. Lehn, *Pure Appl. Chem.* **1978**, *50*, 871.

[15] J. M. Lehn, *Supramolecular Chemistry — Concepts and perspectives*, Tokyo **1995**.

[16] E. Weber (Ed.), *Supramolecular Chemistry I - Directed Synthesis and Molecular*

Recognition **1993**.

[17] G. Tillet, B. Boutevin, B. Ameduri, *Prog. Ploym. Sci.* **2011**, *36*, 191.

[18] W. Jones, C. N. R. Rao, *Supramolecular organization and materials design*, Cambridge University Press, Cambridge **2008**.

[19] T. Nakanishi (Ed.), *Supramolecular Soft Matter: Applications in Materials and Organic Electronics* **2011**.

[20] E. Elacqua, D. S. Lye, M. Weck, *Acc. Chem. Res.* **2014**, *47*, 2405.

[21] M. Krogsgaard, V. Nue, H. Birkedal, *Chem. Eur. J.* **2016**, *22*, 844.

[22] L. Voorhaar, R. Hoogenboom, *Chem. Soc. Rev.* **2016**, *45*, 4013.

[23] N. Kamaly, B. Yameen, J. Wu, O. C. Farokhzad, *Chem. Rev.* **2016**, *116*, 2602.

[24] Y. Li, D. Maciel, J. Rodrigues, X. Shi, H. Tomas, *Chem. Rev.* **2015**, *115*, 8564.

[25] X. Sun, T. D. James, *Chem. Rev.* **2015**, *115*, 8001.

[26] C. Heinzmann, C. Weder, L. M. de Espinosa, *Chem. Soc. Rev.* **2016**, *45*, 342.

[27] E. Krieg, M. M. C. Bastings, P. Besenius, B. Rybtchinski, *Chem. Rev.* **2016**, *116*, 2414.

[28] X. Ma, H. Tian, *Acc. Chem. Res.* **2014**, *47*, 1971.

[29] M.-O. M. Piepenbrock, G. O. Lloyd, N. Clarke, J. W. Steed, *Chem. Rev.* **2010**, *110*, 1960.

[30] T. Jungst, W. Smolan, K. Schacht, T. Scheibel, J. Groll, *Chem. Rev.* **2016**, *116*, 1496.

[31] X. Ma, Y. Zhao, *Chem. Rev.* **2015**, *115*, 7794.

[32] J. Hu, S. Liu, *Acc. Chem. Res.* **2014**, *47*, 2084.

[33] W. Xia, M. Ni, C. Yao, X. Wang, D. Chen, C. Lin, X.-Y. Hu, L. Wang, *Macromolecules* **2015**, *48*, 4403.

[34] S. Y. An, S. M. Noh, J. H. Nam, J. K. Oh, *Macromol. Rapid Commun.* **2015**, *36*, 1255.

[35] C. L. Lewis, E. M. Dell, *J. Polym. Sci. Part B: Polym. Phys.* **2016**, *54*, 1340.

[36] J. P. Gong, Y. Katsuyama, T. Kurokawa, Y. Osada, *Adv. Mater.* **2003**, *15*, 1155.

[37] M. A. Haque, T. Kurokawa, J. P. Gong, *Polymer* **2012**, *53*, 1805.

[38] Q. Chen, H. Chen, L. Zhu, J. Zheng, *Macromol. Chem. Phys.* **2016**, *217*, 1022.

[39] C. W. Peak, J. J. Wilker, G. Schmidt, *Colloid Polym. Sci.* **2013**, *291*, 2031.

[40] J. W. Steed, D. R. Tumer, K. J. Wallace (Eds.), *Core Concepts in Supramolecular Chemistry and Nanochemistry*.

[41] Z. Cui, W. Wang, M. Obeng, M. Chen, S. Wu, I. Kinloch, B. R. Saunders, *Soft matter* **2016**, *12*, 6985.

[42] C. K. Pandiyarajan, M. Rubinstein, J. Genzer, *Macromolecules* **2016**, *49*, 5076.

[43] S. Kondo, T. Hiroi, Y.-S. Han, T.-H. Kim, M. Shibayama, U.-i. Chung, T. Sakai, *Adv. Mater.* **2015**, *27*, 7407.

[44] Z. Tang, J. Huang, B. Guo, L. Zhang, F. Liu, *Macromolecules* **2016**, *49*, 1781.

[45] D. Wang, J. Guo, H. Zhang, B. Cheng, H. Shen, N. Zhao, J. Xu, *J. Mater. Chem. A* **2015**, *3*, 12864.

[46] Y. You, W. Huang, A. Zhang, Y. Lin, *J. Polym. Sci. Part A: Polym. Chem.* **2016**, *54*, 3760.

[47] P. Lin, S. Ma, X. Wang, F. Zhou, *Adv. Mater.* **2015**, *27*, 2054.

[48] Y. Huang, M. Zhong, Y. Huang, M. Zhu, Z. Pei, Z. Wang, Q. Xue, X. Xie, C. Zhi, *Nat. Commun.* **2015**, *6*, 10310.

[49] M. Zhong, Y.-T. Liu, X.-Y. Liu, F.-K. Shi, L.-Q. Zhang, M.-F. Zhu, X.-M. Xie, *Soft matter* **2016**, *12*, 5420.

[50] Z. S. Kean, J. L. Hawk, S. Lin, X. Zhao, R. P. Sijbesma, S. L. Craig, *Adv. Mater.* **2014**, *26*, 6013.

[51] J. Guo, C. Yuan, M. Guo, L. Wang, F. Yan, *Chem. Sci.* **2014**, *5*, 3261.

[52] T. Kakuta, Y. Takashima, T. Sano, T. Nakamura, Y. Kobayashi, H. Yamaguchi, A. Harada, *Macromolecules* **2015**, *48*, 732.

[53]M. Nakahata, Y. Takashima, H. Yamaguchi, A. Harada, *Nat. Commun.* **2011**, *2*, 511.

[54] H. Xu, J. Nishida, W. Ma, H. Wu, M. Kobayashi, H. Otsuka, A. Takahara, *ACS Macro Lett.* **2012**, *1*, 457.

[55] C. Zhang, G. G. Cano, P. V. Braun, *Adv. Mater.* **2014**, *26*, 5678.

[56] M. Nakahata, Y. Takashima, A. Hashidzume, A. Harada, *Angew. Chem. Int. Ed.* **2013**, *52*, 5731.

[57] Y. Zheng, A. Hashidzume, A. Harada, *Macromol. Rapid Commun.* **2013**, *34*, 1062.

[58] C. Ma, T. Li, Q. Zhao, X. Yang, J. Wu, Y. Luo, T. Xie, *Adv. Mater.* **2014**, *26*, 5665.

[59] K. Miyamae, M. Nakahata, Y. Takashima, A. Harada, *Angew. Chem. Int. Ed.* **2015**, *54*, 8984.

[60] S. Tan, J. Cui, Q. Fu, E. Nam, K. Ladewig, J. M. Ren, E. H. H. Wong, F. Caruso, A. Blencowe, G. G. Qiao, *ACS Appl. Mater. Interfaces* **2016**, *8*, 6219.

[61] C. B. Rodell, J. W. MacArthur, S. M. Dorsey, R. J. Wade, L. L. Wang, Y. J. Woo, J. A. Burdick, *Adv. Funct. Mater.* **2015**, *25*, 636.

[62] L. Ouyang, C. B. Highley, C. B. Rodell, W. Sun, J. A. Burdick, *ACS Biomater. Sci. Eng.* **2016**.

[63] Y. Liu, K. Ai, L. Lu, *Chem. Rev.* **2014**, *114*, 5057.

[64] H. Xu, J. Nishida, H. Wu, Y. Higaki, H. Otsuka, N. Ohta, A. Takahara, *Soft matter* **2013**, *9*, 1967.

[65] Z. Guo, K. Ni, D. Wei, Y. Ren, *RSC Adv* **2015**, *5*, 37377.

[66] M. Nakahata, S. Mori, Y. Takashima, A. Hashidzume, H. Yamaguchi, A. Harada, *ACS Macro. Lett.* **2014**, *3*, 337.

[67] Y. Dong, W. Wang, O. Veiseh, E. A. Appel, K. Xue, M. J. Webber, B. C. Tang, X.-W. Yang, G. C. Weir, R. Langer, D. G. Anderson, *Langmuir* **2016**, *32*, 8743.

[68] C. Zhang, M. D. Losego, P. V. Braun, *Chem. Mater.* **2013**, *25*, 3239.

[69] B. Zhang, Z. A. Digby, J. A. Flum, E. M. Foster, J. L. Sparks, D. Konkolewicz, *Polym. Chem.* **2015**, *6*, 7368.

[70] N. Xu, J. Han, Z. Zhu, B. Song, X. Lu, Y. Cai, *Soft matter* **2015**, *11*, 5546.

[71] J. Chen, Q. Su, R. Guo, J. Zhang, A. Dong, C. Lin, J. Zhang, *Macromol. Chem. Phys.* **2017**, *218*, 1700166.

[72] S. Coulibaly, C. Heinzmann, F. L. Beyer, S. Balog, C. Weder, G. L. Fiore, *Macromolecules* **2014**, *47*, 8487.

[73] W. Weng, X. Fang, H. Zhang, H. Peng, Y. Lin, Y. Chen, *Eur. Polym. J.* **2013**, *49*, 4062.

[74] S. C. Grindy, R. Learsch, D. Mozhdehi, J. Cheng, D. G. Barrett, Z. Guan, P. B. Messersmith, N. Holten-Andersen, *Nat. Mater.* **2015**, *14*, 1210.

[75] Q. Song, H. Chen, S. Zhou, K. Zhao, B. Wang, P. Hu, *Polym. Chem.* **2016**, *7*, 1739.

[76] O. Altintas, M. Artar, G. ter Huurne, I. K. Voets, A. R. A. Palmans, C. Barner-Kowollik, E. W. Meijer, *Macromolecules* **2015**, *48*, 8921.

[77] E. S. Place, N. D. Evans, M. M. Stevens, *Nat. Mater.* **2009**, *8*, 457.

[78] K. Y. Lee, D. J. Mooney, *Chem. Rev.* **2001**, *101*, 1869.

[79] M. A. Daniele, A. A. Adams, J. Naciri, S. H. North, F. S. Ligler, *Biomaterials* **2014**, *35*, 1845.

[80] M. He, Z. Wang, Y. Cao, Y. Zhao, B. Duan, Y. Chen, M. Xu, L. Zhang, *Biomacromolecules* **2014**, *15*, 3358.

[81] Y. P. Singh, N. Bhardwaj, B. B. Mandal, *ACS Appl. Mater. Interfaces* **2016**, *8*, 21236.

[82] M. M. Fitzgerald, K. Bootsma, J. A. Berberich, J. L. Sparks, *Biomacromolecules* **2015**, *16*, 1497.

[83] Y. Shu, T. Hao, F. Yao, Y. Qian, Y. Wang, B. Yang, J. Li, C. Wang, *ACS Appl. Mater. Interfaces* **2015**, *7*, 6505.

[84] V. X. Truong, K. M. Tsang, G. P. Simon, R. L. Boyd, R. A. Evans, H. Thissen, J. S. Forsythe, *Biomacromolecules* **2015**, *16*, 2246.

[85] L. Bidault, M. Deneufchatel, C. Vancaeyzeele, O. Fichet, V. Larreta-Garde, *Biomacromolecules* **2013**, *14*, 3870.

[86] T. C. Suekama, J. Hu, T. Kurokawa, J. P. Gong, S. H. Gehrke, *ACS Macro Lett.* **2013**, *2*, 137.

[87] J. Yeom, S. H. Bhang, B.-S. Kim, M. S. Seo, E. J. Hwang, H. Cho, J. K. Park, S. K. Hahn, *Bioconjugate Chem.* **2010**, *21*, 240.

[88] Q. Chen, H. Chen, L. Zhu, J. Zheng, *J. Mater. Chem. B* **2015**, *3*, 3654.

[89] A. S. Hoffman, *Adv. Drug Deliv. Rev.* **2012**, *64*, 18.

[90] T. Vermonden, R. Censi, W. E. Hennink, *Chem. Rev.* **2012**, *112*, 2853.

[91] N. Morimoto, T. Endo, M. Ohtomi, Y. Iwasaki, K. Akiyoshi, *Macromol. Biosci.* **2005**, *5*, 710.

[92] A. Kumar, S. K. Samal, R. Dash, U. Ojha, *J. Mater. Chem. B* **2014**, *2*, 7429.

[93] P. Zhang, G. Li, *Prog. Ploym. Sci.* **2016**, *57*, 32.

[94] Y. Hu, Z. Du, X. Deng, T. Wang, Z. Yang, W. Zhou, C. Wang, *Macromolecules*

2016, *49*, 5660.

[95] D. Döhler, H. Peterlik, W. H. Binder, *Polymer* **2015**, *69*, 264.

[96] M. Pan, Q.-J. Yuan, X.-L. Gong, S. Zhang, B.-J. Li, *Macromol. Rapid Commun.* **2016**, *37*, 433.

[97] J. Li, J. A. Viveros, M. H. Wrue, M. Anthamatten, *Adv. Mater.* **2007**, *19*, 2851.

[98] S. Tamesue, K. Yasuda, S. Noguchi, T. Mitsumata, T. Yamauchi, *ACS Macro Lett.* **2016**, *5*, 704.

[99] K. Saha, S. S. Agasti, C. Kim, X. Li, V. M. Rotello, *Chem. Rev.* **2012**, *112*, 2739.

[100] S. K. Vashist, E. Lam, S. Hrapovic, K. B. Male, J. H. T. Luong, *Chem. Rev.* **2014**, *114*, 11083.

[101] Y. Shiraki, K. Tsuruta, J. Morimoto, C. Ohba, A. Kawamura, R. Yoshida, R. Kawano, T. Uragami, T. Miyata, *Macromol. Rapid Commun.* **2015**, *36*, 515.

[102] Q. Wu, L. Wang, H. Yu, J. Wang, Z. Chen, *Chem. Rev.* **2011**, *111*, 7855.

[103] N. Ganesan, A. P. Gadre, M. Paranjape, J. F. Currie, *Anal. Biochem.* **2005**, *343*, 188.

[104] S. Kang, Y. H. Bae, *J. Control. Release* **2003**, *86*, 115.

[105] K. Belal, F. Stoffelbach, J. Lyskawa, M. Fumagalli, D. Hourdet, A. Marcellan, L. D. Smet, V. R. de La Rosa, G. Cooke, R. Hoogenboom, P. Woisel, *Angew. Chem. Int. Ed.* **2016**, *55*, 13974.

[106] X. Hu, J. Zhou, M. Vatankhah-Varnosfaderani, W. F. M. Daniel, Q. Li, A. P. Zhushma, A. V. Dobrynin, S. S. Sheiko, *Nat. Commun.* **2016**, *7*, 12919.

[107] A. Kugimiya, T. Takeuchi, *Biosens. Bioelectron.* **2001**, *16*, 1059.

[108] A. V. Kabashin, P. Evans, S. Pastkovsky, W. Hendren, G. A. Wurtz, R. Atkinson, R. Pollard, V. A. Podolskiy, A. V. Zayats, *Nat. Mater.* **2009**, *8*, 867.

[109] A. J. Haes, R. P. van Duyne, *J. Am. Chem. Soc.* **2002**, *124*, 10596.

[110] M. Wakao, S. Watanabe, Y. Kurahashi, T. Matsuo, M. Takeuchi, T. Ogawa, K. Suzuki, T. Yumino, T. Myogadani, A. Saito, K.-I. Muta, M. Kimura, K. Kajikawa, Y. Suda, *Anal. Chem.* **2017**, *89*, 1086.

[111] J.-F. Masson, *ACS Sens.* **2017**, *2*, 16.

[112] A. R. Zarei, F. Barghak, *J. Anal. Chem.* **2017**, *72*, 430.

[113] M. Piliarik, L. Párová, J. Homola, *Biosens. Bioelectron.* **2009**, *24*, 1399.

[114] A. Aulasevich, R. F. Roskamp, U. Jonas, B. Menges, J. Dostálek, W. Knoll, *Macromol. Rapid Commun.* **2009**, *30*, 872.

[115] Y. Wang, C.-J. Huang, U. Jonas, T. Wei, J. Dostalek, W. Knoll, *Biosens. Bioelectron.* **2010**, *25*, 1663.

[116] D. Kuckling, M. E. Harmon, C. W. Frank, *Macromolecules* **2002**, *35*, 6377.

[117] M. E. Harmon, D. Kuckling, C. W. Frank, *Macromolecules* **2003**, *36*, 162.

[118] D. Kuckling, P. Pareek, *Polymer* **2008**, *49*, 1435.

[119] H. R. Culver, J. R. Clegg, N. A. Peppas, *Accounts of chemical research* **2017**, *50*, 170.

[120] S. M. Heilmann, J. K. Rasmussen, L. R. Krepski, *J. Polym. Sci. A Polym. Chem.* **2001**, *39*, 3655.

[121] S. K. Schmitt, D. J. Trebatoski, J. D. Krutty, A. W. Xie, B. Rollins, W. L. Murphy, P. Gopalan, *Biomacromolecules* **2016**, *17*, 1040.

[122] X. Mu, J. Qiao, L. Qi, P. Dong, H. Ma, *ACS Appl. Mater. Interfaces* **2014**, *6*, 21346.

[123] J. T. Lai, D. Filla, R. Shea, *Macromolecules* **2002**, *35*, 6754.

[124] C.-W. Wang, W.-T. Yu, H.-P. Lai, B.-Y. Lee, R.-C. Gao, K.-T. Tan, *Anal. Chem.* **2015**, *87*, 4231.

[125] M. E. Harmon, D. Kuckling, P. Pareek, C. W. Frank, *Langmuir* **2003**, *19*, 10947.

[126] C. D. Vo, D. Kuckling, H.-J. P. Adler, M. Schnhoff, *Colloid Polym. Sci.* **2002**, *280*, 400.

[127] S. Gupta, D. Kuckling, K. Kretschmer, V. Choudhary, H.-J. Adler, *J. Polym. Sci. A Polym. Chem.* **2007**, *45*, 669.

[128] D. Kuckling, H. P. Adler, L. Ling, W. D. Habicher, Arndt K., *polym. Bull.* **2000**, *44*, 269.

[129] V. H. Pérez-Luna, M. J. O'Brien, K. A. Opperman, P. D. Hampton, G. P. López, L. A. Klumb, P. S. Stayton, *J. Am. Chem. Soc.* **1999**, *121*, 6469.

[130] A. Vagias, K. Sergelen, K. Koynov, P. Košovan, J. Dostalek, U. Jonas, W.

Knoll, G. Fytas, *Macromolecules* **2017**, *50*, 4770.

[131] C. E. Argarahal, I. D. Kuntz, S. Birken, R. Axel, C. R. Cantorl, *Nucleic Acids Res.* **1986**, *14*, 1871.

[132] S. Gao, N. Koshizaki, H. Tokuhisa, E. Koyama, T. Sasaki, J.-K. Kim, J. Ryu, D.-S. Kim, Y. Shimizu, *Adv. Funct. Mater.* **2010**, *20*, 78.

[133] X. Hong, E. A. H. Hall, *Analyst* **2012**, *137*, 4712.

[134] M. E. Stewart, C. R. Anderton, L. B. Thompson, J. Maria, S. K. Gray, J. A. Rogers, R. G. Nuzzo, *Chem. Rev.* **2008**, *108*, 494.

[135] V. G. Kravets, F. Schedin, R. Jalil, L. Britnell, R. V. Gorbachev, D. Ansell, B. Thackray, K. S. Novoselov, A. K. Geim, A. V. Kabashin, A. N. Grigorenko, *Nat. Mat.* **2013**, *12*, 304.

[136] K. V. Sreekanth, Y. Alapan, M. ElKabbash, E. Ilker, M. Hinczewski, U. A. Gurkan, A. de Luca, G. Strangi, *Nat. Mater.* **2016**, *15*, 621.

[137] X. Li, Y. Wang, L. Wang, Q. Wei, *Chem. Commun.* **2014**, *50*, 5049.

[138] T. L. Sun, T. Kurokawa, S. Kuroda, A. B. Ihsan, T. Akasaki, K. Sato, M. A. Haque, T. Nakajima, J. P. Gong, *Nat. Mater.* **2013**, *12*, 932.

[139] J.-Y. Sun, X. Zhao, W. R. K. Illeperuma, O. Chaudhuri, K. H. Oh, D. J. Mooney, J. J. Vlassak, Z. Suo, *Nature* **2012**, *489*, 133.

[140] S. Zhang, A. M. Bellinger, D. L. Glettig, R. Barman, Y.-A. L. Lee, J. Zhu, C. Cleveland, V. A. Montgomery, L. Gu, L. D. Nash, D. J. Maitland, R. Langer, G. Traverso, *Nat. Mater.* **2015**, *14*, 1065.

[141] Z. Tang, J. Huang, B. Guo, L. Zhang, F. Liu, *Macromolecules* **2016**, *49*, 1781.

[142] C. Zhang, M. D. Losego, P. V. Braun, *Chem. Mater.* **2013**, *25*, 3239.

[143] M. Toma, U. Jonas, A. Mateescu, W. Knoll, J. Dostalek, *J. Phys. Chem. C* **2013**, *117*, 11705.

[144] Q. Zhang, Y. Wang, A. Mateescu, K. Sergelen, A. Kibrom, U. Jonas, T. Wei, J. Dostalek, *Talanta* **2013**, *104*, 149.

[145] A. Steffen, C. Thiele, S. Tietze, C. Strassnig, A. Kämper, T. Lengauer, G. Wenz, J. Apostolakis, *Chem. Eur. J.* **2007**, *13*, 6801.

[146] G. Wenz, C. Strassnig, C. Thiele, A. Engelke, B. Morgenstern, K.

Hegetschweiler, *Chem. Eur. J.* **2008**, *14*, 7202.

[147] M. Gade, A. Paul, C. Alex, D. Choudhury, H. V. Thulasiram, R. Kikkeri, *Chem. Commun.* **2015**, *51*, 6346.

[148] Y. Liu, R. Cao, Y. Chen, J.-Y. He, *J. Phy. Chem. B* **2008**, *112*, 1445.

[149] A. Samanta, B. J. Ravoo, *Chem. Eur. J.* **2014**, *20*, 4966.

[150] A. Charlot, R. Auzély-Velty, *Macromolecules* **2007**, *40*, 1147.

[151] S. K. Osman, F. P. Brandl, G. M. Zayed, J. K. Teßmar, A. M. Göpferich, *Polymer* **2011**, *52*, 4806.

[152] Z. Huang, K. Qin, G. Deng, G. Wu, Y. Bai, J.-F. Xu, Z. Wang, Z. Yu, O. A. Scherman, X. Zhang, *Langmuir* **2016**, *32*, 12352.

[153] D. A. Armbruster, T. Pry, *Clin. Biochem. Rev.* **2008**, *29*, 49.

[154] A. K. Dwivedi, R. Singh, A. Singh, K.-H. Wei, C.-Y. Wu, P.-C. Lyu, H.-C. Lin, *Macromolecules* **2016**, *49*, 5587.

[155] G. González-Gaitano, T. Sanz-García, G. Tardajos, *Langmuir* **1999**, *15*, 7963.

[156] H. Mwakibete, R. Cristantino, D. M. Bloor, E. Wyn-Jones, J. F. Holzwarth, *Langmuir* **1995**, *11*, 57.

[157] M. Lin, P. Song, G. Zhou, X. Zuo, A. Aldalbahi, X. Lou, J. Shi, C. Fan, *Nat. Protoc.* **2016**, *11*, 1244.

[158] L. Wu, X. Qu, *Chem. Soc. Rev.* **2015**, *44*, 2963.

[159] S. Zhang, R. Geryak, J. Geldmeier, S. Kim, V. V. Tsukruk, *Chem. Rev.* **2017**, *117*, 12942.

[160] B. Liu, Y. Li, H. Wan, L. Wang, W. Xu, S. Zhu, Y. Liang, B. Zhang, J. Lou, H. Dai, K. Qian, *Adv. Funct. Mater.* **2016**, *26*, 7994.

[161] C. L. Sawyers, *Nature* **2008**, *452*, 548.

[162] S.-Y. Zhang, W. Shi, P. Cheng, M. J. Zaworotko, *J. Am. Chem. Soc.* **2015**, *137*, 12203.

[163] P. A. Canney, M. Moore, P. M. Wilkinson, R. D. James, *Brit. J. Cancer* **1984**, *50*, 765.

[164] G. B. Mills, W. H. Moolenaar, *Nat. Rev. Cancer* **2003**, *3*, 582.

[165] Y. Wang, H. Pei, Y. Jia, J. Liu, Z. Li, K. Ai, Z. Lu, L. Lu, *J. Am. Chem. Soc.*

2017, *139*, 11616.

[166] W. H. Moolenaar, *J. Biol. Chem.* **1995**, *270*, 12949.

[167] J. M. Onorato, P. Shipkova, A. Minnich, A.-F. Aubry, J. Easter, A. Tymiak, *J. Lipid Res.* **2014**, *55*, 1784.

[168] T. Kishimoto, T. Matsuoka, S. Imamura, K. Mizuno, *Clin. Chim. Acta* **2003**, *333*, 59.

[169] J.-h. Chen, F. Zou, N.-d. Wang, S.-w. Xie, X. Zhang, *Bioorg. Med. Chem. Lett.* **2000**, *10*, 1691.

[170] L. Seballos, J. Z. Zhang, R. Sutphen, *Anal. Bioanal. Chem.* **2005**, *383*, 763.

[171] Z. Zheng, W.-C. Geng, J. Gao, Y.-Y. Wang, H. Sun, D.-S. Guo, *Chem. Sci.* **2018**, *9*, 2087.

[172] M. Lan, W. Liu, Y. Wang, J. Ge, J. Wu, H. Zhang, J. Chen, W. Zhang, P. Wang, *ACS Appl. Mater. Interfaces* **2013**, *5*, 2283.

[173] D. Yao, Z. Lin, J. Wu, *ACS Appl. Mater. Interfaces* **2016**, *8*, 5847.

[174] A. G. Brolo, *Nat. Photonics* **2012**, *6*, 709.

[175] P. Singh, *Sensor Actuat. B Chem.* **2016**, *229*, 110.

[176] W. D. Wilson, *Science* **2002**, *295*, 2103.

[177] J. N. Anker, W. P. Hall, O. Lyandres, N. C. Shah, J. Zhao, R. P. van Duyne, *Nat. Mater.* **2008**, *7*, 442.

[178] N. de-los-Santos-Alvarez, M. J. Lobo-Castañón, A. J. Miranda-Ordieres, P. Tuñón-Blanco, *Biosens. Bioelectron.* **2009**, *24*, 2547.

[179] J. Wang, A. Munir, H. S. Zhou, *Talanta* **2009**, *79*, 72.

[180] W. U. Wang, C. Chen, K.-h. Lin, Y. Fang, C. M. Lieber, *P. Natl. Acad. Sci. USA* **2005**, *102*, 3208.

[181] S. Zeng, K. V. Sreekanth, J. Shang, T. Yu, C.-K. Chen, F. Yin, D. Baillargeat, P. Coquet, H.-P. Ho, A. V. Kabashin, K.-T. Yong, *Adv. Mater.* **2015**, *27*, 6163.

[182] P. Zijlstra, P. M. R. Paulo, M. Orrit, *Nat. Nanotechnol.* **2012**, *7*, 379.

[183] N. Maccaferri, K. E. Gregorczyk, T. V. A. G. de Oliveira, M. Kataja, S. van Dijken, Z. Pirzadeh, A. Dmitriev, J. Åkerman, M. Knez, P. Vavassori, *Nat. Commun.* **2015**, *6*, 6150.

[184] Y. Shen, J. Zhou, T. Liu, Y. Tao, R. Jiang, M. Liu, G. Xiao, J. Zhu, Z.-K. Zhou, X. Wang, C. Jin, J. Wang, *Nat. Commun.* **2013**, *4*, 2381.

[185] D. Kuckling, M. E. Harmon, C. W. Frank, *Macromolecules* **2002**, *35*, 6377.

[186] G. Pelossof, R. Tel-Vered, X.-Q. Liu, I. Willner, *Chem. Eur. J.* **2011**, *17*, 8904.

[187] J.-E. Lee, Chung, Lee, Kyungwha J., K. Shin, D. H. Kim, *Adv. Funct. Mater.* **2015**, *25*, 6716.

[188] Y. Hayashi, R. Matsuda, T. Maitani, K. Imai, W. Nishimura, K. Ito, M. Maeda, *Anal. Chem.* **2004**, *76*, 1295.

[189] P. D. Ross, S. Subramanian, *Biochemistry* **1981**, *20*, 3906-3102.

[190] Z. Huang, K. Qin, G. Deng, G. Wu, Y. Bai, J.-F. Xu, Z. Wang, Z. Yu, O. A. Scherman, X. Zhang, *Langmuir* **2016**, *32*, 12352.

[191] Daniel Buenger, Fuat Topuz, Juergen Groll, *Prog. Ploym. Sci.* **2012**, *37*, 1678.

[192] H.-J. Schneider, *Angew. Chem. Int. Ed.* **2009**, *48*, 3924.

[193] S. S. Babu, V. K. Praveen, A. Ajayaghosh, *Chem. Rev.* **2014**, *114*, 1973.

[194] A. Forootan, R. Sjöback, J. Björkman, B. Sjögreen, L. Linz, M. Kubista, *Biomol. Detect. Quan.* **2017**, *12*, 1.

[195] Enyi Ye, Pei Lin Chee, Ankshita Prasad, Xiaotian Fang, Cally Owh, Valerie Jing Jing Yeo, Xian Jun Loh, *Mater. Today* **2014**, *17*, 194.

[196] Wei Lu, Xiaoxia Le, Jiawei Zhang, Youju Huang, Tao Chen, *Chem. Soc. Rev.* **2017**, *46*, 1284.

[197] R. Baron, C.-H. Huang, D. M. Bassani, A. Onopriyenko, M. Zayats, I. Willner, *Angew. Chem. Int. Ed.* **2005**, *44*, 4010.

[198] D.-W. Kim, S.-G. Lim, C.-H. Jun, *Org. Lett.* **2006**, *8*, 2937.

[199] N. Kimizuka, T. Kawasaki, K. Hirata, Kunitake T., *J. Am. Chem. Soc.* **1998**, *120*, 4094.

[200] J. H. Yoon, Y. J. Park, J. H. Lee, J. Yoo, C.-H. Jun, *Org. Lett.* **2005**, *7*, 2889.

[201] M. C. Young, E. Liew, J. Ashby, K. E. McCoy, R. J. Hooley, *Chem. Commun.* **2013**, *49*, 6331.

[202] K. Zhang, G. B. Fahs, M. Aiba, R. B. Moore, T. E. Long, *Chem. Commun.* **2014**, *50*, 9145.

[203] P. Tecilla, S.-K. Chang, A. D. Hamilton, *J. Am. Chem. Soc.* **1990**, *112*, 9586.

[204] Tecilla P., A. D. Hamilton, *J. Chem. Soc. Chem. Commun.* **1990**.

[205] W. H. Binder, C. Kluger, M. Josipovic, C. J. Straif, G. Friedbacher, *Macromolecules* **2006**, *39*, 8092.

[206] W. H. Binder, C. Kluger, C. J. Straif, G. Friedbacher, *Macromolecules* **2005**, *38*, 9405.

[207] S. Bosch, L. Zeininger, F. Hauke, A. Hirsch, *Chem. Eur. J.* **2014**, *20*, 2537.

[208] S. Chen, Y. Deng, X. Chang, H. Barqawi, M. Schulz, W. H. Binder, *Polym. Chem.* **2014**, *5*, 2891.

[209] S. Chen, M. Rocher, C. Ladavière, J.-F. Gérard, F. Lortie, J. Bernard, *Polym. Chem.* **2012**, *3*, 3157.

[210] A. Croom, K. B. Manning, M. Weck, *Macromolecules* **2016**, *49*, 7117.

[211] A. Dirksen, U. Hahn, F. Schwanke, M. Nieger, J. N. H. Reek, F. Vögtle, L. de Cola, *Chem. Eur. J.* **2004**, *10*, 2036.

[212] J. T. Lai, D. Filla, R. Shea, *Macromolecules* **2002**, *35*, 6754.

[213] S. Gupta, D. Kuckling, K. Kretschmer, V. r. Choudha, H. J. Adler, *J. Polym. Sci. Polym. Chem.* **2007**, *45*, 669.

[214] D. T. Browne, J. Eisinger, N. J. Leonard, *J. Am. Chem. Soc.* **1968**, *90*, 7302.

[215] J. Schmidt, R. Schmidt, F. Würthner, *J. Org. Chem.* **2008**, *73*, 6355.

[216] S. Guernelli, M. F. Laganà, E. Mezzina, F. Ferroni, G. Siani, D. Spinelli, *Eur. J. Org. Chem.* **2003**, *2003*, 4765.

[217] K. Hirose, *J. Incl. Phenom. Macro. Chem.* **2001**, *39*, 193.